



# DISSERTATION

Titel der Dissertation

Photolithographic Synthesis of Microarrays

Verfasserin

Mag. Nicole Kretschy

angestrebter akademischer Grad

Doktorin der Naturwissenschaften (Dr. rer.nat.)

Wien, 2015

Studienkennzahl lt.  
Studienblatt:

A 796605419

Dissertationsgebiet  
lt. Studienblatt:

Chemie

Betreuerin /  
Betreuer:

B.Sc. MSc PhD Mark Manuel  
Somoza



## **Acknowledgement**

I am thankful to my supervisor, Mark Manuel Somoza whose expertise, understanding, guidance and support made it possible for me to work on a topic that was of great interest to me.

I would like to thank my colleagues Matej Sack, Kathrin Hölz, and Jory Liétard for their precious advice during the work on my thesis.

I wish to express gratitude to Veronika Somoza, Ann-Katrin Holik, Babara Rohm, Masad J. Damha, Nicole L. W. Franssen-van Hal, Pepijn van der Putte, Klaus Hellmuth, Stefan Matysiak, and Klaus-Peter Stengele for providing me their cooperation and help during my research.

My special thanks to Prof. Christopher Gerner and Prof. Martin Bilban for being willing to be my evaluators of my PhD thesis.

I am grateful to my parents Renate and Erfried Kretschy and to my partner Thomas Walter for their loving support.

# Table of Contents

1. Introduction	5
1.1. What is a Microarray?	5
1.2. Peptide Microarrays	5
1.3. Protein Microarrays	7
1.4. Biological Background	9
1.5. DNA Microarrays	12
1.6. RNA Microarrays	22
1.7. Motivation	29
1.8. List of Publications	32
1.9. Publications	33
1.9.1. Next-Generation o-Nitrobenzyl Photolabile Groups for Light-Directed Chemistry and Microarray Synthesis	34
1.9.5. Optimized light-directed synthesis of aptamer microarrays	39
1.9.3. Base-cleavable microarrays for the characterization of DNA and RNA oligonucleotides synthesized in situ by photolithography	47
1.9.2. Comparison of the sequence-dependent fluorescence of the cyanine dyes Cy3, Cy5, DyLight DY547 and DyLight DY647 on single-stranded DNA	51
1.9.6. Nonivamide enhances miRNA let-7d expression and decreases adipogenesis PPAR $\gamma$ expression in 3T3-L1 cells	56
1.9.4. Simultaneous light-directed synthesis of mirror-image microarrays in a photochemical reaction cell with flare suppression	67
2.0. Conclusions	72
3.0 Abstract	75
4.0. Zusammenfassung	76
5.0. References	78

# **1. Introduction**

The aim of this project is to optimize the synthesis of deoxyribonucleic acid (DNA) and ribonucleic acid (RNA) microarrays. This includes not only the synthesis itself, but many additional aspect related to the synthesis which have to be considered. First I want to mention the most known types of microarrays, such as peptide, protein and DNA microarrays, and the recently developed RNA microarrays, and applications which this method encompasses. These three types have some parts of the synthesis in common, and some arrays have evolved out of existing methods like the light directed synthesis of DNA microarrays which is used in this thesis as a main method.

## **1.1. What is a Microarray?**

A microarray is a collection of microscopic specific molecules attached to a specific location on a surface. There are a large numbers of variations of microarrays. They can be divided into four main groups: peptide-, protein-, DNA- and RNA-microarrays.

## **1.2. Peptide Microarrays**

### **1.2.1. Peptides**

Peptides are naturally occurring molecules composed of amino acids and typically linked by covalent bonds between their amino and carboxyl groups. They are involved in almost all biological functions. The development of therapeutics based on a peptides play an important role in the treatment of many diseases. A way to analyze the biological function and their involvement in the development of critical diseases in a highly effective way is the synthesis of peptide microarrays (1).

## **1.2.2. Types of Peptide Microarrays and Applications**

There two ways to synthesize a peptide microarray: light-directed parallel chemical synthesis and spotting array methods.

### **1.1.2.1. Light-directed parallel chemical synthesis**

The parallel on-chip synthesis is an in situ synthesis method which enables the synthesis of thousands peptides simultaneously. The common photolabile groups are NVOC (6-Nitroveratryloxycarbonyl chloride) or MeNPOC ([R,S]-1-[3,4-[methylene-dioxy]-6-nitrophenyl] ethyl chloroformate) and are removed by a spatially addressable illumination performed using a photomask. Light-directed parallel chemical synthesis limits the size of the peptides that can be synthesized, therefore only small peptides can be synthesized. This is due the synthetic challenges including purity and stability.

### **1.1.2.2. Spotted Arrays**

The spotting method involves the presynthesis of a peptide library followed by the transfer the libraries onto a solid substrate (1,2). The spotting of the presynthesized peptide products is managed by an automatic arrayer. The preparation of the libraries can be accelerated by using different methods such as parallel synthesis, split and mix synthesis and reagent mixtures, among others.

Glass slides are typical substrates, due to their low cost, their low intrinsic fluorescence, and their ability to provide a homogeneous chemical surface for immobilizing biochemical at very high density. The efficiency of the density peptide microarray can be increased by functionalization of the surface, the usage of a conjugates and also the usage of a robotic arm to spot the peptides. These improvements enable the synthesis of high density Peptide microarrays, which has become a screening tool to determine enzyme substrate specificities (1,3) and for the characterization of protein kinases, protease and peptide-peptide and protein

peptide interactions (4,1) as well as in many others fields.

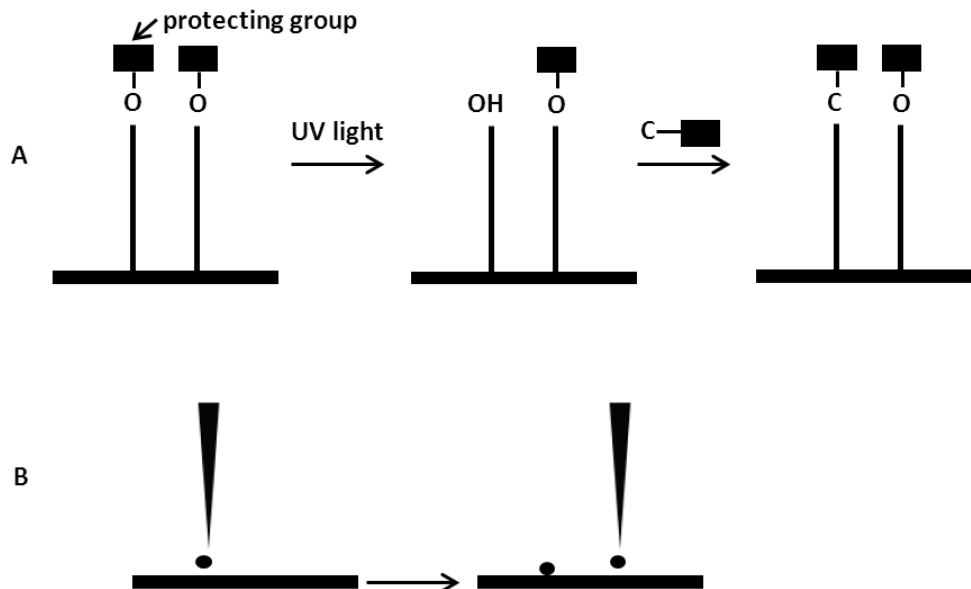


Figure 1. Schematic representation of (A) in-situ synthesis of peptides using photolithographic technique; (B) in situ generation of peptides via spotting microarray approach.

## 1.3. Protein Microarrays

### 1.3.1. Proteins

Proteins are composed of bioactive polypeptides, but the polypeptide is only a bioactive protein if it folds into a specific three-dimensional structure (5). The sequence of the polypeptide determines the functional structure of the protein and therefore also the biological function. There are many shapes in which a protein can appear for example ball like shaped with an irregular surface (globular proteins) or shaped like long fibers (fibrous proteins). This difference causes the specific recognizing and binding abilities of a protein (6).

The multiplicity of functions performed within living organisms arises from a huge number of, for example, catalytic proteins. These proteins convert the

ligands into other molecules, and are also involved in replicating DNA, as well as in regulatory protein-protein interaction to inhibit or increase some crucial biological processes (6, 7). This is only a small sample of the function of proteins. Thus the understanding of the protein activities in a complex cellular system is very important for many fields of research such as tumor biology or pharmacogenosy. In the next chapter an introduction on the most commonly used methods to analyze the protein activities is given.

### **1.3.2. Types of Protein Microarrays and Applications**

Protein microarrays can contain thousands of different proteins, for example antigens, antibodies, enzymes. The proteins are immobilized on discrete spatial locations on a solid surface (8). Usually they are divided into three groups: analytical microarrays, functional microarrays, and reverse phase microarrays, which are show in Fig. 2

On an analytical microarray, a library of antibodies, aptamers, or affibodies are typically arrayed on a glass microscope slide (9). These are used as capture molecules as they have a high affinity to the corresponding binding molecules. A field of applications for analytical microarrays is the profiling of a complex mixture of proteins in order to measure binding affinities, specificities, and protein expression levels of the proteins in the mixture (10).

The difference between an analytical array and a functional array is the size of the protein determined. Functional arrays contain a full-length of functional proteins or protein domains. They are typically used to analyze a large number of protein interactions, such as protein-protein, protein-DNA, protein-RNA, protein-phospholipid, and protein-small molecule interactions.

Reverse phase microarrays are composed of lysates of isolated tissues which are arrayed onto a slide using a contact pin microarrayer. The lysates are probed with antibodies against the target protein which allows the detection of the antibodies,



by using chemiluminescent, fluorescent, or colorimetric assays. The reference peptides which are printed on the slides as well allow enabling the protein quantification of the sample lysates (9). Reverse phase microarrays are used to determine the presence of altered proteins like post-translational modification that may be the result of diseases such as cancer (9, 11).

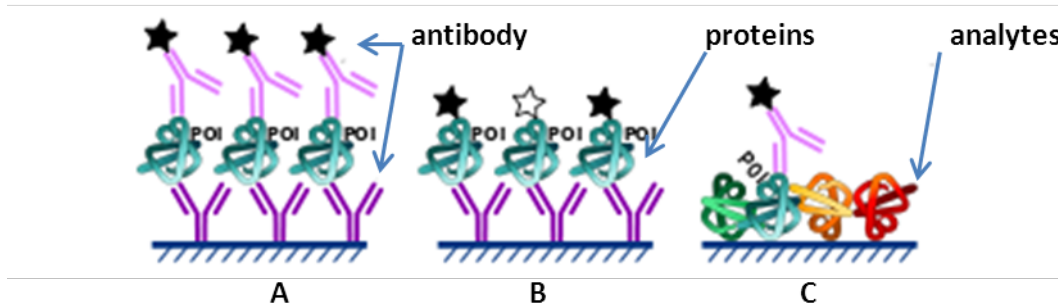


Figure 2. “Types of protein arrays” by Philippe Hupé is licensed under CC BY-SA 3.0.  
 A) analytical- B) functional- C) reverse phase microarray

## 1.4. Biological Background

### 1.4.1. What is DNA?

DNA as the carrier of our hereditary information allows our cells to store, retrieve, and translate the genetic instructions which are required to make and maintain a living organism (12). DNA is stored within every single cell in the human body and has a unique double helix structure which provides enhanced stability and protects from several chemical modifications by the environment. DNA is not completely protected as there are influences such as ionizing radiation, smoke or chemical substances which can alter the DNA through mutations and cause diseases.

## 1.4.2. Structure and Function of DNA

A DNA molecule is composed of two DNA chains which are presented as two long polynucleotides and they can consist of four different nucleosides: thymine, adenine, cytosine and guanine. Every nucleoside is able to bind to a specific nucleoside assuming that it is complementary to the nucleoside sequence of its partner strand. For example thymine is complementary to adenine, and guanine is complementary to cytosine and vice versa. A deoxyribose is attached to a phosphate group and builds the “backbone” of the polynucleotide chain. The nucleotide pairs are covalently linked together by hydrogen bonds in a double stranded chain. Through the deoxyribose the DNA becomes more stable and therefore the ideal carrier of the hereditary information (13).

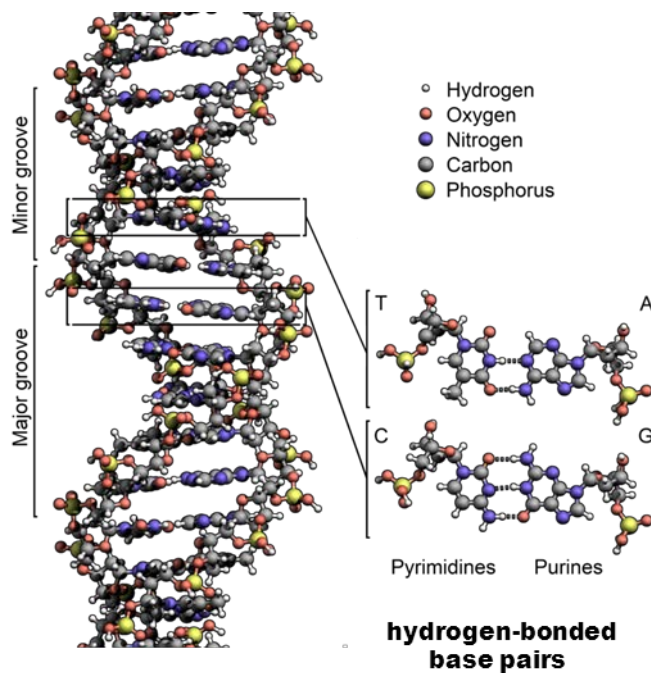


Figure 3. “The structure of DNA showing with detail showing the structure of the four bases, adenine, cytosine, guanine and thymine, and the location of the major and minor groove” by Zephyris is licensed under CC BY-SA 3.0

## 1.4.3 Gene Expression

### 1.4.3.1. Transcription

For the synthesis of a protein, the DNA is needed as a template for messenger RNA synthesis. The process starts with the unwinding of DNA strand by a helicase enzyme. One of the two strands is used as a template for the RNA synthesis. During the synthesis a transient double-stranded RNA-DNA hybrid with the growing RNA chain is formed. The template strand has two ends, the 5' and the 3'. The RNA is synthesized by the RNA polymerase from the 5' to the 3' end. The RNA polymerase binds to specific DNA regions called promoters. For successful binding several transcription factors are required. The RNA polymerase begins to elongate on the RNA strand by adding the ribonucleotide monophosphate residue (AMP, CMP, GMP or UMP) to the free 3' hydroxyl group at the 3' end of the growing RNA chain (14).

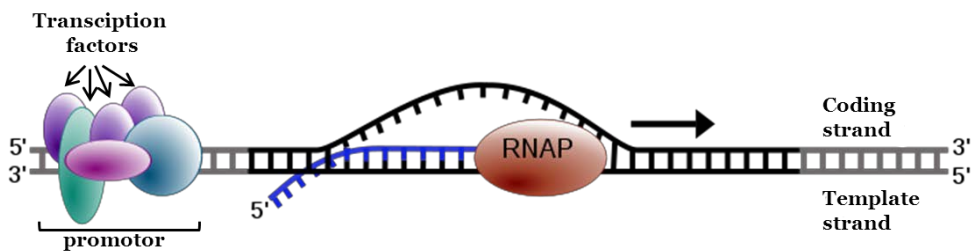


Figure 4. “The process of transcription is carried out by RNA polymerase (RNAP), which uses DNA (black) as a template and produces RNA (blue)” by Forluvoft is licensed under Public Domain .

### 1.4.3.1. RNA processing

After the cleavage reaction, the primary transcript undergoes a series of processing reactions. One of these reactions is the RNA splicing where unwanted internal segments (exons) are removed and the remaining segments (introns) are

rejoined. Furthermore the primary transcript is capped due to the adding of methylated nucleoside, 7-methylguanosine to the first 5' nucleotide of the RNA transcript. The link between the 7-methylguanosine and the 5' nucleotide is enabled by a special 5'-5' phosphodiester bond. Afterwards the primary transcript is polyadenylated by the adding of several adenylates (i.e. AMP) residues to the poly A tail.

The final 3' end of the strand, which was synthesized by the Polymerase II, is determined by a post-transcriptional cleavage reaction on the poly A tail. The transcription is stopped after the Polymerase I and III recognize a specific transcription termination site (14).

#### **1.4.3.1. Translation**

After the termination of the transcription the mRNAs migrate from the nucleus to the cytoplasm. Only the central segment of mRNA is translated. The flanking segment, 5' and 3' untranslated regions are cut and facilitate the binding of the mRNA on the ribosome, where the translation takes place. Each codon of the mRNA sequence consists of three nucleotides which are decoded sequentially in order to specify individual amino acids. The process is mediated by tRNAs (transfer RNA); a tRNA is composed of 74-95 nucleotides and is covalently bound to a specific amino acid. Each tRNA has a binding site which includes an anticodon triplet which is complementary to the codon in the mRNA sequence. Amino acids are incorporated continuously into the growing polypeptide chain. The carboxyl group of the last incorporated amino acid reacts with the amino group of the incoming amino acid, thereby they are bound together. The reaction is catalyzed by the peptidyl transferase activity of the ribosome.

The primary products of the translation are often modified for example by chemical modification (hydroxylation, phosphorylation, etc.) of the side chains of single amino acids or the addition of different types of carbohydrate or lipid groups (14).

## **1.5. DNA Microarrays**

### **1.5.1. Existing Fabrications Strategies of DNA Microarrays**

The first fabrication method for DNA microarrays was reported 1982 where cytoplasmic RNA was isolated from a mouse transplantable colon carcinoma. Double stranded DNA, which was complementary to the isolated RNA, was synthesized and was inserted into a plasmid using HindIII linkers. The recombinant molecules were cloned into *Escherichia coli*. Clones were spotted on sterile nitrocellulose filters and grown on L-agar plates. Furthermore the clones were screened with the labeled complementary DNA synthesized from isolated RNA of the tumor or normal mouse colon, liver, or kidney to test if the cloned sequence was present (16).

In 1987 this approach was expanded using a cDNA library by Augenlicht et al (17). The gene expression level of 4000 cloned complementary sequences in an increasingly advanced stage were isolated from the mucosa of normal and neoplastic human large intestine from colonic epithelial cells was screened (17). The use of microarrays, with a small format and with a higher density, for gene expression profiling was first reported in 1995 (18). A high speed printing device was used to spot 48 cDNAs, amplified with PCR, from *Arabidopsis thaliana* clones onto a microscope slide. To attach and denature the DNA, the printed arrays were processed by chemical and heat treatment. After that the array was hybridized with fluorescent cDNA synthesized from total *Arabidopsis* mRNA and scanned with a laser scanner (18).

A whole eukaryotic genome was arrayed for the first time by Deval A. Lashkari et al. in 1997 (19). Sequence information, from public databases, was used to locate the predicted ORFs (open reading frames) of yeast and appropriate primers for amplification were chosen. The primers were used to enable the amplification of yeast ORFs in 96-well plates by PCR. The ORFS are arrayed by the use of an automated micro array device. The products of the PCR were printed onto glass

surfaces, hybridized with fluorescently labeled samples and scanned with a laser confocal scanning microscope (19).

Currently, there are two methods to synthesize a DNA Microarray: Solid phase synthesis of DNA Microarrays and in situ synthesis of oligonucleotides on a solid substrate.

## **1.5.2. Solid phase synthesis of DNA Microarrays**

### **1.5.2.1. Synthesis**

The solid phase synthesis enables the synthesis of oligonucleotide up to a base length of a hundred bases. As a substrate, a controlled-pore-glass (CPG) is used. This has deep pores in which the oligonucleotide synthesis takes place. The synthesis proceeds in the 3' to 5' direction. The size of the pores determines the maximum length of the oligonucleotides that can be synthesized (20).

Phosphoramidites are covalently bonded to next phosphoramidite. The first phosphoramidite couples, in the presence of an activator, to the free hydroxyl group of a CPG substrate (21). Any remaining free 5'-hydroxyl groups are capped to simplify the final purification of the oligonucleotide chain. The newly created phosphite triester linkage are oxidized. After the deprotection of the 5' protecting group the cycle starts again.

### **1.5.2.2. Protecting groups**

Protecting groups are used to stabilize the phosphoramidite and to prevent interaction with some other molecules. Except for thymine, each base has a protecting group, which is usually a benzoyl group for dA and dC and an isobutyryl group for dG (22). The 5' hydroxyl of the phosphoramidite is protected by a 4,4' dimethoxytrityl (DMT) group (20).

### 1.5.2.3. Deprotection

The DMT protecting group can be easily removed during the synthesis with a dilute acid, typically dichloroacetic or trichloroacetic acid in methylene chloride. After the successful removal, an orange color is visible in the line. The quantity of color released is representative of the completeness of the coupling reaction, and can be measured photometrically. With each step a very high coupling efficiency (>99%) can be achieved (22). The base protecting groups have to be removed after the synthesis, normally by an ammonium hydroxide treatment (20). The phosphate is protected by the 2-cyanoethyl protecting group (22).

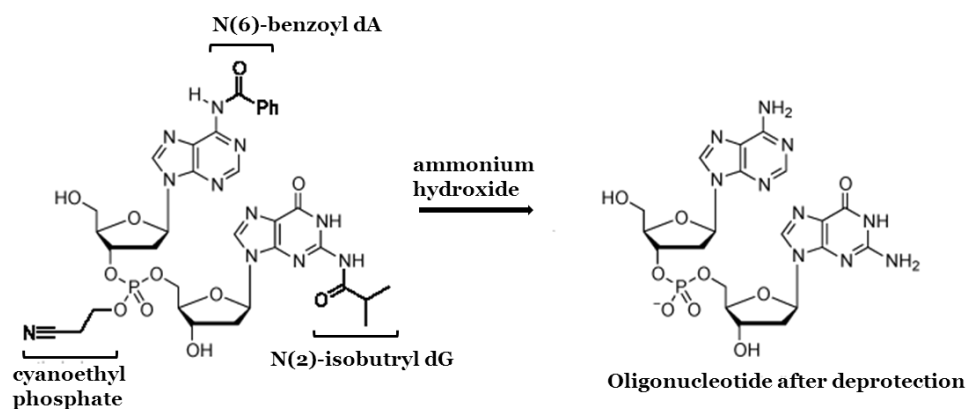


Figure 5. Mechanism of deprotection of an oligonucleotide.

### 1.5.2.4. Application

The products of the synthesis can be used for several biological approaches such as DNA sequencing, PCR applications, and site-specific mutagenesis (23).

### **1.5.2.5. Advantages and disadvantages of solid support synthesis**

Solid support synthesis use large excess of reagents which drive the reactions quickly to completion. Purification of the synthesized oligonucleotides simple because unreacted 5'-hydroxyl group are capped and can be removed using HPLC or gel electrophoresis (21). The yield of a synthesis is high (22), but with each synthesis only a single oligonucleotide sequence can be synthesized at a time (20).

### **1.5.3. Light directed in situ synthesis of high-density DNA Microarrays**

#### **1.5.3.1. Existing Fabrications Strategies**

##### Light-generated oligonucleotide arrays for rapid DNA sequence analysis

*Ann Caviani Pease, Dennis Solas, Edward J. Sullivan, Maureen T. Cronin, Christopher P. Holmes, Stephen P.A. Fodor*

A matrix of 256 spatially defined oligonucleotide probes was generated by using photolabile 5'-protected N-acyl-deoxynucleoside phosphoramidites, surface linker chemistry and light-directed oligonucleotide synthesis. To test the coupling efficiencies of the photoprotected nucleosides two different methods were developed. In the first method a glycol linker was attached and detritylated. Then MeNPoc-deoxynucleoside-O-cyanoethyl phosphoramidite coupled to the free hydroxyl group. A DMT-deoxynucleoside-cyanoethyl phosphoramidite was added as reporter amidite, and should couple to any unreacted hydroxyl groups remaining from the first coupling reaction. After that the trityl effluents were collected and quantified by absorption spectroscopy to determine the coupling efficiencies. They were measured assuming a high coupling efficiency of the reporter amidite.

The second method includes photoprotected nucleosides which are directly attached to the glass substrate. In a light-directed synthesis, the spatial control and the quality of the products depend on the pattern of illumination and the order of



chemical coupling reagents. With each cycle another part of the array was illuminated. After the deprotection the nucleosides are coupling on the free hydroxyl group. The process is continued to build four regions of mononucleotides. Another region of the substrate was then illuminated. Finally a fluorescent deoxynucleoside phosphoramidite (FAM-phosphoramidite) was coupled. It was assumed that the FAM-phosphoramidite couples on the newly exposed hydroxyl groups and the previously unreacted hydroxyl groups. The coupling efficiency was determined by scanning for fluorescence signals and-by the measurement of the ratio of fluorescence intensities of the two sites.

The results show that the coupling efficiencies of the first method were around 95% to 100% and of the second method between 85% and 98% (24).

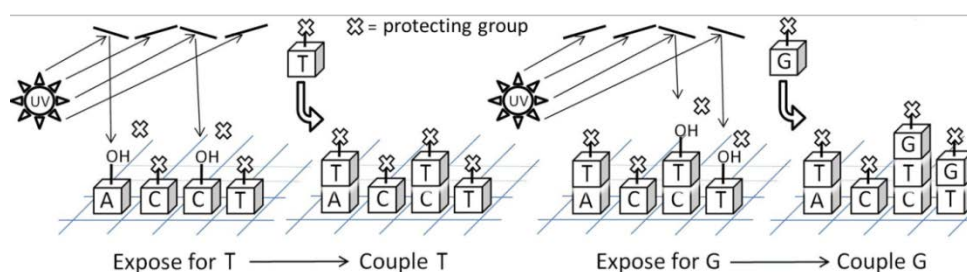


Figure 6. Light-directed synthesis of oligonucleotides. The thymine phosphoramidite is introduced into the reaction flow cell and couples to these hydroxyl groups. A subsequent coupling of guanine is initiated by directing micromirrors to illuminate the third and fourth microarray positions. After exposure, the guanine phosphoramidite is introduced and couples, extending the DNA sequences at positions three and four.

#### Light-directed, spatially addressable parallel chemical synthesis.

*Fodor SP, Read JL, Pirrung MC, Stryer L, Lu AT, Solas D.*

In these studies the usage of the light directed synthesis was tested. Therefore peptide arrays and dinucleotide arrays are used. The peptide arrays consist of two different sequences. The arrays are created on the entire surface by a protecting step, followed by three coupling steps and one addition spatially localized

deprotection step. The spatially localized deprotection step was performed by a 50  $\mu\text{m}$  checkerboard mask. After the deprotection the array was treated with N $\alpha$ -tert-butylloxycarbonyl-O-tert-butyl-L-tyrosine. The array was probed with two different antibodies to identify the two sequences. The set of tested peptides are expanded to 1024 per array and performed like the previous one.

For the combinatorial synthesis nucleosides are used, there the light directed and chemical syntheses were combined. The products are formed by the pattern and order of mask and by the order of reactants. The synthesis includes twenty coupling and illumination steps. As a protecting group NVOC (6-Nitroveratryloxycarbonyl chloride) and for the detection of the sequences two different fluorescence labels were used (25).

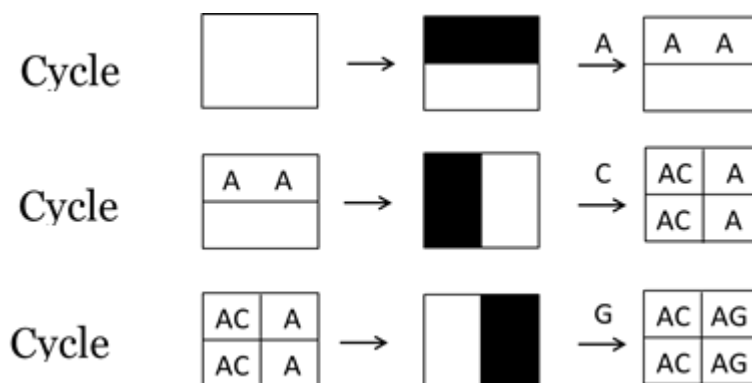


Figure 7. (a) Masks used to synthesize AC, AG and from reactants Adenine, Cytosine and Guanine. The synthesis includes three photolysis and chemical cycles.

In 1991 the original application of this technology was developed by Affymetrix. But the difference between this and the presently used method is the usage of a digital micromirror device instead of photolithographic masks (27).

### 1.5.3.2. Synthesis

DNA microarrays are made using the technique of maskless array synthesis (MAS). Figure 5 shows a 3-D visualization of the optical system of the MAS

system. The MAS instrument can be divided into two systems, an optical system and a chemical delivery system.

The chemical system consists of a modified Perspective Biosystems Expedite 8909 synthesizer, which delivers solvents and reagents to the functionalized glass surface where the microarray synthesis takes place. The optical system is similar to that of a photolithographic system, but it uses a digital micromirror device instead of photomasks to deliver patterned ultraviolet light. The pattern displayed on the micromirror device is transferred to the synthesis surface, where photocleavable protecting groups on the phosphoramidites at the 5' termini of the oligonucleotides are removed by according to this pattern (see Figure 8). Reagent delivery and light exposures are synchronized and controlled by a computer, which is also responsible for the storage and order of virtual masks which are displayed on the micromirror array.

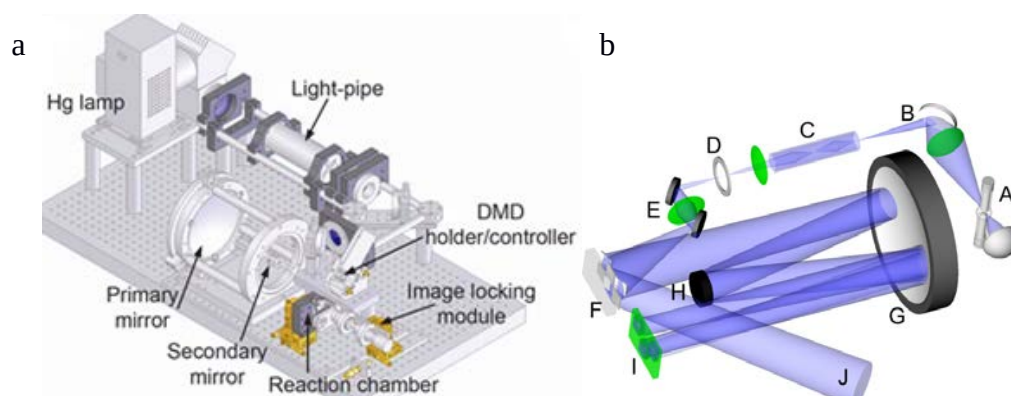


Figure 8. a) 3-D visualization of the MAS optical system with labels indicating the major components. b) Schematic of the optical system of the maskless array synthesizer. A. High pressure mercury short-arc lamp. B. Dichroic mirror. C. Homogenizing light pipe. D. Shutter. E. Folding mirrors. F. Micromirror array. G. Offner relay primary mirror. H. Offner relay secondary mirror. I. Reaction chamber illuminated by ON mirrors. J. Light dump from OFF mirrors.

In comparison to the solid-phase synthesis the cycle where a phosphoramidite is added to the growing oligonucleotide chain is similar, except of some significant differences. The removal of the NPPOC protecting group from the 5'-hydroxyl

terminus during the synthesis is performed by the UV light from the I-line of mercury lamp, in the presence of an organic base, and thereby enables the coupling during the next synthetic cycle (27).

Before the photodeprotection starts, the synthesis area is dried with helium. Oxidation of the phosphites is not required during the cycle if a non-acid activator, such as DCI (dicyanoimidazole) is used. But, at a minimum a final oxidation is still needed. The cycle is illustrated with 5'-NPPOC DNA phosphoramidites in Figure 7.

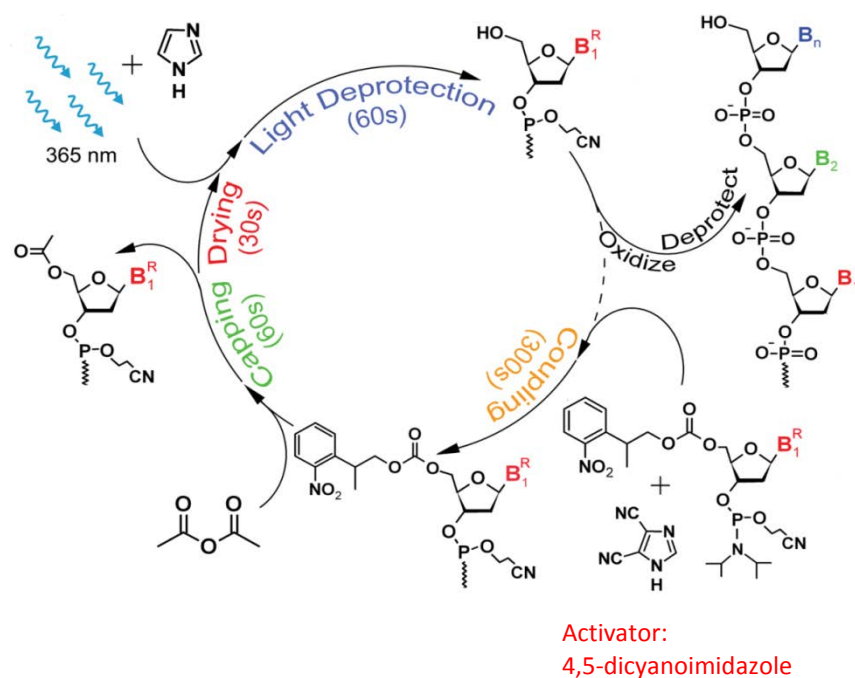


Figure 9. Phosphoramidite synthesis cycle in maskless, light-directed synthesis of microarrays.

### 1.5.3.3. Protecting groups

The chemistry is similar to that used in solid-phase oligonucleotide synthesis only the protecting groups of the bases are different, namely dA is protected by the tac (t-butyl phenoxyacetyl) group, dC is protected by isobutyryl group and dG is protected by the ipac (2-(4-isopropylphenoxy) acetyl) group. The primary

modification is the 5'-nitrophenylpropyloxycarbonyl (NPPOC) photocleavable protecting group.

#### **1.5.3.4. Deprotection**

After synthesis, the base and phosphate protecting groups need to be removed by ethylenediamine/ethanol treatment.

#### **1.5.3.5. Coupling efficiencies**

The key parameter for determining the performance of the DNA phosphoramidites is the coupling efficiency. The coupling efficiency determines the DNA chain length which can be obtained with a reasonable yield. The coupling efficiencies of all five protecting groups were tested by Agbavwe et al. The measured coupling efficiencies were: 99.8% (dA), 98.0% (dC), 98.6% (dG), 99.4% (dT), and 99.0% (global fit of all four base data). (27).

#### **1.5.3.6. Labeling Strategies**

Cy3 and Cy5 which are commonly used in nucleic acid labeling applications are covalently bound to the 5' termini of both single- and double-stranded DNA (28). Cy3 has an absorbance maximum of 550 nm and an emission maximum of 570 nm and is more stable to visible light than Cy5. Cy5 has an absorbance maximum of 649 nm and an emission maximum of 670 nm (29, 30).

#### **1.5.3.7. Application**

DNA microarrays are high-throughput methods and enable the exploration of the preferential binding of complementary nucleic acid sequences to simultaneously measure the expression levels of thousands of genes. This includes the comparison

of the expression levels between normal, diseased, or drug treated cells. This creates the possibility to detect patterns of differentially expressed genes which provides biomarkers or fingerprints of diseases or toxicities (31, 32).

Another application field for DNA microarrays is the analysis of genomic DNA for example to analyze the genetic characterization of immortalized prostate epithelial cells before and after conversion to tumorigenicity. The hybridization of the microarray with the genomic DNA of the mutant strains and their isogenic parental wild-type strains was shown. It was revealed that they were aneuploid for whole chromosomes or chromosomal segments (33).

## **1.6. RNA Microarrays**

### **1.6.1. RNA vs. DNA**

It is known that RNA is an extremely versatile biopolymer as it has storage abilities like the DNA/the storage capability similar to the DNA but the RNA (ribonucleic acid) has additional secondary structure abilities that enhance its enzymatic and bioaffinity properties. Due to their versatility the molecule plays an important role in many basic biological systems including translation, gene expression, regulation and suppression, and biocatalysis. There are five main differences between RNA and DNA:

1. RNA has the nucleobase uracil instead of thymine
2. RNA has a ribose as sugar
3. RNA normally occurs single stranded
4. RNA is less stable than DNA
5. RNA has enhanced enzymatic and bioaffinity properties (15, 35).

## 1.6.2. Existing Fabrications Strategies

### Immobilized RNA switches for the analysis of complex chemical and biological mixtures

*Sukeerthi Seetharaman, Maris Zivarts, Narasimhan Sudarsan, Ronald R. Breaker*

A prototype of a RNA array was developed using RNA switches. The RNA switches were modified by using allosteric selection to fabricate a series of self-cleaving hammerhead ribozymes. They can be activated by addition of specific metals such as cobalt, cadmium, nickel and zinc and have the ability to sense five additional analytes with similar kinetics characteristics of AR1 such are 3',5', cyclic guanosine monophosphate (cGMP), 3',5'-cyclic cytosine monophosphate (cCMP), cyclic adenosine monophosphate (cAMP), flavin mononucleotide (FMN), and theophylline. AR1 is an allosteric ribozyme and consists of a structurally distinct ribozyme and allosteric domains and can be activated in the presence of  $\text{CO}_2^+$ .

To construct prototype RNA array, the six additional RNA switches (AR2–AR7) with a format identical to that of AR1 were generated. This ribozyme normally self-cleaves in the presence of divalent magnesium or of its corresponding effector. The RNA switches (AR1-AR7) are immobilized by a 5'-thiophosphate group on the gold surface. Due to the immobilization the RNA switches become HS-RNA switches. These RNA switches are arrayed on columns 1-7 and they are treated with nine different analytes (Figure 10)

Row A was treated under the permissive reaction conditions in the presence of 1 mM  $\text{Co}_2^+$ , which results in a positive signal in A1. A loss of the positive signal was observed by adding the corresponding factor which reflects the release of the 3'-cleavage fragment into the reaction solution as a result of ribozyme cleavage. The results further show that an alteration of the signal is visible in each of the appropriate pixels of rows B–G in the positive and negative images as long as the corresponding effectors are present (36).

## Fabricating RNA Microarrays with RNA–DNA Surface Ligation Chemistry

*Hye Jin Lee , Alastair W. Wark , Yuan Li , and Robert M. Corn*

By using RNA-DNA ligation a single stranded (ss) RNA microarray was created. First a ssDNA microarray was produced by the chemical attachment of 3'-thiol-modified, 5'-phosphate-terminated ssDNA to a gold substrate. The surface was modified to form a thiol-reactive maleimide-terminated surface. These "anchor" DNA ( $D_A$ ) array elements were hybridized with template DNA ( $D_T$ ) and probe RNA ( $R_P$ ) to form a nicked duplex substrate and were afterwards exposed to a solution containing T4 DNA ligase. The ligase forms a phosphodiester bond between the 5'-phosphate of the surface-attached ssDNA and the 3'-hydroxyl group of unmodified RNA. This happens in the presence of a complementary ssDNA template. After that the array is rinsed with urea to remove and denature the template DNA and the ligase to create bioactive ss RNA elements (Figure 11).

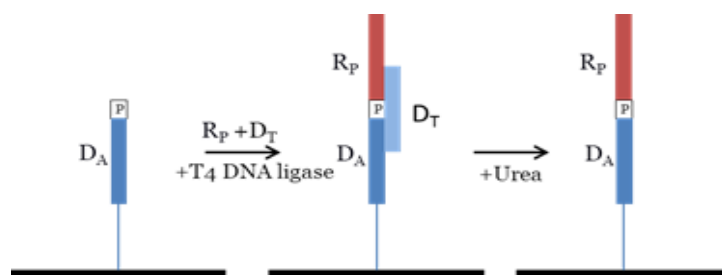


Figure 10a-d. The fabrication of an RNA microarray element. –a-c)] Different fabrication steps, d) Image of the fabricated RNA microarray.

As a next step each surface ligation reaction was characterized by using in situ SPRI measurements in three different experiments. The successfully ligation is determined the reflectivity of the hybridization experiments. The three experiments include: The hybridization of the RNA microarray with the complementary sequence ( $D_c$ ) resulting in an increase of 1.5% in  $\Delta R$  ( $R$ =reflectivity) due the hybridization absorption of  $D_c$  onto the  $R_P$  array elements. The exposure of the ligated ss RNA microarray to a solution of RNase S



accomplished the hydrolysis of single-stranded RP array elements in a separate experiment resulting in a loss of 2.5% loss of R in SRP image (SRPI surface plasmon resonance imaging). In an additional enzymatically study, the hybridization of Rp microarray with Dc causes the formation of DC–RP heteroduplexes. The heteroduplexes were hydrolyzed by RNase H resulting in 3.2% loss of R in the SRP image. In the case of RNase H the ligation process can be repeated to create a new ss RNA array because RNase H cleaves the phosphodiester bonds in RNA to produce 5′-phosphate and 3′-hydroxyl termini (Figure 12) (37).

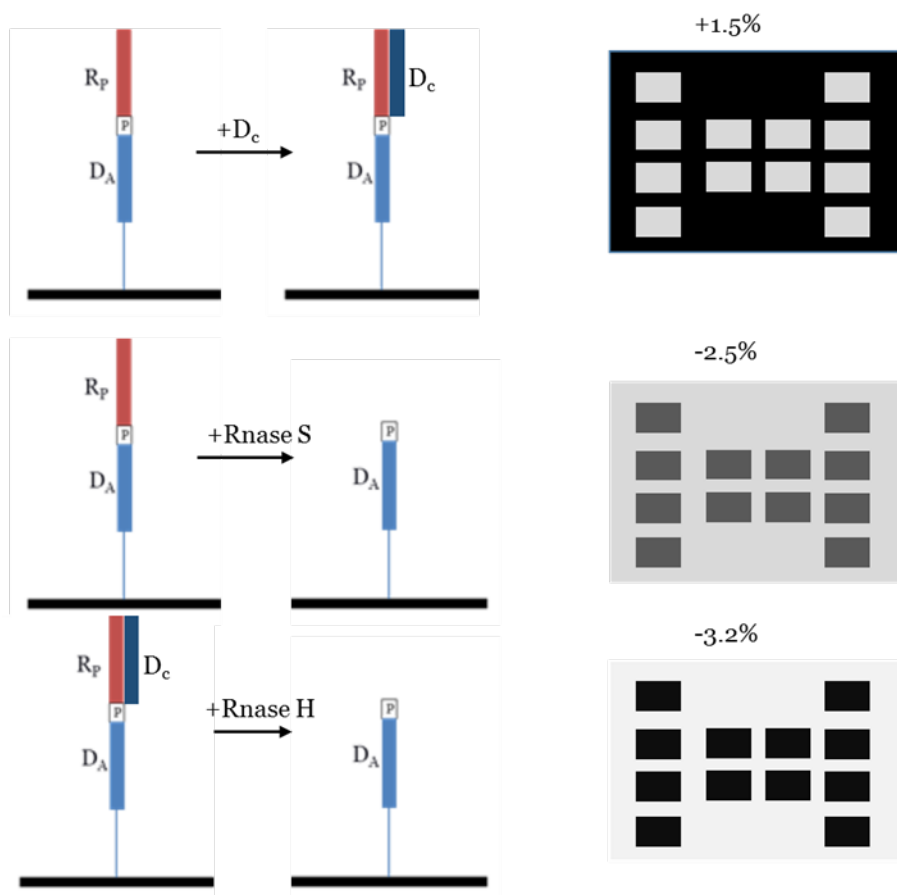


Figure 12. Schematics and accompanying SPR difference images of a hybridizations-and hydrolysis experiment.

### 1.6.3. Protecting groups for solid phase RNA synthesis for the 2'-hydroxyl group of RNA

In addition of the common DNA protection groups which were mentioned before, the RNA needs additional protection on the 2'-hydroxyl position and also carefully controlled deprotection conditions. These are the existing protecting groups for solid phase RNA synthesis.

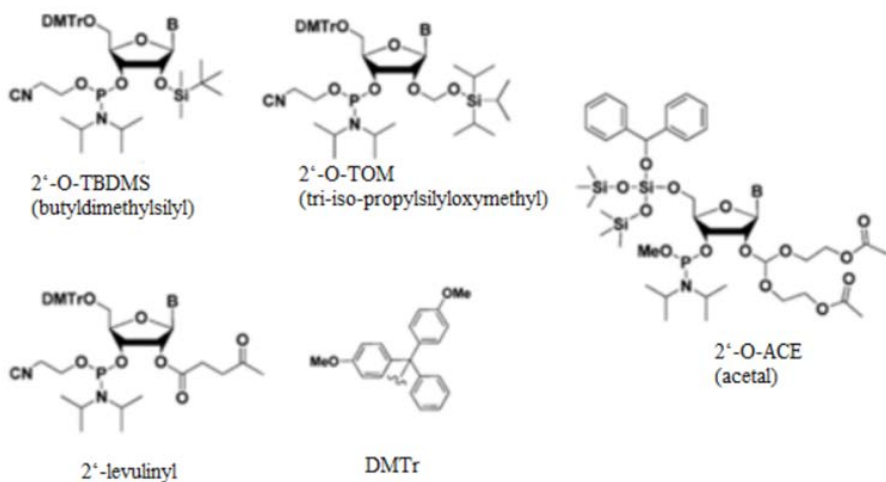


Figure 11. Protecting groups for solid phase RNA synthesis for the 2'-hydroxyl group of RNA

For solid phase synthesis a CPG solid support is usually used as a substrate. By adding a Q linker (hydroquinone-*O,O'*-diacetic acid linker) to the solid support it is possible to cleave the RNA strand by a brief fluoride treatment. (38):

### 1.6.4. Coupling efficiency

The performance of the deprotection determines the coupling efficiency of the phosphoramidite. All the protecting groups need a special treatment to achieve a complete deprotection. The coupling efficiencies of all five protecting groups were tested by Lackey et al by synthesizing on a hydroquinone-*O,O'*-diacetic acid CPG solid support a different protecting schemes is needed. To assess optimize

coupling and kinetic efficiencies for the RNA phosphoramidite, monomer coupling times were set to 1 and 10 min. The coupling efficiency of the tested sequence which includes all four bases and with all four different protecting groups was identified by HPLC analysis (Table 1).

Table 1. Comparative Study of 21-nt RNAs Synthesized from Various Chemistries<sup>a</sup>, Lackey et al, *Acetal Levulinyl Ester (ALE) Groups for 2'-Hydroxyl Protection of Ribonucleosides in the Synthesis of Oligoribonucleotides on Glass and Microarrays*, J. Am. Chem. Soc., 2009. 131(24): p. 8496-8502

2'-O-PG	found MW <sup>b</sup>	T <sub>m</sub> (°C)	10 min coupling % purity <sup>c</sup>	avg coupling yield <sup>d</sup>	1 min coupling % purity <sup>e</sup>	avg coupling yield <sup>e</sup>
TBDMS	6616.4	59.8	70.6	98.4	45.4	96.3
TOM	6616.5	60.1	67.2	98.1	32.0	94.7
ACE	6616.5	59.5	81.8 <sup>f</sup>	99.0	n.d.	n.d.
ALE	6616.2	59.4	76.2	98.7	61.8	97.7

a) Base sequence: r(GCUUGAAGUCUUAAUUA)-d(TT), b) Calculated molecular weight: 6617 g/mol, c) % yield calculated by HPLC (% area of major peak), d) Calculated from 10 min coupling time, e) Calculated from 1 min coupling time, f) Coupling time unknown.

### 1.6.5. Newly developed protecting group for light directed in situ synthesis for the 2'-hydroxyl group of RNA.

Existing fabrication strategies in the synthesis of RNA microarrays involve immobilization of a presynthesized RNA strand through enzymatic and chemical ligation steps, which can involve limitation of the complexity and versatility of the microarray. Moreover such methods can lead to degradation of the RNA as they are handled in the deprotected form. This encloses the need for deprotection methods which performs the deprotection during the synthesis.

The protecting group should also be compatible with the glass substrate and should not interfere with the NPPOC photolabile group, so this exclude fluoride labile 2'-O-protecting groups and photolabile groups as possible protecting group. Another requirement to synthesize on a glass solid surface is that 2'-OH

protecting group should not sterically interfere with the coupling reaction. 2'-acetal- and 2'-orthoester-based protecting groups could, in principle, work on a chip if the 5'- and base protecting groups could be converted to chip-compatible groups, and if the conditions required to deblock these acid (or base) labile protecting groups were adapted as to minimize the detachment of the RNA from its surface to remove the DMT group from the 5'-position of the RNA. Therefore a new protecting group was developed, the acetal levulinyl ester group. This group has two advantages in comparison with the existing levulinyl group. It cannot migrate by virtue of its acetal function and the 5'-O-DMTr 2'-O-ALE monomers (Figure 12) can be prepared in higher yields (38).

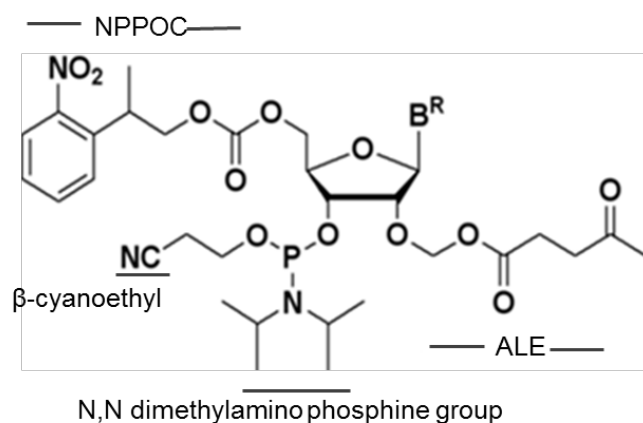


Figure 13. Acetal levulinyl ester group

### 1.6.6. Applications

RNA microarrays offer the potential to accelerate high-throughput screenings of RNA aptamers as well as to probe RNA–protein and RNA–RNA interactions of biological interest (38).

## 1.7. Motivation

DNA microarrays are a high-throughput method and enable the exploration of the expression levels of thousands of genes simultaneously. Each microarray design needs adapted conditions for the optimized synthesis. In general this includes the synthesis, deprotection, and hybridization. There are several methods to achieve an optimization of the synthesis, for example by using different protecting groups, by using different fluorescence labels, or by using a modified photochemical reaction cell.

An overview over the originally and nowadays commonly used protection groups was already given above. The commonly used NPPOC group is well established and its versatility is already proven. But the intensive research-in this area offers many newly developed modified photolabile protecting groups. The advantage of using another photolabile protecting group with a different type of intra-and intermolecular energy transfer or with a higher absorptivity would possibly decrease the synthesis time. Therefore we tested two different photolabile protecting groups and compared the efficiency of them with the NPPOC group.

Another aim of this study is to find easier ways to analyze the synthesized DNA more efficiently. After the synthesis the DNA is still attached to the substrate surface. In general the verification determination of the quality of the synthesis is achieved by a hybridization experiment, in which a complementary sequence of the quality control is hybridized to the DNA on the surface. While this can determine the quality of the synthesis itself, no statement can be made about sufficient deprotection after synthesis. The base protecting groups, and in the case of RNA the ALE group, is still attached after synthesis. They have to be removed by an additional deprotection step. To verify the sufficiency of these deprotection process such as HPLC or MS which can possibly be used for this verification although for these methods it is necessary to cleave the DNA from the surface. For solid support synthesis there is already a method developed but this method is not compatible with the in-situ synthesis of microarrays. In the cooperation with the

University of Montreal we try to develop such a method.

The photochemical cell is where the synthesis takes place and it enables exact positioning of the substrate. The optical system has to be focused onto this position. The cell is constructed in such a way that the liquid can reach the synthesis area very easily. The substrate is fixed by four screws so that the focus cannot be changed. Between the substrate and the cell there is a gasket which, in combination with the tighten screws, prevents the leaking of the cell. However, the total synthesis time and the consumption of solvents and reagents are still a significant economic constraint. So we modified the photochemical reaction cell to possibly enhance the efficiency.

There are many techniques of labelling single stranded DNA or RNA. The most common ones are cyanine dyes such as Cy3 and Cy5 as the most established representatives. They are covalently attached to the 5' end of single-stranded DNA. It is known that the intensity of the hybridizations signal is sequence dependent. It is essential to find the sequence depended pattern of a dye to understand the interaction between the dye and the sequence and further to know how this affects the hybridization signal. DY547 and DY647 are becoming widely used for nucleic acid labeling but the sequence dependence is not explored yet. For a better understanding of sequence-dye interaction and to determine the sequence dependence pattern of DY547 and DY647 we tested and compared those with the already well-established Cy3 and Cy5 dyes in a DNA Microarray experiment. The better understanding of sequence dye interaction may lead to insights into sequence-specific biophysical properties of nucleic acids, such as DNA rigidity, which affects DNA-protein interactions.

Each design of a microarray needs specific conditions whose optimization is also important for the synthesis of DNA microarrays, to ensure the quality of the synthesis. DNA microarrays offer the possibility to synthesize DNA aptamer arrays. DNA aptamers are small oligonucleotides derived by an in-vitro selection process called SELEX (Systematic Evolution of Ligands by Experimental enrichment). They are used in variety of different fields and are important

candidates for therapeutic and diagnostic applications. Their particularly suitability is justified by their high affinity and specificity for their target molecules. DNA microarrays are composed of aptamers immobilized on a solid substrate. They are providing the possibility of simultaneous scanning of over hundred thousand nucleic acid sequences with specificities and binding affinities to detect the pathogenesis of a disease on a post transcriptional level, for example. Not much was known about the optimal synthesis of oligonucleotide microarrays used in hybridization-based genomics applications. In these studies we explored the development of optimal synthesis of DNA aptamer arrays.

Gene expression experiments are the most common applications for DNA Microarrays, which can be used in variety of fields which was already mentioned before. But especially the interaction between nutrients and their effects on the gene expression is not fully explored but constantly present. The overgrowth of adipose tissue is associated with overweight, obesity and subsequent diseases like diabetes type II, chronic inflammation, dementia, and macrovascular diseases. Capsaicin (CAP), the most abundant capsaicinoid in red pepper, has also an effect on adipose which is already proved in 3T3-L1 cells. In cooperation with the Nutrition Department of the University of Vienna we investigate whether a less pungent structural analog of CAP, nonivamide (NV), has similar effects on lipid accumulation in 3T3-L1 cells and whether TRPV1 receptor activation and miRNA regulation is involved in the underlying pathways. The influence of miRNA regulation was tested in a gene expression experiment by using light directed in situ microarray technology. In these experiments all possible mouse miRNAs are included on one array to enable a high-throughput screening on miRNA level.

## 1.8. List of Publications

1) “Simultaneous Light-Directed Synthesis of Mirror-Image Microarrays in a Photochemical Reaction Cell with Flare Suppression” M. Sack, N. Kretschy, B. Rohm, V. Somoza, M. M.Somoza (2013) *Analytical Chemistry* 85(18), 8513-851; <http://dx.doi.org/10.1021/ac4024318>

**Published, contribution: preparation of the microarrays substrate and synthesis of the microarrays**

2) “Optimized Light-Directed Synthesis of Aptamer Microarrays” N.L.W. Franssen-van Hal, P. vander Putte, K. Hellmuth, S. Matysiak, N. Kretschy, M. M. Somoza (2013) *Analytical Chemistry* 85(12), 5950–5957; <http://dx.doi.org/10.1021/ac400746j>

**Published, contribution: synthesis of the microarrays**

3) “Comparison of the Sequence-Dependent Fluorescence of the Cyanine Dyes Cy3, Cy5, DyLight DY547 and DyLight DY647 on Single-Stranded DNA” N. Kretschy and M. M. Somoza (2014) *PLoS ONE* 9(1): e85605; <http://dx.doi.org/10.1371/journal.pone.0085605>

**Published, contribution: microarray design and synthesis, data analysis, preparing the paper**

4) “Base-cleavable microarrays for the characterization of DNA and RNA oligonucleo-tides synthesized in situ by photolithography” Jory Lietard, Nicole Kretschy, Matej Sack, Alexander S. Wahba, Mark M. Somoza Masad J. Damha (2014) *Chemical Communications*, 50, 12903-12906; <http://dx.doi.org/10.1371/10.1039/C4CC05771F>

**Published, contribution: microarray design and synthesis**



5) “Nonivamide enhances miRNA let-7d expression and decreases adipogenesis PPAR $\gamma$  expression in 3T3-L1 cells” Rohm B, Holik AK, Kretschy N, Somoza MM, Ley JP, Widder S, Krammer GE, Marko D, Somoza V. (2015). Journal of Cellular Biochemistry; <http://dx.doi.org/10.1002/jcb.25052>

**Published, contribution: synthesis of the microarrays**

6) “Next-Generation o-Nitrobenzyl Photolabile Groups for Light-Directed Chemistry and Microarrays” Nicole Kretschy, Ann-Katrin Holik, Veronika Somoza, Klaus-Peter Stengele and Mark M. Somoza (2015) Angewandte Chemie International Edition; <http://dx.doi.org/10.1002/anie.201502125>

**Published, contribution: microarray design and synthesis, data analysis, preparing the paper**

Attended conferences:

“Advances in Microarray Technology” March 10-11, 2014

“Aptamers in Medicine and Perspectives”, October 4-5, 2013

## **1.9. Publications**

# Next-Generation *o*-Nitrobenzyl Photolabile Groups for Light-Directed Chemistry and Microarrays\*\*

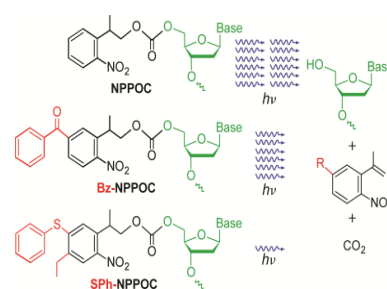
Nicole Kretschy, Ann-Katrin Holik, Veronika Somoza, Klaus-Peter Stengele and Mark M. Somoza\*

**Abstract:** Light as an external trigger is a valuable and easily controllable tool for directing chemical reactions with high spatial and temporal accuracy. Two *o*-nitrobenzyl derivatives, benzoyl- and thiophenol-NPPOC offer significantly improved photo-deprotection efficiency over the commonly used NPPOC group. The two- and twelve-fold increase in photodeprotection efficiency was proven using photolithograph synthesis of microarrays.

Photolabile groups are widely used in chemical synthesis to extend available blocking strategies into a further orthogonal direction,<sup>[1]</sup> for photo-polymerization, cross-linking and functionalization in polymer chemistry,<sup>[2]</sup> for 3D patterning and fabrication,<sup>[3]</sup> and for the creation of biologically-inactivated (caged) molecules that can be activated by light after they are introduced into cells.<sup>[4]</sup> The most commonly used photolabile groups are *o*-nitrobenzyl derivatives; these have proved to be highly versatile, and are used to protect a wide variety of functional groups.<sup>[5]</sup> In contrast to chemically cleavable protecting groups, photolabile groups permit high resolution spatial control of reactions when optical imaging systems deliver the light. Spatial control has proven to be particularly useful for the combinatorial synthesis of biopolymer microarrays. This approach, adopted for the industrial-scale synthesis of microarrays, can produce arrays with  $>10^6$  unique sequences per square centimeter.<sup>[6]</sup> Photolithographic synthesis was first applied to peptide microarrays<sup>[7]</sup> using amino acids with the nitroveratryloxycarbonyl (NVOC) N-terminus protecting group, and then to DNA microarrays using 5'-( $\alpha$ -methyl-2-nitropiperonyl)oxycarbonyl (MeNPOC)<sup>[8]</sup> and dimethoxybenzoin-carbonate (DMBOC)<sup>[9]</sup> phosphoramidites, but the relatively low stepwise yield obtained with these groups limits their use to microarrays of short oligomers.<sup>[10]</sup> The development of the 2-(2-nitrophenyl)-propoxycarbonyl (NPPOC) group, with essentially quantitative yield and significantly higher photolysis quantum yield permitted the manufacture of microarrays of long oligonucleotides.<sup>[11]</sup> High photolytic efficiency, the product of the

absorption coefficient and the photolysis quantum yield ( $\epsilon \cdot \phi$ ), is important in most applications of photolabile groups, not just because of higher yield and increased experimental throughput, but because minimizing irradiation proportionately reduces the risk of photochemical side reactions. The efficiency of the NPPOC group has resulted in its widespread use, not only for genomic DNA microarray synthesis, but also for aptamer,<sup>[12]</sup> gene assembly,<sup>[13]</sup> RNA<sup>[14]</sup> and peptide microarray synthesis,<sup>[15]</sup> carbohydrate chemistry,<sup>[16]</sup> cleavable linkers,<sup>[17]</sup> and caging.<sup>[18]</sup> The photolysis quantum yield of NPPOC is relatively high (0.41 in MeOH), but the low absorptivity ( $\epsilon_{365\text{nm}/\text{MeOH}} \approx 230 \text{ M}^{-1}\text{cm}^{-1}$ ) has led to both the search for derivatives with higher absorptivity<sup>[19]</sup> and the development of photosensitization techniques based on intra- and intermolecular energy transfer from a triplet sensitizer.<sup>[20]</sup> For the most part, however, these derivatives and sensitizers have not proved to be robust replacements for NPPOC in the synthesis of complex microarrays of long oligomers.

Here we evaluate two NPPOC derivatives with greatly improved photolytic efficiencies in the synthesis of microarrays. The two derivatives, benzoyl-2-(2-nitrophenyl)-propoxycarbonyl (Bz-NPPOC) and thiophenol-2-(2-nitrophenyl)-propoxycarbonyl (SPh-NPPOC) (Scheme 1), used as 5'-hydroxyl protecting groups on DNA phosphoramidites, were tested to determine whether they can be used as effective replacements for NPPOC. We will show that microarrays synthesized with these groups are equivalent or better than those synthesized with NPPOC, yet require far less light for photolysis. In the case of photolithographic synthesis, reduced light requirement is a major advantage due to the low numerical aperture (NA) of the optical systems. Low NA is needed to generate sufficiently large depth-of-focus and to reduce synthesis errors due to scattered light, but greatly reduces the amount of usable light that can be obtained from any given source.<sup>[21]</sup>



**Scheme 1.** a) Structures and photocleavage products of 5'-OH NPPOC, Bz-NPPOC and SPh-NPPOC DNA phosphoramidites.

The NPPOC, Bz- and SPh-NPPOC DNA phosphoramidites were evaluated using Maskless Array Synthesis (MAS).<sup>[21-22]</sup> MAS is a proven photolithographic approach for *in situ* synthesis of high-density DNA microarrays for genomics applications, but now also used for the synthesis of arrays of RNA, peptides and carbohydrates. MAS uses an array of digitally-controlled micromirrors to direct light from a Hg lamp to the microarray

[\*] N. Kretschy<sup>[1]</sup>, Prof. M. M. Somoza  
Institute of Inorganic Chemistry, Faculty of Chemistry, University of Vienna, Althanstraße 14 (UZA II), 1090 Vienna (Austria)  
E-mail: mark.somoza@univie.ac.at  
A.-K. Holik<sup>[2]</sup>, Prof. V. Somoza  
Department of Nutritional and Physiological Chemistry, Faculty of Chemistry, Althanstraße 14, 1090 Vienna (Austria)  
Prof. V. Somoza  
Christian Doppler Laboratory for Bioactive Aroma Compounds, University of Vienna, Althanstraße 14, 1090 Vienna (Austria)  
Dr. K.-P. Stengele  
Roche Diagnostics, Nonnenwald 2, 82377 Penzberg (Germany)

[+] These authors contributed equally to this work.

[\*\*] Funding by the University of Vienna, the Faculty of Chemistry of the University of Vienna, the Austrian Science Fund (Grant FWF P23797), the Austrian Federal Ministry of Economy, Family and Youth, and the Austrian National Foundation for Research, Technology and Development is gratefully acknowledged.

Supporting information for this article is available on the WWW under <http://dx.doi.org/10.1002/anie>.

synthesis surface. Light exposure is synchronized with chemical delivery to allow the synthesis of high-complexity microarrays (detailed methods in the Supporting Information).

Figure 1 shows the absorption spectra of the NPPOC-, Bz- and SPh-NPPOC 5'-OH-protected thymidine phosphoramidites, along with the 365, 405 and 436 nm lines from the Hg lamp. The absorbance from NPPOC and Bz-NPPOC are very similar in the relevant spectral region near 365nm, so that the increased photolytic efficiency of Bz-NPPOC is due to increased quantum yield of photolysis. SPh-NPPOC absorption is seven times higher at 365nm, and is significant until about 420 nm, but the spectral overlap with the 365nm line still accounts for >87% of the total (Supporting Information). The 436 nm line is present, but does not contribute; the remaining spectrum is filtered out to prevent DNA damage and heating.

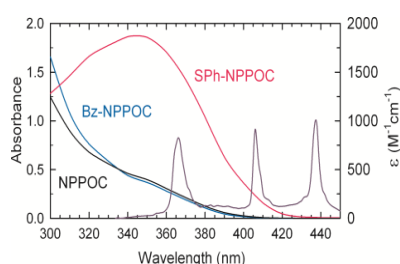


**Figure 1.** Absorption/extinction coefficient spectra of the phosphoramidites in DMSO, along with the high pressure Hg lines at 365, 405 and 436 nm, as measured at the reaction site.

The light exposure necessary to remove the NPPOC, Bz- and SPh-NPPOC protecting groups was determined by creating microarrays with oligonucleotides sharing a common sequence but synthesized using a gradient of light exposures. These arrays were then hybridized with the fluorescently-labeled complementary sequence and scanned. As the exposure increases, the sequence fidelity increases until the full hybridization signal is reached. Microarray synthesis using exposure gradients, followed by hybridization, is a highly sensitive test of photolysis efficiency since the value of each data point is determined by many consecutive photocleavage reactions, all of which need to be successful in order to generate a strong signal. Figure 2 shows the exposure gradients for the three photolabile groups when used to synthesize mixed-base 25 and 60mers. The radiant exposure values for Bz- and SPh-NPPOC were scaled by  $\times 2.1$  and  $\times 12.0$ , respectively, to overlap with the NPPOC data. The precise overlap between the curves indicates that the photolysis kinetics are equivalent but faster for Bz-NPPOC and far faster for SPh-NPPOC.

Although the photolysis is very fast for Bz- and SPh-NPPOC, the overall yield is also highly relevant. To allow an accurate comparison with NPPOC, a microarray was designed containing oligonucleotides sharing a common sequence but synthesized with two chemistries, NPPOC as a reference, and either Bz- or SPh-NPPOC.

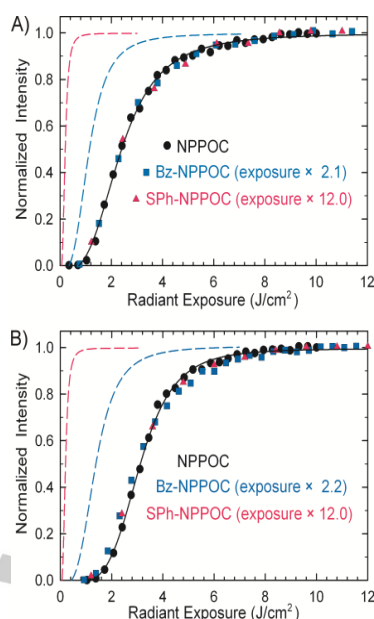


**Figure 2.** Hybridization intensities for A) 60mer and B) 25mer arrays synthesized with an exposure gradient using NPPOC (black circles), Bz-NPPOC (blue squares) and SPh-NPPOC (red triangles). Radiant exposure values for Bz- and SPh-NPPOC are multiplied by 2.1 (2.2) and 12.0, respectively, with original data positions indicated by dashed lines.

The NPPOC-based oligomer synthesis used  $6 \text{ J/cm}^2$  exposures and was compared, on the bases of hybridization intensity, with Bz- or SPh-NPPOC oligomers synthesized using the proportionally lower exposures based on Figure 2, 2.7 and  $0.5 \text{ J/cm}^2$ , respectively. Since NPPOC deprotection proceeds via a photoinduced  $\beta$ -elimination pathway favored by a small concentration of an amine base,<sup>[19b, 23]</sup> the rate of proton abstraction could be limiting under fast deprotection conditions. This might favor longer reactions performed with lower radiant power or the use of higher concentrations of the base in the exposure solvent (imidazole in DMSO). Relative to NPPOC, synthesis with Bz- or SPh-NPPOC results in equal or better hybridization signal under all tested conditions (Figure 3). Lower radiant power resulted in a modest improvement in hybridization intensity, but increased concentration of imidazole in the exposure solvent does not. A higher imidazole concentration does appear to improve signal homogeneity.

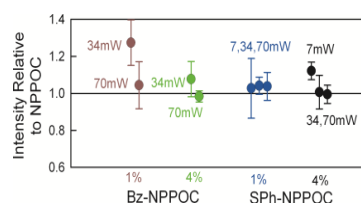


**Figure 3.** Hybridization intensity (relative to NPPOC) of Bz- and SPh-NPPOC for several values of exposure radiant power ( $\text{mW/cm}^2$ ) and for photocleavage reactions carried out in either 1% or 4% imidazole in DMSO ( $w/v$ ) as the exposure solvent. The error bars, the standard deviation of on-array replicates, is used as a measure of synthesis homogeneity.

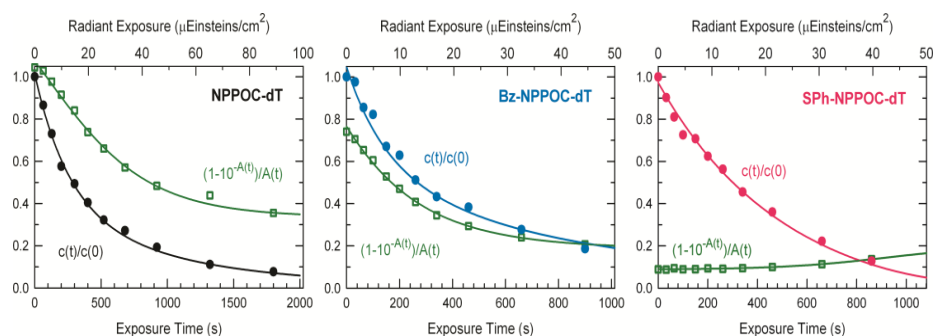


**Figure 4.** Kinetics of the NPPOC-, Bz- and SPh-NPPOC-protected thymidine photolysis with 365nm light. Irradiance was 16.2 mW/cm<sup>2</sup> for NPPOC and Bz-NPPOC, and 15.0 mW/cm<sup>2</sup> for SPh-NPPOC. The  $c(t)/c(0)$  data were fitted according to Equation 1 and numerical integration of the photokinetic factor fit.

The exposure gradients experiments, along with the measured extinction coefficients, provide accurate values for the relative quantum yield of photolysis. The absolute yields were determined by irradiating them in solution and quantifying the compounds and their photoproducts by HPLC. The photokinetic rate law for the concentration  $c$  of the starting compound is given by Equation (1):<sup>[24]</sup>

$$(1) \quad \dot{c} = -1000I_0 \frac{Fd}{V} \frac{1-10^{-A(t)}}{A(t)} \varepsilon \varphi c$$

Where  $I_0$  is the irradiance,  $F$ ,  $d$  and  $V$  are the exposure cross section, path length and sample volume, respectively, and  $A(t)$  is the total absorbance of the sample. Figure 4 shows the decomposition kinetics and photokinetic factors,  $(1-10^{-A(t)})/A(t)$ . The quantum yields  $\varphi$  were obtained by numerical integration of the photokinetic factor. Table 1 summarizes the results, which are highly consistent with the microarray data, with  $\varepsilon \cdot \varphi$  for Bz-NPPOC double that of NPPOC. For SPh-NPPOC the 10-fold value relative to NPPOC is lower than the 12-fold value obtained in the array experiments due to the contribution of the 405 nm Hg line in array synthesis.

**Table 1.** Extinction, quantum yield and photolytic efficiency for the compounds<sup>[a]</sup>.

Compound	$\varepsilon_{365\text{nm}}$ [ $\text{M}^{-1}\text{cm}^{-1}$ ]	$\varphi_{365\text{nm}}$	$\varepsilon \cdot \varphi_{365\text{nm}}$ [ $\text{M}^{-1}\text{cm}^{-1}$ ]
NPPOC	260	0.40	104
Bz-NPPOC	240	0.84	202
SPh-NPPOC	1560	0.68	1064

[a] Molar absorptivity  $\varepsilon$ , photolysis quantum yield  $\varphi$ , photolytic efficiency  $\varepsilon \cdot \varphi$ , all at 365 nm.

To test the potential of these groups under conditions representative of one of the most demanding applications of photolabile groups, high-density gene expression microarrays were synthesized using 5'-NPPOC-, Bz- and SPh-NPPOC phosphoramidites. The design included two replicates of each of at least three unique 60mer probes for each of >45000 human genes, as well as 20 to 100 replicates of quality control and reference sequences, a total of 382536 oligonucleotides. The arrays were tested by hybridization with labeled cDNA produced from a human colon adenocarcinoma cell line (Caco-2). Each of the three chemistries resulted in high-quality microarrays with similar quality assessment metrics results (Supporting

Information). Figure 5 shows details of the images, along with the corresponding  $\log_2$  scatter plots of control vs. treated samples of RMA normalized data.<sup>[25]</sup>

In summary, two highly light-sensitive groups for light-triggered deprotection and spatio-selective synthesis, benzoyl- and thiophenol-NPPOC, have been shown to be superior replacements for NPPOC, one of the most commonly used photolabile groups in chemistry. The 2-fold and 12-fold increase in photodeprotection efficiency for Bz- and SPh-NPPOC, respectively, significantly reduces the production time for photolithographic microarrays and should prove to be a useful replacement for NPPOC and other photolabile groups in many caging, synthetic and triggering applications.

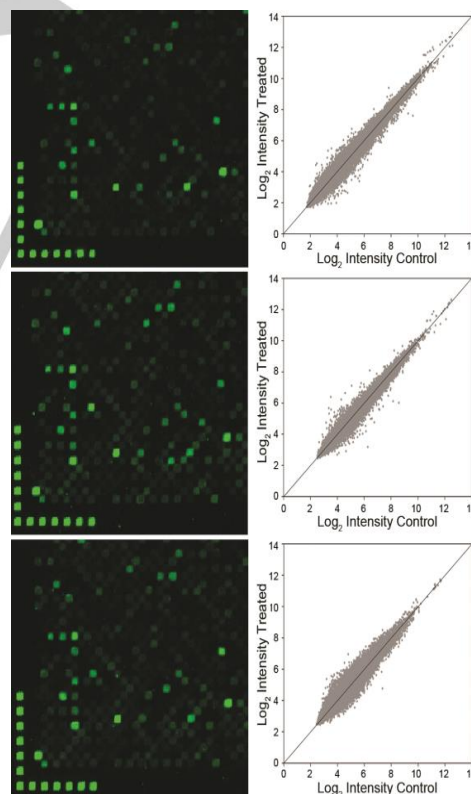


**Figure 5.** Left column: Details of 2.5  $\mu\text{m}$  resolution scan images from gene expression microarrays synthesized with (top to bottom) NPPOC, Bz-NPPOC and SPh-NPPOC and hybridized with Cy3-labeled cDNA. The size of each square-shaped feature is 14 $\times$ 14  $\mu\text{m}$ . Right column: Scatterplots the RMA-processed expression data from the gene expression microarrays synthesized with (top to bottom) NPPOC, Bz- and SPh-NPPOC.

**Keywords:** Photolysis • Photochemistry • Bz-NPPOC • SPh-NPPOC • NPPOC

- [1] a) M. Schelhaas, H. Waldmann, *Angew. Chem., Int. Ed.* 1996, 35, 2056; b) M. Schelhaas, H. Waldmann, *Angew. Chem.* 1996, 108, 2192.
- [2] H. Zhao, E. S. Sterner, E. B. Coughlin, P. Theato, *Macromolecules* 2012, 45, 1723.
- [3] a) J. E. Poelma, B. P. Fors, G. F. Meyers, J. W. Kramer, C. J. Hawker, *Angew. Chem., Int. Ed.* 2013, 52, 6844; b) J. E. Poelma, B. P. Fors, G. F. Meyers, J. W. Kramer, C. J. Hawker, *Angew. Chem.* 2013, 125, 6982.
- [4] a) C. Brieke, F. Rohrbach, A. Gottschalk, G. Mayer, A. Heckel, *Angew. Chem., Int. Ed.* 2012, 51, 8446; b) C. Brieke, F. Rohrbach, A. Gottschalk, G. Mayer, A. Heckel, *Angew. Chem.* 2012, 124, 8572; c) J. Hoffmann, U. Kazmaier, *Angew. Chem., Int. Ed.* 2014, 53, 11356; d) J. Hoffmann, U. Kazmaier, *Angew. Chem.* 2014, 126, 11538.
- [5] P. Klán, T. Šolomek, C. G. Bochet, A. Blanc, R. Givens, M. Rubina, V. Popik, A. Kostikov, *J. Wirz, Chem. Rev.* 2012, 113, 119.
- [6] S. Buus, J. Rockberg, B. Forsström, P. Nilsson, M. Uhlen, C. Schafer-Nielsen, *Mol. Cell. Proteomics* 2012, 11, 1790.
- [7] S. Fodor, J. Read, M. Pirrung, L. Stryer, A. Lu, D. Solas, *Science* 1991, 251, 767.
- [8] M. C. Pirrung, J.-C. Bradley, *J. Org. Chem.* 1995, 60, 6270.
- [9] M. C. Pirrung, L. Fallon, G. McGall, *J. Org. Chem.* 1998, 63, 241.
- [10] G. H. McGall, A. D. Barone, M. Diggelmann, S. P. A. Fodor, E. Gentalen, N. Ngo, *J. Am. Chem. Soc.* 1997, 119, 5081.
- [11] a) M. Beier, J. D. Hoheisel, *Nucleic Acids Res.* 2000, 28, e11; b) M. C. Pirrung, L. Wang, M. P. Montague-Smith, *Org. Lett.* 2001, 3, 1105.
- [12] N. L. W. Franssen-van Hal, P. van der Putte, K. Hellmuth, S. Matysiak, N. Kretschy, M. M. Somoza, *Anal. Chem.* 2013, 85, 5950.
- [13] a) C.-H. Wu, M. R. Lockett, L. M. Smith, *Angew. Chem., Int. Ed.* 2012, 51, 4628; b) C.-H. Wu, M. R. Lockett, L. M. Smith, *Angew. Chem.* 2012, 124, 4706.
- [14] a) J. G. Lackey, D. Mitra, M. M. Somoza, F. Cerrina, M. J. Damha, *J. Am. Chem. Soc.* 2009, 131, 8496; b) C.-H. Wu, M. T. Holden, L. M. Smith, *Angew. Chem., Int. Ed.* 2014, 53, 13514; c) C.-H. Wu, M. T. Holden, L. M. Smith, *Angew. Chem.* 2014, 126, 13732.
- [15] a) K. R. Bhushan, C. DeLisi, R. A. Laursen, *Tetrahedron Lett.* 2003, 44, 8585; b) B. Forsström, B. B. Axnäs, K.-P. Stengele, J. Bühler, T. J. Albert, T. A. Richmond, F. J. Hu, P. Nilsson, E. P. Hudson, J. Rockberg, M. Uhlen, *Mol. Cell. Proteomics* 2014, 13, 1585; c) L. B. Hansen, S. Buus, C. Schafer-Nielsen, *PLoS ONE* 2013, 8, e68902.
- [16] H. Yi, S. Maisonneuve, J. Xie, *Org. Biomol. Chem.* 2009, 7, 3847.
- [17] a) R. Johnsson, J. G. Lackey, J. J. Bogojeski, M. J. Damha, *Bioorg. Med. Chem. Lett.* 2011, 21, 3721; b) J. Lietard, M. R. Hassler, J. Fakhoury, M. J. Damha, *Chem. Commun.* 2014, 50, 15063; c) J. Olejnik, S. Sonar, E. Krzymańska-Olejnik, K. J. Rothschild, *Proc. Natl. Acad. Sci. U. S. A.* 1995, 92, 7590; d) R. Rodebaugh, B. Fraser-Reid, H. Mario Geysen, *Tetrahedron Lett.* 1997, 38, 7653.
- [18] W. Xi, M. Krieger, C. J. Kloxin, C. N. Bowman, *Chem. Commun.* 2013, 49, 4504.
- [19] a) S. Bühler, I. Lagoja, H. Giegrich, K.-P. Stengele, W. Pfeleiderer, *Helv. Chim. Acta* 2004, 87, 620; b) A. Hasan, K.-P. Stengele, H. Giegrich, P. Cornwell, K. R. Isham, R. A. Sachleben, W. Pfeleiderer, R. S. Foote, *Tetrahedron* 1997, 53, 4247; c) K.-P. Stengele, J. Bühler, S. Bühler, E. Kvassiouk, R. Green, T. Prykota, W. Pfeleiderer, *Nucleosides, Nucleotides Nucleic Acids* 2005, 24, 891.
- [20] a) D. Wöll, J. Smirnova, M. Galetskaya, T. Prykota, J. Bühler, K.-P. Stengele, W. Pfeleiderer, U. E. Steiner, *Chem. Eur. J.* 2008, 14, 6490; b) D. Wöll, J. Smirnova, W. Pfeleiderer, U. E. Steiner, *Angew. Chem., Int. Ed.* 2006, 45, 2975; c) D. Wöll, S. Walbert, K.-P. Stengele, T. J. Albert, T. Richmond, J. Norton, M. Singer, R. D. Green, W. Pfeleiderer, U. E. Steiner, *Helv. Chim. Acta.* 2004, 87, 28.
- [21] C. Agbavwe, C. Kim, D. Hong, K. Heinrich, T. Wang, M. M. Somoza, *J. Nanobiotechnol.* 2011, 9.
- [22] a) S. Singh-Gasson, R. Green, Y. Yue, C. Nelson, F. Blattner, M. Sussman, F. Cerrina, *Nat. Biotechnol.* 1999, 17, 974 ; b) M. Sack, N. Kretschy, B. Rohm, V. Somoza, M. M. Somoza, *Anal. Chem.* 2013, 85, 8513.
- [23] H. Giegrich, S. Eisele-Bühler, C. Hermann, E. Kvasnyuk, R. Charubala, W. Pfeleiderer, *Nucleosides Nucleotides* 1998, 17, 1987.
- [24] H. Mauser, G. Gauglitz, *Photokinetics: Theoretical Fundamentals and Applications*, Elsevier Science, 1998.
- [25] R. A. Irizarry, B. Hobbs, F. Collin, Y. D. Beazer-Barclay, K. J. Antonellis, U. Scherf, T. P. Speed, *Biostatistics* 2003, 4, 249.



## Entry for the Table of Contents

## COMMUNICATION

**High-speed photolysis: Bz-NPPOC and SPh-NPPOC are two highly light-sensitive groups for photodeprotection and spatio-selective synthesis.**



*Nicole Kretschy, Ann-Katrin Holik, Veronika Somoza, Klaus-Peter Stengele and Mark M. Somoza\**

**Page No. – Page No.**

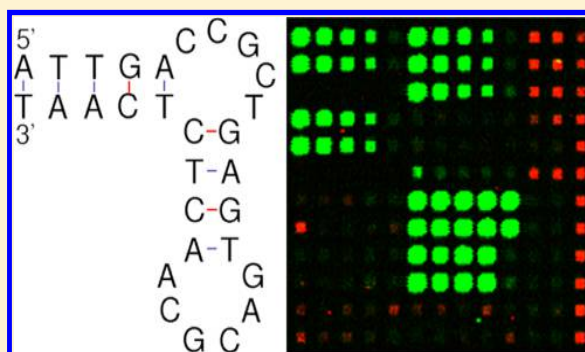
**Next-Generation *o*-Nitrobenzyl Photolabile Groups for Light-Directed Chemistry and Microarrays**

## Optimized Light-Directed Synthesis of Aptamer Microarrays

Nicole L. W. Franssen-van Hal,<sup>†</sup> Pepijn van der Putte,<sup>†</sup> Klaus Hellmuth,<sup>†</sup> Stefan Matysiak,<sup>†</sup> Nicole Kretschy,<sup>‡</sup> and Mark M. Somoza<sup>‡,\*</sup><sup>†</sup>FlexGen, J.H. Oortweg 21, 2333CH Leiden, The Netherlands<sup>‡</sup>Institute of Inorganic Chemistry, University of Vienna, Währinger Strasse 42, A-1090 Vienna, Austria

## Supporting Information

**ABSTRACT:** Aptamer microarrays are a promising high-throughput method for ultrasensitive detection of multiple analytes, but although much is known about the optimal synthesis of oligonucleotide microarrays used in hybridization-based genomics applications, the bioaffinity interactions between aptamers and their targets is qualitatively different and requires significant changes to synthesis parameters. Focusing on streptavidin-binding DNA aptamers, we employed light-directed in situ synthesis of microarrays to analyze the effects of sequence fidelity, linker length, surface probe density, and substrate functionalization on detection sensitivity. Direct comparison with oligonucleotide hybridization experiments indicates that aptamer microarrays are significantly more sensitive to sequence fidelity and substrate functionalization and have different optimal linker length and surface probe density requirements. Whereas microarray hybridization probes generate maximum signal with multiple deletions, aptamer sequences with the same deletion rate result in a 3-fold binding signal reduction compared with the same sequences synthesized for maximized sequence fidelity. The highest hybridization signal was obtained with dT 5mer linkers, and the highest aptamer signal was obtained with dT 11mers, with shorter aptamer linkers significantly reducing the binding signal. The probe hybridization signal was found to be more sensitive to molecular crowding, whereas the aptamer probe signal does not appear to be constrained within the density of functional surface groups commonly used to synthesize microarrays.



Sensitive and accurate multiplexed protein measurements are fundamental for modern biomedical research and clinical practice. Immunoassays exploiting the diversity and specificity of antibody–antigen binding are the most commonly used and widely accepted methods for both single and multiplexed measurements.<sup>1</sup> In recent years, however, aptamers—single-stranded nucleic acids generated by in vitro selection from combinatorial libraries to bind to specific target molecules (SELEX<sup>2–4</sup>)—are providing an alternative path to sensitive protein analysis. Perhaps one of the principal appeals of aptamer-based technology is that it leverages highly developed and versatile chemical synthesis of nucleic acids with in vitro selection to provide a purely chemical development pathway. The tool palette for aptamer synthesis includes not only natural DNA and RNA nucleoside monophosphates, but also non-natural building blocks with modifications at the 2' position, such as 2'-O-methyl, 2'-fluoro-, and 2'-F-ANA;<sup>5–8</sup> more profound sugar modifications, such as locked nucleic acid (LNA) and hexitol nucleic acid (HNA);<sup>9–11</sup> or backbone modifications, such as phosphorodithioate linkages.<sup>12,13</sup> The versatility of phosphoramidite chemistry also extends to the facile synthesis of complex microarrays, traditionally for genomics applications, but readily adaptable to arrays of aptamers, both for aptamer optimization<sup>14,15</sup> and for aptamer-based multiplexed protein detection.<sup>16–18</sup> The widespread use

of oligonucleotide microarrays for high-throughput gene expression studies, as well as other hybridization-based genomics applications, provides the analytical, technological, and manufacturing infrastructure for the development of aptamer microarrays. Aptamer microarrays consist of aptamers immobilized on a solid substrate. Aptamer arrays are promising analytical tools because in vitro selection provides nucleic acid sequences with specificities and binding affinities comparable to those of monoclonal antibodies;<sup>19–21</sup> however, they are more stable<sup>22</sup> as well as easier to synthesize than antibody arrays because of the mature solid-phase oligonucleotide synthesis and spotting technology, and in situ synthesis of oligonucleotide microarrays using phosphoramidite chemistry.<sup>23–27</sup>

At the simplest level, oligonucleotide microarrays consist only of sequences of ~25–60 nucleotides long immobilized on a substrate in a defined pattern. However, in the case of traditional hybridization-based microarray experiments, much effort has been devoted to understanding and optimizing technical parameters influencing aspects such as hybridization kinetics, efficiency, and signal intensity/noise ratio to maximize

Received: March 12, 2013

Accepted: May 14, 2013

Published: May 14, 2013

their analytical power. Clearly, for both aptamer arrays and hybridization-based arrays, sequence design is the most important consideration, but here, we consider the impact of synthesis parameters that also significantly affect microarray performance: microarray surface chemistry, oligonucleotide surface density, sequence fidelity, and surface-to-probe spacer length. We investigate the effect of these parameters on aptamer signal intensity and make direct comparisons with how the same parameters affect signal intensity in analogous hybridization experiments to gain insight into how to best adapt existing oligonucleotide microarray technology for aptamer-based bioaffinity applications.

Surface chemistry is used to modify the glass substrate to enable DNA attachment and, therefore, also determines the surface density of bound probes.<sup>28,29</sup> Surface density strongly influences hybridization intensity and signal due to steric factors.<sup>30</sup> In addition, the surface functionalization serves as a spacer, distancing the probes from the glass surface, which is known to increase hybridization efficiency.<sup>28,31,32</sup> In addition, the surface functionalization changes surface electrostatics and hydrophobicity, which in turn influence hybridization and background intensity.<sup>33–35</sup> Although the surface functionalization also serves as a spacer, additional distance between the surface and the array oligonucleotides can be introduced via specialized linker phosphoramidites or by oligonucleotide sequences, typically poly(dT).<sup>25,36–38</sup> Finally, oligonucleotide sequence fidelity also plays a role in both hybridization and protein binding to aptamers. The relationship between the number and position of mismatches in the case of hybridization on microarrays is fairly predictable,<sup>39,40</sup> but less so in the case of aptamers, in which the effect of mutations is highly variable.<sup>14</sup>

## EXPERIMENTAL SECTION

**Microarray Synthesis.** DNA/aptamer microarrays were fabricated using maskless array synthesis (MAS) as described previously.<sup>27,41</sup> Briefly, microarray substrates were used as received from the manufacturer, with the exception of the hydroxyl-functionalized substrates, which were Schott Nexterion Glass D slides functionalized with *N*-(3-triethoxysilylpropyl)-4-hydroxybutyramide (Gelest SIT8189.5). These slides were loaded into a metal staining rack and completely covered with a 500 mL solution consisting of 10 mg of the silane in 95:5 (v/v) ethanol/water and 1 mL of acetic acid. The slides were covered and gently agitated for 4 h and then rinsed twice for 20 min with gentle agitation in the same solution, but without the silane. The slides were then drained and cured overnight in a preheated vacuum oven (120 °C). The slides were stored in a desiccator cabinet until use.

Microarrays were synthesized directly on the slides using a maskless array synthesizer, which consists of an optical imaging system that uses a digital micromirror device to deliver patterned ultraviolet light near 365 nm to the synthesis surface. Microarray layout and oligonucleotide sequences are determined by selective removal of the 2-(2-nitrophenyl)propyloxycarbonyl (NPPOC) photocleavable 5'-hydroxyl protecting group on the oligonucleotides. Reagent delivery and light exposures are synchronized and controlled by a computer, which also stores and orders the display on the micromirror array. The chemistry is similar to that used in conventional solid-phase oligonucleotide synthesis. The primary modification is the use of NPPOC phosphoramidites. Upon absorption of a photon near 365 nm and in the presence of a weak organic base, 1% (m/v) imidazole in DMSO, the

NPPOC group comes off, leaving a 5'-hydroxyl terminus that is able to react with an activated phosphoramidite during the next synthetic cycle. After synthesis, the microarrays were deprotected in 1:1 (v/v) ethylenediamine in ethanol for 2 h at room temperature, washed twice with water, and stored dry until use.

**Microarray Linker-Length and Exposure-Gradient Experiments.** The effect of spacer length and hybridization and aptamer binding were determined on microarrays synthesized with spots with stepwise increases in thymidine (dT) linker length ("linker gradients") followed by either the St-2-1 streptavidin binding aptamer sequence<sup>42</sup> or a sequence (QC25) of similar length and known to hybridize well (hybridization probes and aptamer sequences are given in Table 1). The effect of sequence fidelity on hybridization and aptamer binding were determined with microarrays synthesized with a light-exposure gradient. Spots synthesized with lower light exposure are insufficiently deprotected and therefore have deletion errors. These arrays were synthesized with a fixed-

**Table 1. Streptavidin Binding Aptamer Sequence St-2-1 and Mutant Sequences Derived from St-2-1, along with the Sequences Used in the Hybridization Experiments<sup>a</sup>**

name	sequence	length	affinity (%)
St-2-1	ATT GAC CGC TGT GTG ACG CAA CAC TCA AT	29	85 ± 3
St-2-A	GCT ATT GAC CGC TGT GTG ACG CAA CAC TCA ATA GC	35	86 ± 3
St-2-T-1	TTG ACC GCT GTG TGA CGC AAC ACT CAA	27	73 ± 6
St-2-T-2	TGA CCG CTG TGT GAC GCA ACA CTC A	25	25 ± 7
St-2-T-3	GAC CGC TGT GTG ACG CAA CAC TC	23	23 ± 5
St-2-R-1	ATT GAC GCG TGT GAC GCA ACA CTC AAT	27	60 ± 4
St-2-R-2	TAT TGA GTG TGA CGC AAC ACT CAA TA	26	13 ± 7
St-2-M-1	ATT GAC CTC TGT GTG ACG CAA CAC TCA AT	29	21 ± 5
St-2-M-2	ATT GAC CGC TGT GTG ACT CAA CAC TCA AT	29	11 ± 8
St-2-M-3	ATT GAC CGC TGT GTA ACG CAA CAC TCA AT	29	12 ± 3
St-2-1_rev	TAA CTC ACA ACG CAG TGT GTC GCC AGT TA	29	
QC1	CTG TTC TGC ATC CTG CCT TTA CAT T	25	
QC3	GTT TGA GAC CAG TCT GAC CAA CAT G	25	
QC6	TCT ACT ATC CCT AAG CCC ATT TCT C	25	
QC8	GTT GTC ACA CAT ACA CTG CTC GAA A	25	
QC11	CGG GCG GTC TCA ATC AAG CAT GGA TTA CGG TGT TTA CTC TGT CCT GCG GT	50	
QC13	AGA GGA TGA CAA GGA CAC AAT CGT GCT CCC ATC TGT ATT CTT TAC GAA CT	50	
QC25	GTC ATC ATC ATG AAC CAC CCT GGT C	25	

<sup>a</sup>Binding affinity was determined by Bing et al. in a competition assay with FAM-labeled St-2-1. On our arrays, St-2-1\_rev was used as a negative control sequence. The correlation between the affinity data and microarray binding data is given in Figure 6.



length dT 5mer linker and an exposure gradient between 0.2 and 18 J/cm<sup>2</sup> at 365 nm. There is an exponential relationship between exposure and deprotection, with 6 J/cm<sup>2</sup> corresponding to ~99% NPPOC removal, and 12 J/cm<sup>2</sup> corresponding to >99.9% removal (1% and <0.1% deletions per synthesis cycle, respectively).<sup>27</sup>

Exposure gradient and spacer gradient microarrays were hybridized in an adhesive chamber (SecureSeal SA200, Grace Biolabs) with a solution consisting of 0.3 pmol of 5'-Cy3-labeled probe, 40 μg of herring sperm DNA, and 200 μg of acetylated BSA in 400 μL of MES buffer (100 mM MES, 1 M NaCl, 20 mM EDTA, 0.01% Tween-20). After 2 h of rotation at 42 °C, the chamber was removed, and the microarrays were vigorously washed in a 50 mL centrifuge tube with 30 mL of nonstringent wash buffer (SSPE; 0.9 M NaCl, 0.06 M phosphate, 6 mM EDTA, 0.01% Tween-20) for 2 min and then, similarly, with stringent wash buffer (100 mM MES, 0.1 M NaCl, 0.01% Tween-20) for 1 min. Finally, the microarrays were dipped for a few seconds in the final wash buffer (0.1 × SSC) and then dried with a microarray centrifuge. Arrays were scanned with a Molecular Devices GenePix 4400A, and the intensity data were extracted with GenePix Pro.

**Aptamer Array QC Hybridization.** To determine the quality of the synthesized aptamer arrays, the arrays were hybridized with a mixture containing 15 different 25-mer and 50-mer Cy3-labeled QC oligomers (QC1-5, Sigma Genosis, UK; QC6-15, IDT, Belgium) varying in concentration from 0.01 to 100 pM. A solution of 5xSSC/0.1% SDS (SSC, AccuGene Lonza, Belgium; SDS, Sigma, USA) was used as the hybridization buffer. The hybridization mixture was preheated for 5 min at 95 °C, and a volume of 440 μL was used for hybridization in Agilent-one backing slides (G2534-60005, Agilent). Arrays were hybridized over 18 h in an Agilent oven at 45 °C. After hybridization, arrays were quickly rinsed with 6xSSPE/0.01% Tween-20 at room temperature (r.t.) (SSPE, AccuGene Lonza, Belgium; Tween-20, Sigma, Switzerland), washed at r.t. with 6xSSPE/0.01% Tween-20 for 1 min, washed at 45 °C with 0.6xSSPE/0.01% Tween-20 for 10 min, and washed at r.t. with 6xSSPE/0.01% Tween-20 for 10 min. Finally, arrays were dried by centrifugation and scanned at PMT10 using the Agilent High-Resolution C Scanner. Data were extracted using ImaGene 7.5 software.

**On-Array Streptavidin Binding Assay.** To determine the optimal synthesis parameters for on-array aptamer binding experiments, arrays were used to monitor binding of streptavidin to aptamer sequences on the array after the quality check by QC hybridization. First, the arrays were prewetted with 5xSSC/0.01% Tween-20 for 30 min at 45 °C. Next, the arrays were blocked with SuperblockT20 (Thermo Scientific) for 30 min at room temperature (r.t.). After blocking, the arrays were incubated with streptavidin (ProSpec, USA) using an incubation mixture containing 1xPBS/1 mM MgCl<sub>2</sub>/0.01% Tween-20/1% BSA/10 μg per mL streptavidin (PBS, Ambion, USA; MgCl<sub>2</sub>, Sigma, Germany; BSA, Sigma, USA). Incubation was performed at r.t. for 30 min. After streptavidin incubation, the arrays were rinsed three times with 1xPBS/1 mM MgCl<sub>2</sub>/0.05% Tween-20 and subsequently washed with the same buffer for 75 min at r.t., then the arrays were incubated for 30 min at r.t. with Cy5-labeled biotin, using a mixture containing 1xPBS/1 mM MgCl<sub>2</sub>/0.01% Tween-20/1 nM Biotin-dT<sub>5</sub>-Cy5 (IDT). After biotin incubation, the arrays were rinsed three times with 1xPBS/1 mM MgCl<sub>2</sub>/0.05% Tween-20, and subsequently washed with the same buffer for 30 min at r.t. After a final

quick rinse with deionized water, the arrays were dried by centrifugation and scanned at PMT10 using the Agilent high-resolution C scanner. Data were extracted using ImaGene 7.5 software.

## RESULTS AND DISCUSSION

**Influence of T-Spacer Length on Aptamer Binding vs DNA Hybridization.** To test the influence of dT-spacers on the ability of the St-2-1 aptamer (Table 2) to bind to

**Table 2. St-2-1 Binding Data for Microarrays Synthesized on Different Substrates**

surface	dT <sub>10</sub> spacer				rel SD <sup>b</sup> ST-2-1
	R <sup>2</sup> <sup>a</sup>	ST-2-1 signal	ST-2-1/ ST-2-1_rev	ST-2-1/ backgrnd	
UltraGAPS	0.90	154	8.5	9.2	33
Schott E	0.18	35	1.3	1.8	52
Schott A+	0.83	56	2.3	2.7	97
Hydroxyl	0.72	48	3.0	3.4	55

<sup>a</sup>R<sup>2</sup> is the linearity with the binding affinity data from Bing et al.<sup>42</sup> <sup>b</sup>Rel SD of refers to the 14 replicates of ST-2-1 on the microarray.

streptavidin, an array was synthesized on hydroxyl-functionalized substrates, with the aptamer sequence on spacers ranging in length from an oligo-dT 1mer to 25mers. The linkers were synthesized without capping steps to preserve equal probe density. To make a direct comparison with the influence of the spacers on DNA hybridization on the microarrays, the same array design was synthesized with the 25mer sequence (GTC ATC ATC ATG AAC CAC CCT GGT C). In both cases, the surface functionalization contributes ~10 carbon-carbon bond lengths to the spacer, approximately equivalent to 2 dTs. Figure 1 summarizes the results of these experiments, which indicate that there is an optimum spacer length in both cases: dT<sub>5</sub> for hybridization and dT<sub>11</sub> for aptamer binding. In the case of hybridization on microarrays, it is known that a spacer improves hybridization by making the probe more accessible; on the other hand, excessively long spacers can hinder hybridization, presumably because ssDNA forms a random coil on the surface, allowing the probe to be covered, or “dissolved” in a mass of linker DNA.<sup>31</sup>

The effect of spacer length on hybridization can be clearly seen in experiments with radiolabeled DNA. Shchepinov et al.<sup>30</sup> found a signal maximum with 10 couplings of a spacer phosphoramidite, equivalent to a total length of about 100 carbon-carbon bonds. Fluorescent labeling of the target sequence obscures the effect due to interactions between the fluorescent dye and the microarray substrate. Proximity to the surface greatly increases the fluorescence of cyanine dyes in hybridization experiments.<sup>37</sup> We have also observed this effect with microarrays synthesized with oligonucleotides of increasing lengths terminated by a coupling with a Cy3 or Cy5 phosphoramidite (data not shown). The results in Figure 1 are the convolution of the two effects and indicate that the optimum spacer length for the aptamer is significantly longer than the optimum in the hybridization studies. That the St-2-1 aptamer binding signal decreases after 11 dTs is in contrast with the results for the IgE-binding aptamer, for which the signal is proportional to the oligo(dT) length up to at least dT 20mers.<sup>14</sup> Lao et al.<sup>43</sup> also found that the fluorescence signal from human α-thrombin HTQ and HTDQ aptamer binding was significantly higher for a dT<sub>12</sub> vs a dT<sub>6</sub> spacer, but did not

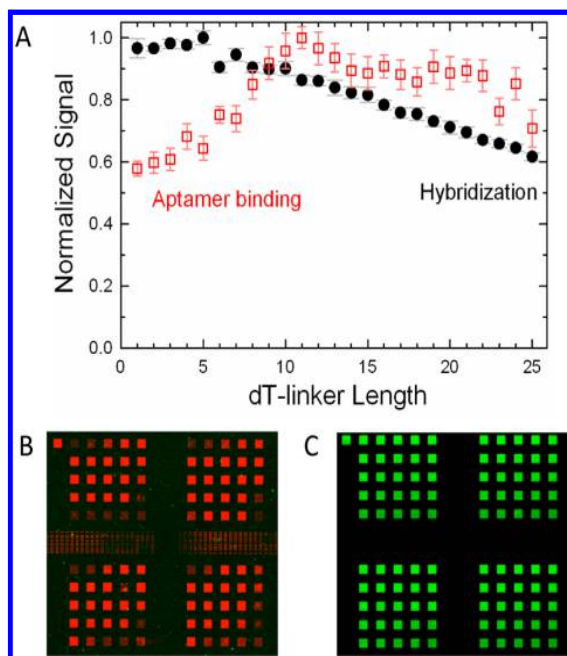


**Figure 1.** (A) Normalized fluorescent signals vs linker length from the St-2-1 aptamer binding assay (red empty squares), and from the equivalent 25mer hybridization experiment. (B) Microarray image of aptamer linker gradient showing four replicates and with the length increasing from left to right and from top to bottom in 25 steps from 1 to 25 dTs. (C) Equivalent image of hybridization experiment. Each of the square features on the microarray is synthesized using a  $10 \times 10$  array of  $16 \mu\text{m}$  DMD mirrors.

explore other oligo(dT) lengths. In all of these cases, the labeling dyes used were cyanine dyes, which suggests that specific aptamer properties, rather than dye–substrate interactions, are the source of the differing spacer requirements, but we cannot exclude the possibility that differences between Cy3- and Cy5-labeling account for the difference. Nevertheless, it seems likely that the optimum spacer length for aptamer microarrays will need to be independently optimized for each aptamer and for each labeling dye.

**Role of Sequence Fidelity and Surface Density in Aptamer Binding vs Hybridization.** The tolerance of aptamer microarrays to sequence error is important for maximizing the binding signal. Sequence fidelity is particularly relevant in the case of in situ microarray synthesis, for which postsynthesis oligonucleotide purification is not possible. Phosphoramidite chemistry has been optimized to yield average stepwise coupling efficiencies well above 99% for DNA monomers and  $\sim 99\%$  for RNA monomers, for both solid-phase synthesis and in situ synthesis on microarrays,<sup>27,44</sup> but other sources of error, most prominently depurination, reduce the overall yield further.<sup>45</sup> Spotted microarrays may use HPLC- or gel electrophoresis-purified oligonucleotides to reach a sequence purity greater than  $\sim 85\%$ , although the value for this level of purity has not been established for aptamer applications or for traditional microarray applications. In addition to lacking the option of oligonucleotide purification, in situ microarray synthesis results in a significantly higher error rate as a result of the additional complexity associated with the simultaneous synthesis of large numbers of sequences.<sup>25,27</sup> Here, we take advantage of the high degree of control afforded by maskless array synthesis (MAS) to assess the sequence fidelity requirement of hybridization vs protein binding to aptamers.

When a single, short sequence is synthesized on a microarray substrate with MAS, the minimal complexity results in very high fidelity oligonucleotides. This is a result of the elimination of stray light effects present when multiple sequences are synthesized simultaneously as well as by the intrinsically low rate of depurination and other side reactions in the MAS chemistry, which does not use acidic conditions and requires minimal exposure to oxidants.<sup>27</sup> Synthesis errors can then be introduced in a controlled manner by reducing the UV light exposure, which results in decreased NPPOC cleavage and, hence, the introduction of deletion errors.

Figure 2 (black squares) shows the results from a hybridization experiment on a microarray synthesized with a

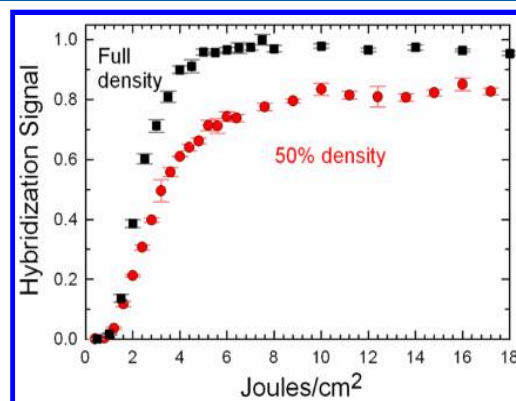


**Figure 2.** Normalized hybridization fluorescent signals for a single 25mer sequence synthesized with a photodeprotection light exposure gradient between 0.2 and  $18 \text{ J/cm}^2$ . The black squares are from a microarray synthesized for maximum surface density of oligonucleotides. The red circles are from an equivalent experiment, but with the oligonucleotide surface density reduced by 50% by a partial light exposure followed by capping. The microarray layout is the same as for the data shown in Figure 1, but with 25 exposure steps replacing the 25 linker steps.

light exposure gradient between 0.2 and  $18 \text{ J/cm}^2$  at 365 nm. The fraction of NPPOC groups cleaved with a given light exposure is a first-order exponential with the form  $1 - e^{-t/\tau}$ , where  $t$  is the light exposure and  $\tau$  is a rate constant of  $\sim 1.3 \text{ J/cm}^2$ .<sup>27</sup> The fraction of sequences with no deletion errors is therefore  $\sim (1 - e^{-t/\tau})^n$ , where  $n$  is the sequence length. Microarray features (“spots”) that receive the lowest exposures have a very low surface density of hybridizable oligonucleotides (“hybridizable” is defined here as capable of forming a hybrid under typical stringent hybridization conditions), but the hybridization signal increases rapidly to reach a maximum around  $6 \text{ J/cm}^2$ . At this exposure,  $\sim 5\%$  of the NPPOC groups remain attached ( $12 \text{ J/cm}^2$  is required for  $>99.9\%$  photodeprotection). This is a clear indication that microarrays used in hybridization experiments have a very high error tolerance. For the 25mer sequence used in these experiments, the  $6 \text{ J/cm}^2$  optimum exposure results in  $\sim 75\%$  of sequences with at least one deletion error. Surface density of oligonucleotides plays a role in this effect, as it is known that hybridization efficiency decreases quickly with oligonucleotide surface density, presumably due to steric crowding.<sup>31,46</sup>

We hypothesized that microarray hybridization efficiency remains constant above a certain oligonucleotide fidelity threshold because then the critical parameter is the density of hybridizable oligonucleotides, rather than just the density of the oligonucleotides. This is because the single-to-double-stranded

transition doubles both the surface density of oligonucleotides and the density of charged groups, hindering further hybridization. In addition, the much higher persistence length of dsDNA ( $\sim 50$  nm<sup>47</sup>) vs ssDNA ( $\sim 2$  nm<sup>48</sup>) may restrict diffusion near the surface and thereby inhibit further hybridization.

To test this hypothesis, we reduced the surface density by 50% after the linker synthesis using a light exposure corresponding to a 50% NPOC cleavage ( $2$  J/cm<sup>2</sup>) and capped the resulting 5'-OH groups with a dimethoxytrityl-dT phosphoramidite (DMT-dT) coupling.<sup>49</sup> The same 25mer sequence as above was then synthesized with an exposure gradient, and the results are plotted alongside those of the full density experiment in Figure 2 (red circles). These data indicate that the hybridization signal reaches  $\sim 80\%$  of the intensity of the full density results. In addition, the light exposure resulting in maximum signal shifts higher, to at least  $10$  J/cm<sup>2</sup> or perhaps more, as the slope remains slightly positive up to  $18$  J/cm<sup>2</sup>. These results are compatible with our hypothesis. Specifically, the signal is much higher than 50%, indicating that hybridization on the full density array, and at exposures greater than  $6$  J/cm<sup>2</sup>, is constrained by molecular crowding. In addition, the optimum light exposure of the 50% density data is much higher, indicating that with reduced molecular crowding, the increase in sequence fidelity resulting from greater light exposures leads to increased hybridization. The optimum light exposure also depends on sequence length, with light exposure gradients of 60mers reaching a maximum hybridization signal at  $\sim 3$  J/cm<sup>2</sup> (Supporting Information Figure S1), which is also in agreement with the crowding hypothesis, since longer sequences result in a greater mass of DNA on the surface.

The St-2-1 aptamer binds to the 60 kDa protein streptavidin, a much bulkier macromolecule than the 8 kDa complementary 25mer sequence in the hybridization experiments. In addition, the St-2-1 aptamer forms a double-stranded structure with two loops, which may further increase molecular crowding at the microarray surface. As a result, we hypothesized that St-2-1 aptamer microarrays would have a lower optimal oligonucleotide density. We also hypothesized that the aptamer array would be less error-tolerant than the comparable hybridization array. The sensitivity of aptamers to sequence fidelity was explored by Katilius et al.,<sup>14</sup> who used in situ synthesized microarrays to determine the effect of mutations on the affinity of the IgE-binding aptamer. They found that the majority of single mutations result in near complete loss of binding. Similar experiments exploring the effects of defects on hybridization affinity, also on microarrays, indicated that hybridization is significantly less error-sensitive.<sup>40</sup>

To test the role of sequence fidelity and surface density in aptamer microarrays, we synthesized the St-2-1 aptamer with the same light exposure gradient as in the hybridization experiment above. Figure 3 (black squares) shows that the optimum exposure,  $11$  J/cm<sup>2</sup>, is almost twice that of the hybridization experiment, confirming that the aptamer is more sensitive to errors. Another feature of these data is that after the optimum exposure, the aptamer binding signal drops significantly, which may be an indication of molecular crowding. To test whether the aptamer binding signal is constrained by crowding, the same array was resynthesized with the surface density reduced by 50% after the linker synthesis using the same partial exposure and capping procedure as above. The signal intensity of the 50% density array is shown in

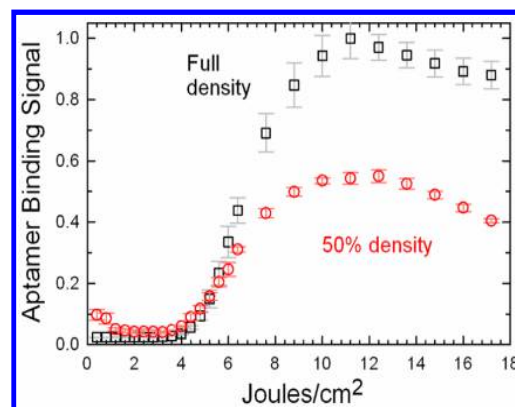


**Figure 3.** Normalized streptavidin binding signal for a St-2-1 aptamer sequence synthesized with a photodeprotection light exposure gradient between  $0.2$  and  $18$  J/cm<sup>2</sup>. The black squares represent data from a microarray synthesized with a maximum surface density of oligonucleotides. The red circles are from an equivalent experiment, but with a microarray with an oligonucleotide surface density reduced by 50%.

Figure 3 (red circles). The data show that the binding signal is reduced by approximately 50%, indicating that, unlike the hybridization results, binding is not significantly constrained by molecular crowding at the normal microarray oligonucleotide surface densities. The curves in Figure 3 exhibit a clear drop at very high light exposures. Since the maxima and the extent of subsequent decline is similar for both surface densities, the effect cannot be attributed to crowding.

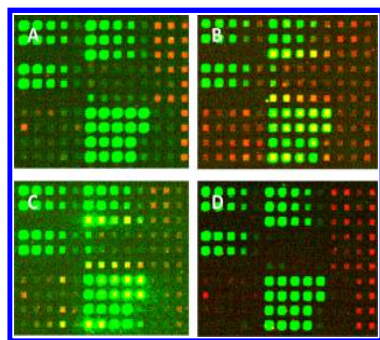
By  $12$  J/cm<sup>2</sup>, the photodeprotection is essentially complete ( $\sim 99.9\%$ ), and additional exposure would not significantly improve the sequence fidelity. Since aptamers appear to be much more sensitive to sequence error than hybridization probes, we speculate that the drop in signal is a consequence of errors introduced by the very high light exposure itself. It is well-known that high doses of UV-A are capable of inducing both single-strand DNA breaks and pyrimidine dimers.<sup>50</sup> This result indicates that methods to increase the aptamer surface density, for example, by using substrates functionalized at a higher density (see below) or by the use of branching phosphoramidites, could be effective in increasing aptamer binding signal.

**Influence of the Substrate on Aptamer Binding and DNA Hybridization.** Surface chemistry is necessary to modify the glass surface to enable the initial phosphoramidite coupling reaction. This surface functionalization determines the surfaced density of bound oligonucleotides. Functionalization chemistry may also affect hybridization by increasing the distance to the glass surface and by changing the surface electrostatics and hydrophobicity, properties which are also known to influence hybridization and nonspecific target binding and, hence, background intensity.<sup>33–35</sup> To evaluate the effect of surface chemistry on both aptamer binding and hybridization, we synthesized microarrays containing a variety of hybridization probes and aptamers on four different types of functionalized glass substrates: Corning UltraGAPS (Gamma Amino Propyl Silane), Schott Nexterion Slide A+ (GAPS;  $1.0 \pm 0.3 \times 10^{12}$  molecules/cm<sup>2</sup>), Schott Nexterion ring-opened Slide E (epoxysilane,  $5.6 \pm 0.3 \times 10^{12}$  molecules/cm<sup>2</sup>). Surface densities were provided by Schott, but not Corning. The fourth substrate was functionalized in-house as described in the



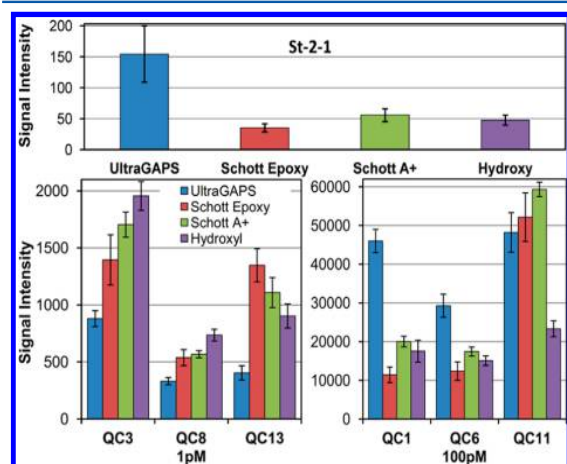
Experimental Section and have a surface hydroxyl density of about  $2.7 \times 10^{12}$  molecules/cm<sup>2</sup>.<sup>49</sup>

Figure 4 shows sections of fluorescent images from the same microarray design synthesized on the four substrate types. The



**Figure 4.** Fluorescent images of sections of microarrays synthesized on different substrates. (A) Corning UltraGAPS, (B) Schott Epoxy ring-opened, (C) Schott A+, (D) Schott Glass D hydroxyl-functionalized with *N*-(3-triethoxysilylpropyl)-4-hydroxybutyramide. Green features are hybridization signals from Cy3-labeled sequences. Red features are from Cy5-labeled biotin binding to the streptavidin–aptamer pairs. A scheme identifying the sequences corresponding to the spots can be found in the Supporting Information. The arrays were synthesized with light exposures of 11 J/cm<sup>2</sup> and with  $32 \times 32 \mu\text{m}$  features (4 DMD mirrors) separated by gaps of 48  $\mu\text{m}$ . All images were acquired with the same scanner settings.

microarrays include both aptamers and hybridization probes but were synthesized with light exposures of 11 J/cm<sup>2</sup> to maximize aptamer binding signals. To maximize their comparability, all four microarrays were synthesized consecutively from the same batch of reagents and monomers, and the hybridization assays, followed by the aptamer binding assay, were performed on the four arrays in parallel. Differences in signal and background intensity are apparent for both the aptamer binding signal (Red/Cy5) and hybridization signals (Green/Cy3). The charts in Figure 5 compare the aptamer



**Figure 5.** Aptamer binding and hybridization signal comparison between microarrays synthesized with four different surface chemistries (left to right): Corning UltraGAPS/amino-modified; Schott E/epoxy-modified, ring-opened; Schott A+/amino-modified; and in-house hydroxyl-functionalized. Top: St-2-1 aptamer–streptavidin binding signal. Bottom: hybridization signal for three probes hybridized with 1 and 100 pM complementary sequences. Error bars are the standard deviation among replicates.

binding and hybridization signals between microarrays synthesized on the different surfaces and with a dT<sub>10</sub> spacer. There is a substantial substrate-dependent difference in aptamer signal, with the UltraGAPS giving a much higher signal than the other substrates. Table 2 gives additional data on the ratios of signal-to-control, signal-to-background, and relative standard deviations of the aptamer signal on the four substrates, and the UltraGAPS substrate leads to substantially better results in all these categories. Since both the UltraGAPS and the A+ substrates are  $\gamma$ -aminopropyl silane functionalized, the higher signal from the UltraGAPS slide may indicate that this substrate is manufactured with a higher density of functional groups than the A+ substrates. Among the three substrates with known surface densities of functional groups, there is no correlation between surface density and aptamer binding signal. However, we cannot exclude that differences among the substrates, other than surface density, are responsible.

Hybridization data from the same microarrays are also shown in Figure 5. Each microarray included the probes described in Table 1: QC1, and QC11, the complementary sequences to which were included in the hybridization solution at a concentration of 100 pM. The complementary sequence probes QC3, QC8, and QC13 were present in the hybridization solution at a concentration of 1 pM. Whereas the UltraGAPS substrate performed substantially better than the other substrates in the aptamer binding assay, none of the substrates was clearly superior in the hybridization data. There is a clear indication in the data that the relationship between hybridization signal and substrate is heterogeneous and sequence-specific, suggesting that the surface chemistry significantly influences both hybridization and aptamer binding.

**On-Array Streptavidin Binding Assay under Optimized Conditions.** To test the suitability of the optimized synthesis conditions (11mer dT linker, 11J/cm<sup>2</sup> light deprotection) for on-array aptamer screening, a panel of streptavidin-binding aptamers were chosen as a model. In 2010, Bing et al. described the streptavidin-binding aptamer St-2-1 and a series of St-2-1-derived mutated sequences and their binding affinity for streptavidin measured in a competition assay with FAM-labeled St-2-1.<sup>42</sup> The percentage FAM-labeled St-2-1 replaced by the tested aptamer was determined as a measure of binding affinity for the aptamer (Table 1). In Figure 6, the on-array signals for the St-2-1 variants of Table 1 are plotted against the affinity data described in Bing et al., resulting in a correlation coefficient of 0.92.

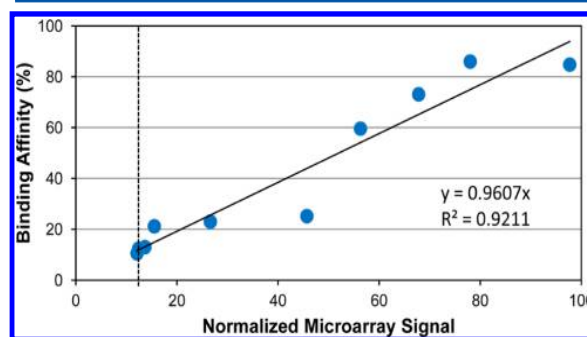


**Figure 6.** Correlation between data of an on-array aptamer binding assay (14 replicate spots on array) and an off-array competition experiment published by Bing et al. Blue dots are the St-2-1 and the mutated variants of St-2-1 shown in Table 1. Dotted line indicates the signal of the negative control St-2-1<sub>rev</sub>.

Figure 7 shows the effect of single mutations in the 29-mer St-2-1 aptamer sequence. For every position, all possible

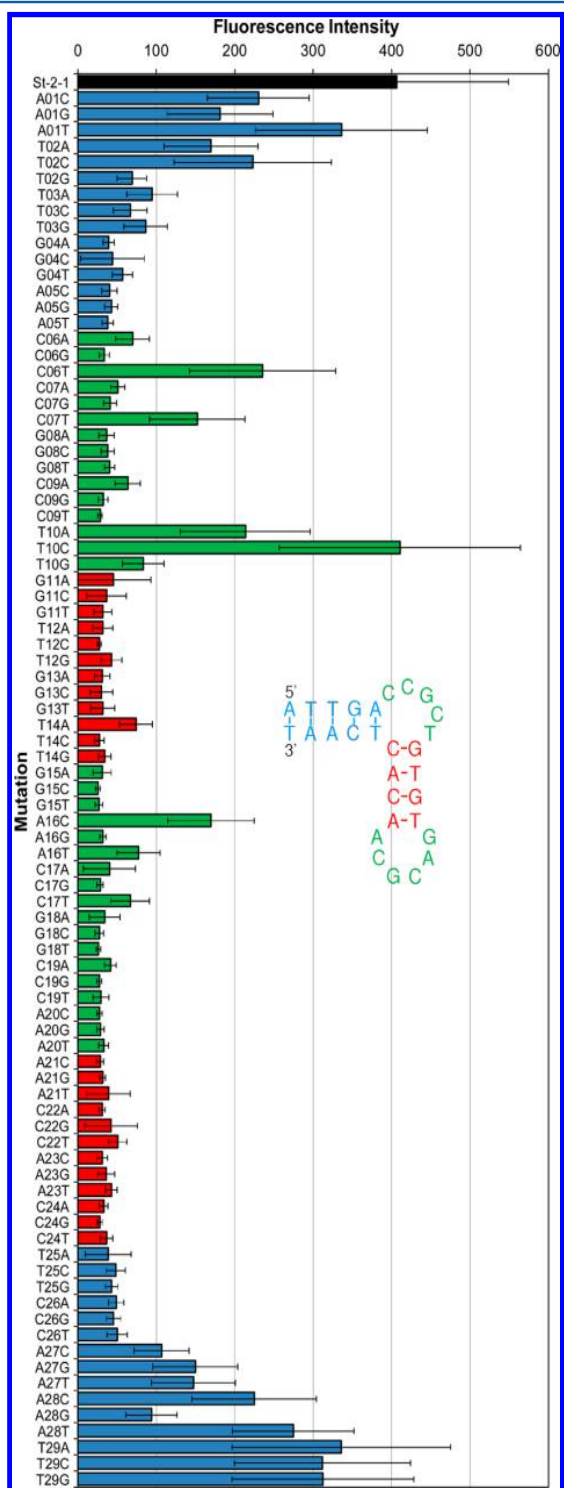


**Figure 7.** Effect of mutations in the 29-mer St-2-1 aptamer sequence on the binding affinity. Binding was tested using an on-array streptavidin binding assay. Black bar, St-2-1; blue bars, mutation in the terminal stem; green bars, mutation in the bulges; red bars, mutation in the sequences between the bulges. Error bars are based on 12 replicates on the array. Signal negative control St-2-1\_rev =28.4.

variants were tested, resulting in 87 mutants. The single mutations appear to be less critical in the terminal stem

sequence when the mutation is at a distance of four or more bases from the bulge (Figure 7, blue bars). Single mutations in the central stem between both bulges are highly critical (Figure 7, red bars). This is in agreement with the findings of Bing et al., who found that the hairpin bulge structure is critical for streptavidin binding. Most single mutations in the bulges are critical. In their paper, Bing et al. describe that G8, G15, and G18 are important to maintain good binding, and we observe the same in our data. Replacing the G at these positions by one of the other bases lowers the binding affinity to the level of the negative control. Mutant T10C appears to be the only mutant with the same binding affinity as St-2-1.

Figure 8 shows the results of mutants that had one base pair replacement in the double stranded parts of St-2-1. All 27

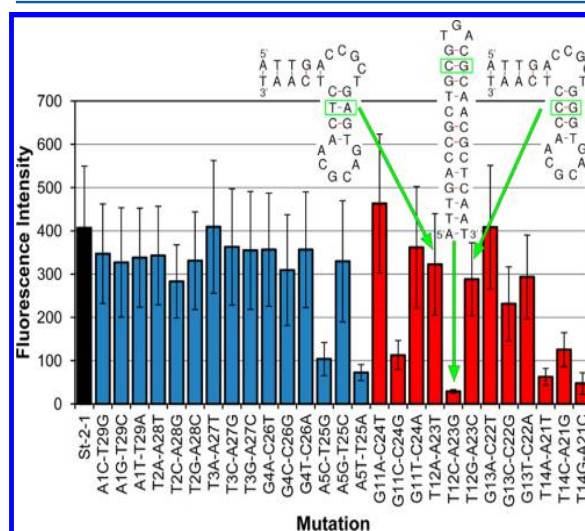


**Figure 8.** Effect of base pair replacements in the double-stranded parts of St-2-1. Binding was tested using an on-array streptavidin binding assay. Black bar, St-2-1; blue bars, mutation in the terminal stem; red bars, mutation in the sequence between the bulges. Error bars are based on 12 replicates on the array. Secondary structure of the variants A<sub>12</sub>T<sub>23</sub>, G<sub>12</sub>C<sub>23</sub>, and C<sub>12</sub>G<sub>23</sub>. The structural variant C<sub>12</sub>G<sub>23</sub> correlates with reduced streptavidin binding on-array.

possible base pair replacements were present on the array (12 replicates). From the results, it can be seen that base pair T<sub>14</sub>A<sub>21</sub> is most critical, since every other combination tested at this position resulted in a significant loss of signal in the streptavidin binding assay. Furthermore, there are a few other replacements that lower the binding affinity significantly, at positions A<sub>5</sub>T<sub>25</sub> (replacement by C<sub>5</sub>G<sub>25</sub> or T<sub>5</sub>A<sub>25</sub>) and T<sub>12</sub>A<sub>23</sub> (replacement by C<sub>12</sub>G<sub>23</sub>). The insets in Figure 8 show the secondary structure of the variants A<sub>12</sub>T<sub>23</sub>, G<sub>12</sub>C<sub>23</sub>, and C<sub>12</sub>G<sub>23</sub>. In accordance with the data from the on-array streptavidin-binding assay, mutant C<sub>12</sub>G<sub>23</sub> is structurally distinct from St-2-1 and has a much reduced binding affinity, whereas mutants A<sub>12</sub>T<sub>23</sub> and G<sub>12</sub>C<sub>23</sub> are structurally similar to St-2-1 and retain a similar binding affinity (DNA structures from <http://mfold.rna.albany.edu/?q=mfold/dna-folding-form>).<sup>51</sup> Together, these data show that aptamer arrays are a powerful tool for aptamer screening.

## CONCLUSIONS

Using the versatility of in situ synthesis of oligonucleotide microarrays, we have explored the impact of synthesis parameters on aptamer microarray performance and made

direct comparisons with similar hybridization-based arrays. The results indicate that, relative to traditional hybridization assays, aptamer microarray detection can be significantly improved by increasing the spacer length and by maximizing oligonucleotide sequence fidelity. Aptamer microarrays also appear to be less sensitive than hybridization microarrays to molecular crowding, proving a pathway for further improvement. The functionalization chemistry of the glass substrate also significantly affects the aptamer binding signal, either by modifying the oligonucleotide surface density, or via electrostatic or hydrophobic interactions with the aptamers or target protein. Aptamers are likely to prove more heterogeneous than hybridization probes in regard to optimum microarray parameters because of their varied 3-D structures and modes of interactions with their targets, and therefore, additional synthesis optimizations with a variety of aptamers will be necessary to understand the full extent of variability.

## ■ ASSOCIATED CONTENT

### Supporting Information

Additional information as noted in text. This material is available free of charge via the Internet at <http://pubs.acs.org>.

## ■ AUTHOR INFORMATION

### Corresponding Author

\*E-mail: [mark.somoza@univie.ac.at](mailto:mark.somoza@univie.ac.at).

### Notes

The authors declare no competing financial interest.

## ■ ACKNOWLEDGMENTS

M.M.S. gratefully acknowledges financial support from the University of Vienna, the Faculty of Chemistry of the University of Vienna, and the Austrian Science Fund (FWF P23797).

## ■ REFERENCES

- (1) Kingsmore, S. F. *Nat. Rev. Drug Discovery* **2006**, *5*, 310–321.
- (2) Robertson, D. L.; Joyce, G. F. *Nature* **1990**, *344*, 467–468.
- (3) Ellington, A. D.; Szostak, J. W. *Nature* **1990**, *346*, 818–822.
- (4) Tuerk, C.; Gold, L. *Science* **1990**, *249*, 505–510.
- (5) Rhie, A.; Kirby, L.; Sayer, N.; Wellesley, R.; Disterer, P.; Sylvester, I.; Gill, A.; Hope, J.; James, W.; Tahiri-Alaoui, A. *J. Biol. Chem.* **2003**, *278*, 39697–39705.
- (6) Green, L. S.; Jellinek, D.; Bell, C.; Beebe, L. A.; Feistner, B. D.; Gill, S. C.; Jucker, F. M.; Janjic, N. *Chem. Biol.* **1995**, *2*, 683–695.
- (7) Dowler, T.; Bergeron, D.; Tedeschi, A. L.; Paquet, L.; Ferrari, N.; Damha, M. J. *Nucleic Acids Res.* **2006**, *34*, 1669–1675.
- (8) Deleavey, G. F.; Watts, J. K.; Alain, T.; Robert, F.; Kalota, A.; Aishwarya, V.; Pelletier, J.; Gewirtz, A. M.; Sonenberg, N.; Damha, M. J. *Nucleic Acids Res.* **2010**, *38*, 4547–4557.
- (9) Koshkin, A. A.; Singh, S. K.; Nielsen, P.; Rajwanshi, V. K.; Kumar, R.; Meldgaard, M.; Olsen, C. E.; Wengel, J. *Tetrahedron* **1998**, *54*, 3607–3630.
- (10) Obika, S.; Nanbu, D.; Hari, Y.; Morio, K.-i.; In, Y.; Ishida, T.; Imanishi, T. *Tetrahedron Lett.* **1997**, *38*, 8735–8738.
- (11) Hendrix, C.; Rosemeyer, H.; Verheggen, I.; Van Aerschot, A.; Seela, F.; Herdewijn, P. *Chem.—Eur. J.* **1997**, *3*, 110–120.
- (12) King, D. J.; Bassett, S. E.; Li, X.; Fennewald, S. A.; Herzog, N. K.; Luxon, B. A.; Shope, R.; Gorenstein, D. G. *Biochemistry* **2002**, *41*, 9696–9706.
- (13) Yang, X.; Bassett, S. E.; Li, X.; Luxon, B. A.; Herzog, N. K.; Shope, R. E.; Aronson, J.; Prow, T. W.; Leary, J. F.; Kirby, R.; Ellington, A. D.; Gorenstein, D. G. *Nucleic Acids Res.* **2002**, *30*, e132.
- (14) Katilius, E.; Flores, C.; Woodbury, N. W. *Nucleic Acids Res.* **2007**, *35*, 7626–7635.
- (15) Fischer, N. O.; Tok, J. B.-H.; Tarasow, T. M. *PLoS ONE* **2008**, *3*, e2720 EP.
- (16) Collett, J. R.; Cho, E. J.; Ellington, A. D. *Methods* **2005**, *37*, 4–15.
- (17) Collett, J. R.; Cho, E. J.; Lee, J. F.; Levy, M.; Hood, A. J.; Wan, C.; Ellington, A. D. *Anal. Biochem.* **2005**, *338*, 113–123.
- (18) Cho, E. J.; Collett, J. R.; Szafranska, A. E.; Ellington, A. D. *Anal. Chim. Acta* **2006**, *564*, 82–90.
- (19) Brody, E. N.; Gold, L. *Rev. Mol. Biotechnol.* **2000**, *74*, 5–13.
- (20) Hesselberth, J.; Robertson, M. P.; Jhaveri, S.; Ellington, A. D. *Rev. Mol. Biotechnol.* **2000**, *74*, 15–25.
- (21) Conrad, R.; Keranen, L. M.; Ellington, A. D.; Newton, A. C. *J. Biol. Chem.* **1994**, *269*, 32051–32054.
- (22) Wilson, D. S.; Nock, S. *Curr. Opin. Chem. Biol.* **2001**, *6*, 81–85.
- (23) Fodor, S. P.; Read, J. L.; Pirrung, M. C.; Stryer, L.; Lu, A. T.; Solas, D. *Science* **1991**, *251*, 767–773.
- (24) Singh-Gasson, S.; Green, R. D.; Yue, Y.; Nelson, C.; Blattner, F.; Sussman, M. R.; Cerrina, F. *Nat. Biotechnol.* **1999**, *17*, 974–978.
- (25) LeProust, E. M.; Peck, B. J.; Spirin, K.; McCuen, H. B.; Moore, B.; Namsaraev, E.; Caruthers, M. H. *Nucleic Acids Res.* **2010**, *38*, 2522–2540.
- (26) Lackey, J. G.; Mitra, D.; Somoza, M. M.; Cerrina, F.; Damha, M. J. *J. Am. Chem. Soc.* **2009**, *131*, 8496–8502.
- (27) Agbavwe, C.; Kim, C.; Hong, D. G.; Heinrich, K.; Wang, T.; Somoza, M. M. *J. Nanobiotechnol.* **2011**, *9*, 57.
- (28) Beaucage, S. L. *Curr. Med. Chem.* **2001**, *8*, 1213–1244.
- (29) Halliwell, C. M.; Cass, A. E. G. *Anal. Chem.* **2001**, *73*, 2476–2483.
- (30) Shchepinov, M. S.; Case-Green, S. C.; Southern, E. M. *Nucleic Acids Res.* **1997**, *25*, 1155–1161.
- (31) Southern, E.; Mir, K.; Shchepinov, M. *Nat. Genet.* **1999**, *21*, 5–9.
- (32) Maskos, U.; Southern, E. M. *Nucleic Acids Res.* **1992**, *20*, 1679–1684.
- (33) Walter, J.-G.; Kokpinar, O.; Friehs, K.; Stahl, F.; Scheper, T. *Anal. Chem.* **2008**, *80*, 7372–7378.
- (34) Taylor, S.; Smith, S.; Windle, B.; Guiseppi-Elie, A. *Nucleic Acids Res.* **2003**, *31*, e87.
- (35) Vainrub, A.; Pettitt, B. M. *J. Am. Chem. Soc.* **2003**, *125*, 7798–7799.
- (36) Li, Y.; Lee, H. J.; Corn, R. M. *Anal. Chem.* **2007**, *79*, 1082–1088.
- (37) Zhang, L.; Hurek, T.; Reinhold-Hurek, B. *Nucleic Acids Res.* **2005**, *33*, e166.
- (38) Zhu, G.; Lübbecke, M.; Walter, J.-G.; Stahl, F.; Scheper, T. *Chem. Eng. Technol.* **2011**, *34*, 2022–2028.
- (39) Naiser, T.; Kayser, J.; Mai, T.; Michel, W.; Ott, A. *Phys. Rev. Lett.* **2009**, *102*, 218301.
- (40) Naiser, T.; Ehler, O.; Kayser, J.; Mai, T.; Michel, W.; Ott, A. *BMC Biotechnol.* **2008**, *8*, 48.
- (41) Agbavwe, C.; Somoza, M. M. *PLoS ONE* **2011**, *6*, e22177.
- (42) Bing, T.; Yang, X.; Mei, H.; Cao, Z.; Shangguan, D. *Bioorg. Med. Chem.* **2010**, *18*, 1798–1805.
- (43) Lao, Y. H.; Peck, K.; Chen, L. C. *Anal. Chem.* **2009**, *81*, 1747–1754.
- (44) Wang, T.; Oehrlein, S.; Somoza, M. M.; Perez, J. R. S.; Kershner, R.; Cerrina, F. *Lab Chip* **2011**, *11*, 1629–1637.
- (45) Septak, M. *Nucleic Acids Res.* **1996**, *24*, 3053–3058.
- (46) Peterson, A. W.; Heaton, R. J.; Georgiadis, R. M. *Nucleic Acids Res.* **2001**, *29*, 5163–5168.
- (47) Smith, S. B.; Cui, Y.; Bustamante, C. *Science* **1996**, *272*, 795–798.
- (48) Murphy, M. C.; Raskin, I.; Cheng, W.; Lohman, T. M.; Ha, T. *Biophys. J.* **2004**, *86*, 2530–2537.
- (49) Chen, S.; Phillips, M. F.; Cerrina, F.; Smith, L. M. *Langmuir* **2009**, *25*, 6570.
- (50) Slieman, T. A.; Nicholson, W. L. *Appl. Environ. Microbiol.* **2000**, *66*, 199–205.
- (51) Zuker, M. *Nucleic Acids Res.* **2003**, *31*, 3406–3415.



## Base-cleavable microarrays for the characterization of DNA and RNA oligonucleotides synthesized *in situ* by photolithography†

Cite this: *Chem. Commun.*, 2014, 50, 12903

Received 24th July 2014,  
Accepted 5th September 2014

DOI: 10.1039/c4cc05771f

www.rsc.org/chemcomm

Jory Lietard,<sup>ab</sup> Nicole Kretschy,<sup>b</sup> Matej Sack,<sup>b</sup> Alexander S. Wahba,<sup>a</sup>  
Mark M. Somoza\*<sup>b</sup> and Masad J. Damha\*<sup>a</sup>

**Assessing synthesis efficiency, errors, failed deprotections, and chemical and enzymatic degradation of oligonucleotides on microarrays is essential for improving existing *in situ* synthesis methods, and for the development of new chemistries. We describe the use of LC-MS to analyse DNA and RNA oligonucleotides deprotected and cleaved under basic conditions from microarrays fabricated using light-directed *in situ* chemistry. The data yield essential information on array quality and sequence identity.**

Arrayed DNA onto chips has revolutionized the field of biomedical research,<sup>1–4</sup> most notably in gene expression profiling,<sup>5</sup> by providing an access to large nucleic acid libraries attached to one single support and by allowing the simultaneous screening of thousands of genes. These DNA libraries can originate from PCR products which are then covalently attached to the glass surface<sup>6</sup> or are synthesized *in situ* by ink-jet printing or photolithography,<sup>7–9</sup> taking advantage of the robust phosphoramidite chemistry.<sup>10,11</sup> The quality of the immobilized DNA is one of the crucial parameters governing the reliability of the measurement,<sup>12</sup> and while this parameter can be controlled to some extent for PCR products, the same level of quality assessment is less trivial for *in situ*-synthesized microarrays.

One method for quality control consists of labelling the terminus of each strand on the array with a fluorescent nucleotide and measuring the fluorescence intensity.<sup>13,14</sup> The decrease in intensity as the chain length increases is fitted to an exponential decay curve which then allows for the determination of a stepwise synthesis yield. In addition, this direct labelling and read-out method permits an optimization of the parameters involved in microarray synthesis, thereby enabling a relative control over array quality.<sup>15</sup> However, fluorescence provides at best a relative

measure of sequence completion. The interpretation of the intensity can also be uncertain due to the sequence-dependence of fluorescence,<sup>16</sup> and it certainly cannot identify the source of error.

To be able to chemically separate the grown oligonucleotides from the glass slide and characterize the eluate using conventional analytical methods is an attractive idea, but the decisively small amount of DNA synthesized on-chip ( $\sim 0.1\text{--}1\text{ pmol mm}^{-2}$ )<sup>17</sup> requires the most sensitive detection techniques. In this context, radiolabelling of cleaved DNA followed by gel electrophoresis offers an overview of synthetic quality and it has been successfully applied to the monitoring of microarray synthesis defects, but like fluorescence provides primary information on the distribution of sequence lengths.<sup>9,17,18</sup> Mass spectrometry (MS) is another sensitive method which would provide final evidence of oligonucleotide identity but it has, to our knowledge, only been attempted on microarray surfaces suitable as matrices for MALDI-MS analyses.<sup>19–21</sup>

We therefore wished to develop a method that allows for MS characterization of microarrays fabricated on standard glass microscope slides. In addition to the identification of full-length products, MS would likely detect synthetic failures, degraded material and incompletely deprotected sequences; essential information for the development of new *in situ* chemistries. Indeed, we have recently embarked on the synthesis of RNA microarrays by photolithography<sup>22,23</sup> and the identification by MS of the synthetic RNA analytes is expected to help guide the technology to maturity. Our approach involved the incorporation of a base-labile ester functionality at the 3'-end of the oligonucleotide chain.<sup>24</sup> To do so, we used a custom-made NPPOC-protected dT phosphoramidite with a succinyl group attached to the 3'-OH function (cleavable dT, dT<sup>cleav</sup>, Fig. 1a). Following published protocols,<sup>25</sup> this amidite was coupled for 1 min on silanized glass slides after the synthesis of a pentamer spacer, and the desired oligonucleotide sequence was then fabricated after NPPOC deprotection of the dT<sup>cleav</sup> (Fig. 1b). To verify that dT<sup>cleav</sup> coupled efficiently, we labelled the 5'-end of a dT<sub>10</sub> chain with a Cy3 dye. In parallel, dT decamers fabricated without dT<sup>cleav</sup> were also fluorescently-labelled. Based on the difference

<sup>a</sup> Department of Chemistry, McGill University, Montréal, Québec H3A 0B8, Canada.  
E-mail: masad.damha@mcgill.ca

<sup>b</sup> Institute of Inorganic Chemistry, University of Vienna, 1090 Vienna, Austria.  
E-mail: mark.somoza@univie.ac.at

† Electronic supplementary information (ESI) available: Experimental procedures for microarray fabrication, deprotection and cleavage as well as LC-MS conditions and spectra of all array eluates. See DOI: 10.1039/c4cc05771f

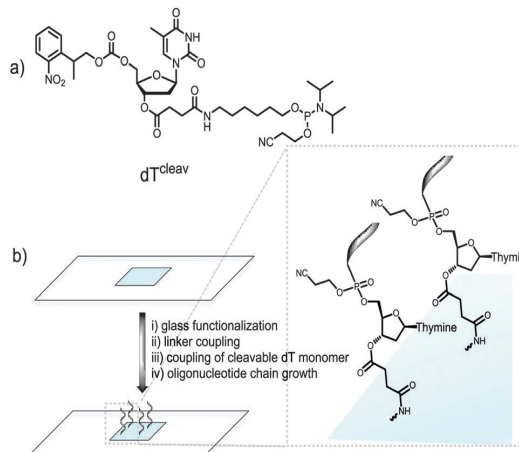


**Fig. 1** (a) Chemical structure of the cleavable dT monomer; (b) schematic illustration of the synthetic steps involved in the fabrication of microarrays containing a cleavable dT unit. Glass functionalization is performed with a silanizing reagent. The linker is typically a dT or dC pentamer chain.

in fluorescence intensity between cleavable and non-cleavable sequences (Fig. S1a, ESI<sup>†</sup>), an 85% coupling yield was calculated for dT<sup>cleav</sup>. Next, the same arrays were treated in concentrated ammonia at r.t. for 2 h and then scanned. The features where cleavable sequences were synthesized underwent a large drop in fluorescence intensity (Fig. S1b, ESI<sup>†</sup>), indicating that the ester function was correctly cleaved and release of the oligonucleotide in solution was almost complete.

We then attempted to collect the chemically-cleaved oligonucleotide. We chose to fabricate a simple dT<sub>13</sub> model sequence according to the procedure depicted in Fig. 1a. After synthesis, the microarray was deprotected in a 1:1 mixture of ethylenediamine (EDA) and toluene (Fig. 2a), an alternative to the conventionally employed EDA/ethanol in DNA array deprotection.<sup>8,26</sup> After 2 h at r.t., the array was thoroughly washed with ACN, dried and the resulting DNA was collected from the surface by applying 100  $\mu$ l of water (Fig. 2b).

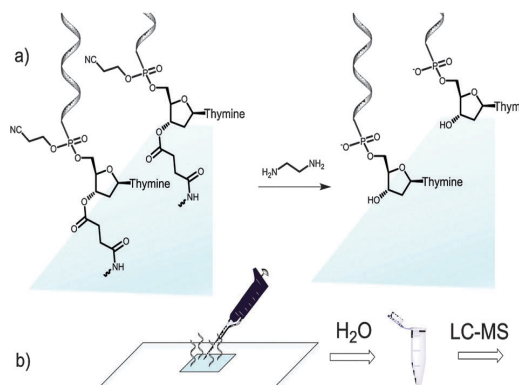


**Fig. 2** Schematic illustration of the cleave-and-collect process of oligonucleotides synthesized on microarrays. (a) DNA oligonucleotides are first deprotected in EDA/toluene 1:1, 2 h, r.t. and the microarray is then washed with ACN (2  $\times$  25 ml); (b) the DNA is then collected by pipetting 100  $\mu$ l H<sub>2</sub>O over the synthesis area. The microarray eluate is concentrated and analysed by LC-MS.

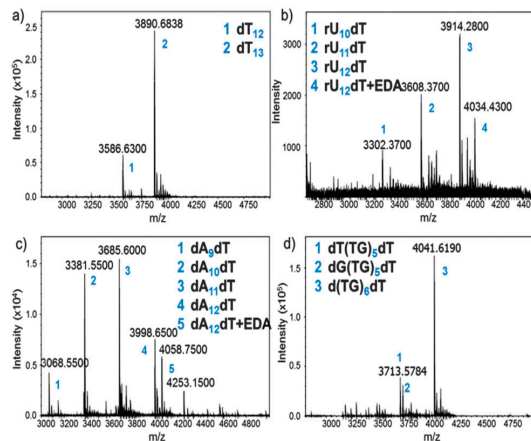


**Fig. 3** MS spectra obtained after deprotection and cleave-and-collect for the following oligonucleotides: (a) dT<sub>15</sub>; (b) rU<sub>12</sub>dT; (c) dA<sub>12</sub>dT; (d) d(TG)<sub>6</sub>dT. Exact masses are shown. EDA: ethylenediamine. Numbers (blue) are referred to in the inset of each MS spectrum.

Quantification of the isolated chip eluate revealed that 20 pmol of material were obtained, consistent with the reported density of available hydroxyl groups on the silanized surface of the substrate.<sup>17</sup> Using a duplicating method developed earlier in our laboratory where two identical arrays are simultaneously fabricated,<sup>27</sup> a single automated run yielded up to 40 pmol of deprotected DNA which were subsequently analysed by liquid chromatography (LC)-electrospray ionization (ESI)-MS.

The MS trace of the cleaved dT<sub>13</sub> is shown in Fig. 3a. The full-length product is detected as a 3'-OH species, demonstrating the correct cleavage at the 3'-ester functionality, together with a significant amount of a shortmer identified as dT<sub>12</sub>. Since the capping step in the synthetic cycle was omitted, the  $n - 1$  oligonucleotides are the result of a single failed coupling. In the absence of capping, the oligonucleotide lengths follow a binomial distribution, which allows estimating the coupling yield based on the relative heights of the MS peaks. The relative peak height in Fig. 3a indicates a 98.3% coupling yield for NPPOC-dT; somewhat lower than values previously calculated by the fluorescence method.

Our cleavage method was then applied to the detection of poly dC (Fig. S11, ESI<sup>†</sup>) and poly dA (Fig. 3c) sequences. Interestingly, the amount of  $n - 1$ ,  $n - 2$  and  $n - 3$  species in crude poly dA samples exceeds those in poly dT and dC arrays. The full-length product, dA<sub>12</sub>dT, is also present in the form of a noncovalent complex with EDA. Nucleobase deprotection is complete in both dA<sub>12</sub>dT and dC<sub>12</sub>dT cases since no trace of remaining phenoxyacetyl (Pac) or isobutyryl (iBu) groups was detected by MS. The characterization of oligonucleotide arrays was also applied to mixmers of two bases and, as shown in Fig. 3d and Fig. S13 (ESI<sup>†</sup>), MS resolution allows for the distinction between two different failure sequences.

Inspired by these results and by a previously reported procedure for the complete deprotection of RNA in EDA without facing degradation,<sup>28</sup> we wished to apply our method to RNA microarrays. A model rU<sub>12</sub>dT array was fabricated using NPPOC 2'-O-ALE rU amidites<sup>22</sup> and was then deprotected as



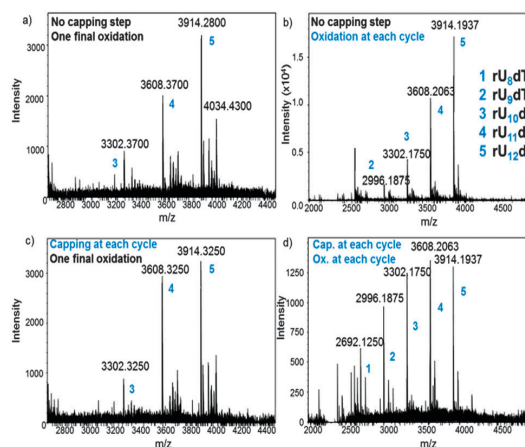


Fig. 4 MS spectra obtained after deprotection and cleave-and-collect for rU<sub>12</sub>dT microarrays under various fabrication conditions: (a) standard protocol without capping and oxidation; (b) an oxidation step is included; (c) a capping step is included; (d) both capping and oxidation steps are included. Exact masses are shown. Numbers 1–5 (blue) are all referred to in the MS spectrum (b).

follows: first, decyanoethylation was conducted in Et<sub>3</sub>N/ACN 2:3 for 6 h at r.t. then ALE removal was performed in buffered hydrazine hydrate in pyridine/AcOH for 2 h at r.t. The intact succinyl ester was finally cleaved by treating the array with dry EDA/toluene for 2 h at r.t. The crude RNA was eluted from the surface by pipetting a small volume of sterilized water, concentrated, quantified (20 pmol per array) and injected on LC-MS. The MS spectrum is shown in Fig. 3b and the major peak corresponds to the full-length, 3'-OH rU<sub>12</sub>dT, which is flanked by a minor peak at +60 Da resulting from a salt complex with EDA. This measurement offers, for the first time, a direct and concrete proof of correct *in situ* synthesis of RNA microarrays. Compared to dT<sub>13</sub> in Fig. 3a, larger amounts of *n* – 1 and *n* – 2 species are also detected, which could be due to either failed couplings or to degradation products arising from cleavage at the internucleotide phosphate. However, the presence of the *n*-mer as the main peak and the lack of 2',3'-phosphorylated shortmers suggest that degradation is limited.

In an attempt to optimize the quality of *in situ* DNA and RNA microarray fabrication, we envisaged to modify a few key parameters in the design protocols and investigate their effect by MS. We performed this study on the dT<sub>13</sub> and rU<sub>12</sub>dT models and considered four factors in the synthesis cycle: coupling time, the activator type, capping and oxidation steps. In DNA and RNA microarray synthesis by photolithography, the oxidation of the phosphite triester linkages can be conducted at the latest stage because deblocking the 5'-OH function does not require an acidic solution. The results as well as a representative panel are shown in Fig. 4 and Fig. S4–S10 (ESI<sup>†</sup>). Including an iodine/water-mediated oxidation or a capping step alone in the synthesis cycle seems to have little effect on array quality (compare Fig. 4b and c to the original array design in Fig. 4a), however when both steps are included, arrays of significantly lower quality were obtained (Fig. 4d). Next, the coupling time was examined and either shortened (from the standard 2 min

to 1 min) or extended (5 min). In both DNA and RNA microarrays, shorter or longer coupling times resulted in arrays of poorer quality (Fig. S7, S8, S19 and S20, ESI<sup>†</sup>). Finally, the conventional 4,5-dicyanoimidazole activator was substituted with tetrazole derivatives, which afforded crude array eluates containing larger amounts of failure sequences (Fig. S9, S10 and S21, ESI<sup>†</sup>).

In summary, a reliable protocol for the deprotection and subsequent cleavage of DNA and RNA microarrays with EDA was developed using a 3'-succinylated dT phosphoramidite. The cleaved DNA microarrays or RNA microarrays are insoluble in the deprotection solution and remain on the glass surface,<sup>28</sup> where they can be collected with water and analysed by LC-ESI-MS. A few picomoles of crude microarray eluates are sufficient to provide a comprehensive overview of chip quality and to monitor the effect of modifying synthesis conditions. Radio-labelling or PCR amplification of the collected DNA/RNA is thus unnecessary. In addition, our approach allows for the first time the assessment of the fidelity of *in situ* RNA microarray synthesis and will have an important impact on the emergence of high-density complex RNA array technology.

The Natural Sciences and Engineering Research Council of Canada (discovery grant to M.J.D.), the Swiss National Science Foundation (Grant #PBBEP2\_146174), The Austrian Science Fund (FWF P23797), ChemGenes Corporation and a McGill Fessenden Grant are gratefully acknowledged for financial support. We would also like to thank Dr Jeremy Lackey for fruitful discussions and FlexGen for the generous donation of the cleavable dT monomer.

## Notes and references

- 1 R. B. Stoughton, *Annu. Rev. Biochem.*, 2005, **74**, 53–82.
- 2 H. M. Fathallah-Shaykh, *Arch. Neurol.*, 2005, **62**, 1669–1672.
- 3 C. Debouck and P. N. Goodfellow, *Nat. Genet.*, 1999, **21**, 48–50.
- 4 M. Andersen, S. Warrick and C. Adams, *Microarray Innovations*, CRC Press, 2009, pp. 215–241.
- 5 D. J. Duggan, M. Bittner, Y. Chen, P. Meltzer and J. M. Trent, *Nat. Genet.*, 1999, **21**, 10–14.
- 6 R. P. Auburn, D. P. Kreil, L. A. Meadows, B. Fischer, S. S. Matilla and S. Russell, *Trends Biotechnol.*, 2005, **23**, 374–379.
- 7 M. Dufva, *Biomol. Eng.*, 2005, **22**, 173–184.
- 8 S. Singh-Gasson, R. D. Green, Y. Yue, C. Nelson, F. Blattner, M. R. Sussman and F. Cerrina, *Nat. Biotechnol.*, 1999, **17**, 974–978.
- 9 E. M. LeProust, B. J. Peck, K. Spirin, H. B. McCuen, B. Moore, E. Namsaraev and M. H. Caruthers, *Nucleic Acids Res.*, 2010, **38**, 2522–2540.
- 10 S. L. Beaucage and M. H. Caruthers, *Tetrahedron Lett.*, 1981, **22**, 1859–1862.
- 11 L. J. McBride and M. H. Caruthers, *Tetrahedron Lett.*, 1983, **24**, 245–248.
- 12 P. Jaluria, K. Konstantopoulos, M. Betenbaugh and J. Shiloach, *Microb. Cell Fact.*, 2007, **6**, 4.
- 13 G. H. McGall, A. D. Barone, M. Diggelmann, S. P. A. Fodor, E. Gentalen and N. Ngo, *J. Am. Chem. Soc.*, 1997, **119**, 5081–5090.
- 14 M. C. Pirrung, L. Fallon and G. McGall, *J. Org. Chem.*, 1998, **63**, 241–246.
- 15 C. Aghabaw, C. Kim, D. Hong, K. Heinrich, T. Wang and M. M. Somoza, *J. Nanobiotechnol.*, 2011, **9**, 57.
- 16 C. Aghabaw and M. M. Somoza, *PLoS One*, 2011, **6**, e22177.
- 17 E. LeProust, H. Zhang, P. Yu, X. Zhou and X. Gao, *Nucleic Acids Res.*, 2001, **29**, 2171–2180.
- 18 K. E. Richmond, M.-H. Li, M. J. Rodesch, M. Patel, A. M. Lowe, C. Kim, L. L. Chu, N. Venkataramaian, S. F. Flickinger, J. Kaysen, P. J. Belshaw, M. R. Sussman and F. Cerrina, *Nucleic Acids Res.*, 2004, **32**, 5011–5018.

- 19 P. Kepper, R. Reinhardt, A. Dahl, H. Lehrach and S. Sauer, *Clin. Chem.*, 2006, **52**, 1303–1310.
- 20 C. F. W. Becker, R. Wacker, W. Bouschen, R. Seidel, B. Kolaric, P. Lang, H. Schroeder, O. Müller, C. M. Niemeyer, B. Spengler, R. S. Goody and M. Engelhard, *Angew. Chem., Int. Ed.*, 2005, **44**, 7635–7639.
- 21 L. Gogolin, H. Schroeder, A. Itzen, R. S. Goody, C. M. Niemeyer and C. F. W. Becker, *ChemBioChem*, 2013, **14**, 92–99.
- 22 J. G. Lackey, D. Mitra, M. M. Somoza, F. Cerrina and M. J. Damha, *J. Am. Chem. Soc.*, 2009, **131**, 8496–8502.
- 23 J. G. Lackey, M. M. Somoza, D. Mitra, F. Cerrina and M. J. Damha, *Chim. Oggi*, 2009, **27**, 30–33.
- 24 K. Maurer, D. Suciú and H. Gao, *US Pat.*, US20090280998 A1, 2009.
- 25 N. L. W. Franssen-van Hal, P. van der Putte, K. Hellmuth, S. Matysiak, N. Kretschy and M. M. Somoza, *Anal. Chem.*, 2013, **85**, 5950–5957.
- 26 E. F. Nuwaysir, W. Huang, T. J. Albert, J. Singh, K. Nuwaysir, A. Pitas, T. Richmond, T. Gorski, J. P. Berg, J. Ballin, M. McCormick, J. Norton, T. Pollock, T. Sumwalt, L. Butcher, D. Porter, M. Molla, C. Hall, F. Blattner, M. R. Sussman, R. L. Wallace, F. Cerrina and R. D. Green, *Genome Res.*, 2002, **12**, 1749–1755.
- 27 M. Sack, N. Kretschy, B. Rohm, V. Somoza and M. M. Somoza, *Anal. Chem.*, 2013, **85**, 8513–8517.
- 28 D. J. Dellinger, Z. Timár, J. Myerson, A. B. Sierzchala, J. Turner, F. Ferreira, Z. Kupihár, G. Dellinger, K. W. Hill, J. A. Powell, J. R. Sampson and M. H. Caruthers, *J. Am. Chem. Soc.*, 2011, **133**, 11540–11556.

# Comparison of the Sequence-Dependent Fluorescence of the Cyanine Dyes Cy3, Cy5, DyLight DY547 and DyLight DY647 on Single-Stranded DNA

Nicole Kretschy, Mark M. Somoza\*

Institute of Inorganic Chemistry, University of Vienna, Vienna, Austria

## Abstract

Cyanine dyes are commonly used for fluorescent labeling of DNA and RNA oligonucleotides in applications including qPCR, sequencing, fluorescence *in situ* hybridization, Förster resonance energy transfer, and labeling for microarray hybridization. Previous research has shown that the fluorescence efficiency of Cy3 and Cy5, covalently attached to the 5' end of single-stranded DNA, is strongly sequence dependent. Here, we show that DY547 and DY647, two alternative cyanine dyes that are becoming widely used for nucleic acid labeling, have a similar pattern of sequence-dependence, with adjacent purines resulting in higher intensity and adjacent cytosines resulting in lower intensity. Investigated over the range of all 1024 possible DNA 5mers, the intensities of Cy3 and Cy5 drop by ~50% and ~65% with respect to their maxima, respectively, whereas the intensities of DY547 and DY647 fall by ~45% and ~40%, respectively. The reduced magnitude of change of the fluorescence intensity of the DyLight dyes, particularly of DY647 in comparison with Cy5, suggests that these dyes are less likely to introduce sequence-dependent bias into experiments based on fluorescent labeling of nucleic acids.

**Citation:** Kretschy N, Somoza MM (2014) Comparison of the Sequence-Dependent Fluorescence of the Cyanine Dyes Cy3, Cy5, DyLight DY547 and DyLight DY647 on Single-Stranded DNA. PLoS ONE 9(1): e85605. doi:10.1371/journal.pone.0085605

**Editor:** Cynthia Gibas, University of North Carolina at Charlotte, United States of America

**Received:** July 31, 2013; **Accepted:** November 28, 2013; **Published:** January 15, 2014

**Copyright:** © 2014 Kretschy, Somoza. This is an open-access article distributed under the terms of the Creative Commons Attribution License, which permits unrestricted use, distribution, and reproduction in any medium, provided the original author and source are credited.

**Funding:** Funding by the University of Vienna, the Faculty of Chemistry of the University of Vienna, and the Austrian Science Fund (FWF P23797) is gratefully acknowledged. The funders had no role in study design, data collection and analysis, decision to publish, or preparation of the manuscript.

**Competing Interests:** The authors have declared that no competing interests exist.

\* E-mail: mark.somoza@univie.ac.at

## Introduction

Fluorescent readout from labeled nucleic acids on solid surfaces or in solution is a common element in a broad range of biotechnological and biophysical methodologies. In most cases, such as in microarray experiments, sequencing-by-synthesis, qPCR, and fluorescence *in situ* hybridization (FISH), the objective is to quantify the abundance of the labeled molecule. In the case of Förster resonance energy transfer (FRET), the magnitude of the transfer of fluorescence energy can be used to determine the distance and/or relative angular orientations between the donor and acceptor. In all of these cases, changes in the fluorescence efficiency of the dye, due to sequence-specific interactions with the labeled strand of DNA or RNA may introduce biases into measurements, either because the measured fluorescence intensity is not proportional to the number of labeled molecules or, in the case of FRET, because the nucleobases between the donor and acceptor are modulating the intensity via an alternative physical process. Previous experiments have shown that the fluorescence of the cyanine dyes Cy3 and Cy5, which are commonly used in nucleic acid labeling applications, are very sensitive to their nucleobase environment, both to nucleobases in solution [1], and covalently bound to the 5' termini of both single- [2], [3] and double-stranded DNA [4].

The cyanine dyes are highly fluorescent molecules that can be modified to cover a wide spectral range, allowing for multiplexing in high-throughput applications. Unlike other classes of dyes, such as the fluorescein and rhodamine derivatives, cyanine dyes are not

quenched by photoinduced charge-transfer interactions with nucleobases, but they are vulnerable to loss of fluorescence due to excited state *cis-trans* isomerization about the linkage between the two indole rings [5]. Cy3 is known to bind to nucleobase monophosphates in solution, and both Cy3 and Cy5 have been shown to stack on the end of double-stranded DNA, like a terminal base pair [6], [7]. This affinity appears to be driven by  $\pi$ -stacking interactions with nucleobases, which also restricts the rotational isomerization of the dyes and increases their fluorescence. The mechanism responsible for sequence-specific fluorescence of oligonucleotides labeled with cyanine dyes is not known, but more rigid base stacks may enhance the ability of the terminal nucleobase to hinder dye isomerization. The rigidity of the base stack is largely determined by its purine content [8], [9] because purines have a larger stacking area and higher free energy for stacking [10], [11], [12].

Our previous results for sequence-dependent fluorescence of Cy3 and Cy5 covalently bound to the 5' end of ssDNA demonstrated that a high purine content results in high intensity analogously to how high GC content results in high melting temperature for complementary sequences; the GA or CT content function almost as random variables, leading to probability distributions that are close to normal distributions [2]. Superimposed on this pattern is, in the brightest sequences, an overrepresentation of dG at the 5' end and an overrepresentation of dA in subsequent positions, and an overrepresentation of dC at the 5' end of the darkest sequences. Experiments with the same sequences, but with a 5' biotin phosphoramidite and subsequent

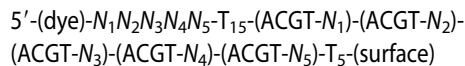
labeling with Cy3- or Cy5- conjugated streptavidin, resulted in a much stronger sequence-dependent fluorescence [2]. One possible explanation for the differences between the results with direct labeling with dye phosphoramidites and indirect labeling via dye-streptavidin-biotin conjugates is that the dye-DNA interactions are highly sensitive to apparently minor changes to the dye structure or tethering mechanism.

The experiments presented here were motivated by an interest to establish the parameters affecting the sequence-dependent fluorescence of cyanine dyes. The DyLight cyanine dyes DY547 and DY647 are structurally similar to Cy3 and Cy5, but differ in how they are tethered to the DNA (Figure 1). In addition, the Cy3 and Cy5 phosphoramidites also include the monomethoxytrityl (MMT) group to allow either 3' labeling, or reverse-phase HPLC purification. The MMT group may affect how the dyes interact with DNA. We were also interested in evaluating whether DY547 and DY647 can be used as direct replacements for Cy3 and Cy5 in sensitive terminal-labeling experiments. Some labeling applications, such as those based 5'-labeled random primers, or amino allyl-dUTP or dye-dNTPs labels randomly incorporated during reverse transcription, should be mostly insensitive to sequence-dependent fluorescence, due to the quasi-random nature of the labeling, but in methods based on labeling of specific sequences, changes in the sequence dependency would affect the results. Beyond improving the accuracy of experiments based on fluorescence labeling of nucleic acids, an understanding of the sequence-dependency of dyes may lead to insights into sequence-specific biophysical properties of nucleic acids, such as DNA rigidity, which affects DNA-protein interactions [13], [14], [15].

## Methods

The *in situ* synthesis of microarrays, including combinatorial arrays of fluorescently labeled ssDNA has been described in detail previously [2], [16], [17], [18], [19], [20]. Briefly, maskless array synthesis (MAS) [21], was used to produce microarrays with 20 or 21 replicates of each of the 1024 5'-labeled experimental

sequences. Dye phosphoramidites (Figure 1) were purchased from Glen Research. In order to produce data unbiased by the different coupling efficiencies of the four DNA phosphoramidites, the following sequence design was used:



The  $N_i$  represent the 5-mer experimental sequences. These are separated by a 15-thymidine linker from a 15-mer with bases customized as shown, that is, with each of the experimental bases subtracted from five copies of sets of all four DNA bases. This design, in conjunction with acetic anhydride capping following each coupling, ensures that all of the sequences which receive the 5'-dye will have the design sequence, which includes the same number of each base, and hence, each experimental sequence has equal number density on the microarray surface. The 15-thymidine linker was chosen to minimize possible long-distance through-the-stack interactions with the downstream nucleobases used to ensure homogenize sequence number density.

After synthesis, the microarrays were vigorously washed for 2 h with acetonitrile to remove traces of dye phosphoramidite from the glass surface. Protecting groups were removed in 2 h with a 1:1 (v/v) solution of ethylenediamine in ethanol. The microarrays were then washed twice with distilled water, dried with argon and immediately scanned using GenePix 4100A. Fluorescence intensity values were extracted from the scan images using NimbleScan v2.1. The fluorescence intensity values were calculated as the average of the 20 or 21 replicates of each sequence, which were randomly arranged on each microarray. Error was calculated as the standard error of the mean (SEM). The consensus sequence logos were generated by ranking the 1024 sequences by fluorescence intensity and then dividing the sequences into eight bins spanning equal ranges of intensity. Consensus logos for each of these octiles of fluorescence intensity were generated using Weblogo (weblogo.berkeley.edu) [22].

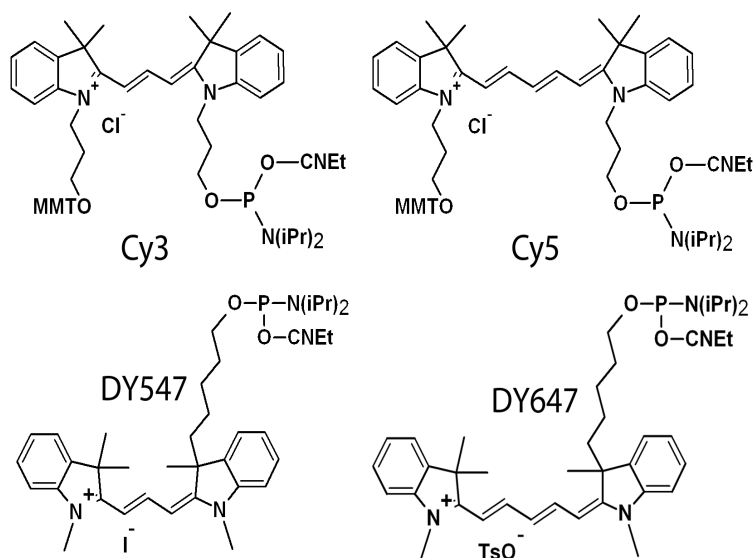


**Figure 1. Molecular structures of the cyanine dye phosphoramidites used in this study: Cy3, Cy5, DY547 and DY647.** Monomethoxytrityl (MMT) groups are present on the Cy-dyes; the 2-cyanoethyl group (CNEt) is the standard phosphate protecting group in oligonucleotide synthesis, and the diisopropyl group (N(iPr)<sub>2</sub>) is displaced during the coupling reaction by the 5'-hydroxyl group to form a phosphate linkage between the terminal nucleoside and the dye.  
doi:10.1371/journal.pone.0085605.g001

## Results and Discussion

All four of the cyanine dyes studied, Cy3, Cy5, DY547 and DY647, interact very similarly with DNA. For all of the dyes, the consensus sequences resulting in the highest fluorescence begin with a 5' guanine followed by multiple adenines; the consensus sequences resulting in the lowest fluorescence always start with a 5' cytosine (Figure 2). While the consensus logos are quite similar for all of the dyes, there are some differences between the Cy-dyes and the DY-dyes. Adenine is almost never found in the least fluorescent Cy-labeled sequences, but does appear in the least fluorescent DY-labeled sequences, particularly in the case of DY547. Cytosine is more common among the brightest DY-labeled sequences compared to the Cy-labeled sequences. Conversely, thymine is often found among the brightest Cy-labeled sequences, but rarely among the brightest DY-labeled sequences.

Although all of the dyes have similar sequence dependence, the magnitude of change of the fluorescence intensity of the DY dyes, over the range of all 1024 sequences, is smaller than that of the Cy dyes, particularly Cy5 (Figure 2B & E). The fluorescence intensity of DY547 falls by ~45% from the brightest (GAAAA) to the least bright sequence (CGTGT). By comparison, the intensity of Cy3 falls slightly more, ~50% over the same range. In the case of Cy3, the brightest of all 1024 sequences is also GAAAA, but the darkest, CGGTT, is similar but not identical. The dye DY647 has the smallest range of fluorescent intensity, which drops by ~40% over the range of all 5-mers. The brightest of the DY647 sequences is GGGGT, highlighting that the consensus sequence for the brightest DY647-labeled DNA oligomers is different from those of the other three dyes (all **GAAAA**); specifically, the 5'-guanine

remains important, but adenines are not dominant in subsequent positions. The darkest Cy5- and DY647-labeled sequence are CGGTC and CTTTT, respectively. In the case of DY647, the darkest sequence is an exact match to the consensus sequence for the lowest octant of fluorescence. The fluorescence intensity of all 1024 5-mers for all four dyes is provided as Data S1 in spreadsheet format as Supporting Information. The individual logos used to make Figure 2 are shown in Figure S1.

We have previously hypothesized that sequence-specific fluorescence results from stacking interactions that modulate the rate of rotational isomerization. The current data is consistent with that hypothesis. Guanine has the largest calculated stacking area, based on B-form stacking geometry: dG (139 Å<sup>2</sup>)>dA (128 Å<sup>2</sup>)>dC (102 Å<sup>2</sup>)>dT (95 Å<sup>2</sup>) [11], and cyanine dyes have the greatest fluorescence in solution along with dG homopolymers [23] and in solution with guanosine monophosphates [1], relative to the other three nucleobases. This suggests that a 5' guanosine is important for fluorescence because this base preferentially stacks with cyanine dyes and restricts fluorescence quenching due to rotational isomerization. Based on the stacking area calculations, a 5' thymine would be predicted to result in the lowest fluorescence, but both the homopolymer and nucleoside monophosphate data indicate that cytosine results in the lowest fluorescence of cyanine dyes, in agreement with all the data presented here. The more distal nucleobases may stabilize or destabilize the interaction of the 5' nucleobase with the dye. It is known that purine stacks in single-stranded DNA are more rigid than pyrimidine stacks and that mixed purine-pyrimidine stacks have intermediate rigidity [8], [9]. Distinctions between purines or between pyrimidines are more

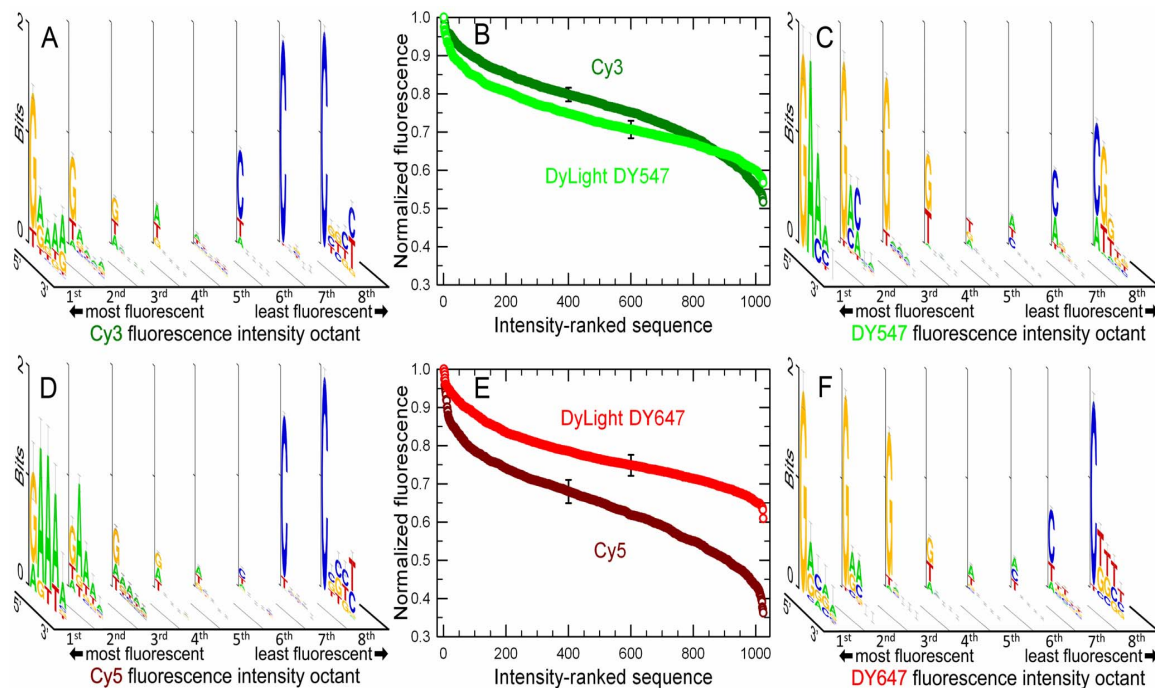


**Figure 2. Fluorescence intensity of cyanine-labeled single-stranded DNA.** (A) Fluorescence intensity consensus sequence logos of all 1024 ssDNA 5-mers labeled with a 5' Cy3 phosphoramidite. Each consensus logo corresponds to those sequences spanning one eighth of the intensity range. (B) Fluorescence intensity of Cy3 and DY547 end-labeled 5-mers, ranked from most to least intense. The Cy3 curve drops by about 50% of the maximum intensity, while the DY547 curve drops about 45%. (C) Consensus sequence logos of all 1024 ssDNA 5-mers labeled with a 5' DY547 phosphoramidite. (D) Consensus sequence logos of all 1024 ssDNA 5-mers labeled with a 5' Cy5 phosphoramidite. (E) Fluorescence intensity of Cy5 and DY647 end-labeled 5-mers, ranked from most to least intense. The Cy5 curve drops by about 65% of the maximum intensity, while the DY647 curve drops about 40%. (F) Consensus sequence logos of all 1024 ssDNA 5-mers labeled with a 5' DY647 phosphoramidite. The single error bars (SEM) on each curve are representative. The z-axis height measures the information content at each site in units of bits. doi:10.1371/journal.pone.0085605.g002

ambiguous. The stacking energy  $\Delta\Delta G^\circ$ , based on ssDNA to dsDNA equilibrium experiments, follows the order  $dA \gg dG > dT \approx dC$  (2.0, 1.3, 1.1 and 1.0 kcal/mol, all  $\pm 0.2$ ) [11], which is consistent with the dominance of adenine in distal positions of the consensus logos for the brightest sequences. However, experiments based on 3' dangling bases have indicated that dA and dG stabilize the stack approximately equally [10], [12]. Although the hypothesis is that stacking interactions are responsible for the observed sequence-dependent fluorescence, deviations from the expected trend suggest that other mechanism also influence dye intensity. For example, dT and dC are occasionally present in the brightest Cy-dye and DY-dye sequences, respectively, and although pyrimidines dominate the darkest sequences, dG is also relatively abundant in distal positions, and DY547 even has a significant representation of dA at the 5' position.

Another of the objectives of the project presented here was to evaluate if the DY-dyes can be used to replace Cy-dyes in experiments that may be sensitive to sequence-dependent fluorescence, such as using fluorescence intensity to quantify the relative abundance of specific nucleic acid sequences. The absorption and emission spectra of Cy3 and DY547, and Cy5 and DY647 are essentially identical, and the DY-dyes have a slightly higher quantum yield [24], but large differences in the pattern of sequence-dependent fluorescence could result in shifts of the relative intensities when substituting dyes. The results presented here indicate that intensities of some labeled sequences would shift, for example, the sequences Cy3-TATAA and Cy5-TATAA are among the brightest, 2<sup>nd</sup> and 13<sup>th</sup> brightest, respectively, while DY547-TATAA and DY647-TATAA are significantly darker, with a rank of 81<sup>st</sup> and 242<sup>nd</sup>, respectively. Nevertheless, since the overall consensus sequence patterns are similar, the relative intensities of most sequences would only change modestly. A significant motivation for using the DY-dyes instead of the Cy-dyes is that the intensity difference between the brightest and darkest sequences are smaller, particularly in comparison with Cy5, so that the probability that a randomly chosen sequence will result in poor fluorescence is lower. To some extent, even applications based on random labeling, for example, genomic DNA or RNA labeling using 5'-labeled random nonamers [25], are subject to sequence-dependent fluorescence biases due to the variable nucleobase content of genes [26]. Quantitative PCR experiments

based on fluorescent reporter oligonucleotides (Molecular beacon or TaqMan probes) are significantly more vulnerable to sequence-dependent fluorescence since a single reporter sequence is chosen for each reaction. Standard curves can at least partially compensate for such biases, but poorly fluorescent reporter probes will inevitably degrade data quality. High-throughput DNA sequencing-by-synthesis is likely to be particularly vulnerable to sequence-dependent fluorescence because all short nucleobase sequences will be repeatedly encountered, and detection failures (deletion errors) from sequences highly unfavorable to fluorescence would be systematic and therefore not detectable with re-sequencing. Furthermore, the optical systems of sequencers need to balance dynamic range of detection with throughput, making them vulnerable to dyes with significant variations in fluorescence [27].

In conclusion, combinatorial microarrays of labeled DNA can effectively determine patterns of sequence-dependent fluorescence. Applying this method to commonly used cyanine dyes indicates that DY547 and DY647 are less likely to result in sequence-dependent labeling artifacts in comparison to Cy3 and Cy5. While many properties of dyes, such as quantum yield, photostability and sensitivity to a variety of environmental factors, can affect signal intensity, sequence-dependent fluorescence may be more likely to introduce systematic biases into experimental results.

## Supporting Information

**Figure S1 Fluorescence intensity consensus logos from Figure 2.** Individual consensus logos for Cy3, DY547, Cy5 and DY647. From left to right, the logos represent each of the eight bins in order of decreasing fluorescence intensity.

(TIF)

**Data S1 Fluorescence intensity data (sequence, normalized intensity, SEM) for all labeling methods in spreadsheet format.**

(XLS)

## Author Contributions

Conceived and designed the experiments: MMS. Performed the experiments: NK. Analyzed the data: NK MMS. Wrote the paper: NK MMS.

## References

- Harvey BJ, Levitus M (2009) Nucleobase-Specific Enhancement of Cy3 Fluorescence. *Journal of Fluorescence* 19: 443–448.
- Aghavwe C, Somoza MM (2011) Sequence-Dependent Fluorescence of Cyanine Dyes on Microarrays. *PLoS ONE* 6: e22177.
- Harvey BJ, Perez C, Levitus M (2009) DNA sequence-dependent enhancement of Cy3 fluorescence. *Photochemical & Photobiological Sciences* 8: 1105–1110.
- Spiriti J, Binder JK, Levitus M, van der Vaart A (2011) Cy3-DNA Stacking Interactions Strongly Depend on the Identity of the Terminal Basepair. *Biophysical Journal* 100: 1049–1057.
- Luby-Phelps K, Mujumdar S, Mujumdar RB, Ernst LA, Galbraith W, et al. (1993) A Novel Fluorescence Ratiometric Method Confirms the Low Solvent Viscosity of the Cytoplasm. *Biophysical Journal* 65: 236–242.
- Iqbal A, Wang L, Thompson KC, Lilley DMJ, Norman DG (2008) The Structure of Cyanine 5 Terminally Attached to Double-Stranded DNA: Implications for FRET Studies. *Biochemistry* 47: 7857–7862.
- Norman DG, Grainger RJ, Uhrin D, Lilley DMJ (2000) Location of cyanine-3 on double-stranded DNA: Importance for fluorescence resonance energy transfer studies. *Biochemistry* 39: 6317–6324.
- Sain A, Chen JZY, Ha B-Y (2006) Persistency of single-stranded DNA: The interplay between base sequences and base stacking. *Physica A: Statistical Mechanics and its Applications* 369: 679–687.
- Solie TN, Schellman JA (1968) The interaction of nucleosides in aqueous solution. *Journal of Molecular Biology* 33: 61–77.
- Doktycz MJ, Paner TM, Amarantunga M, Benight AS (1990) Thermodynamic stability of the 5' dangling-ended DNA hairpins formed from sequences 5'-(XY)<sub>2</sub>GGATAC(T)<sub>4</sub>GTATCC-3', where X, Y = A,T,G,C. *Biopolymers* 30: 829–845.
- Guckian KM, Schweitzer BA, Ren RX-F, Sheils CJ, Tahmassebi DC, et al. (2000) Factors Contributing to Aromatic Stacking in Water: Evaluation in the Context of DNA. *Journal of the American Chemical Society* 122: 2213–2222.
- Turner DH, Sugimoto N, Freier SM (1988) RNA Structure Prediction. *Annual Review of Biophysics and Biophysical Chemistry* 17: 167–192.
- Geggier S, Vologodskii A (2010) Sequence dependence of DNA bending rigidity. *Proceedings of the National Academy of Sciences* 107: 15421–15426.
- Ruan Q, Liu T, Kolbanovskiy A, Liu Y, Ren J, et al. (2007) Sequence Context- and Temperature-Dependent Nucleotide Excision Repair of a Benzo[a]pyrene Diol Epoxide-Guanine DNA Adduct Catalyzed by Thermophilic UvrABC Proteins. *Biochemistry* 46: 7006–7015.
- Sugasawa K, Shimizu Y, Iwai S, Hanaoka F (2002) A molecular mechanism for DNA damage recognition by the xeroderma pigmentosum group C protein complex. *DNA repair* 1: 95–107.
- Aghavwe C, Kim C, Hong D, Heinrich K, Wang T, et al. (2011) Efficiency, Error and Yield in Light-Directed Maskless Synthesis of DNA Microarrays. *Journal of Nanobiotechnology* 9:57.
- Franssen-van Hal NLW, van der Putte P, Hellmuth K, Matysiak S, Kretschy N, et al. (2013) Optimized Light-Directed Synthesis of Aptamer Microarrays. *Analytical Chemistry* 85: 5950–5957.
- Lackey JG, Mitra D, Somoza MM, Cerrina F, Damha MJ (2009) Acetal Levulinyl Ester (ALE) Groups for 2'-Hydroxyl Protection of Ribonucleosides in

- the Synthesis of Oligoribonucleotides on Glass and Microarrays. *Journal of the American Chemical Society* 131: 8496–8502.
19. Lackey JG, Somoza MM, Mitra D, Cerrina F, Damha MJ (2009) In-situ chemical synthesis of rU-DNA chimeras on chips and enzymatic recognition. *Chimica Oggi-Chemistry Today* 27: 30–33.
  20. Sack M, Kretschy N, Rohm B, Somoza V, Somoza MM (2013) Simultaneous Light-Directed Synthesis of Mirror-Image Microarrays in a Photochemical Reaction Cell with Flare Suppression. *Analytical Chemistry* 85: 8513–8517.
  21. Singh-Gasson S, Green RD, Yue YJ, Nelson C, Blattner F, et al. (1999) Maskless fabrication of light-directed oligonucleotide microarrays using a digital micromirror array. *Nature Biotechnology* 17: 974–978.
  22. Schneider TD, Stephens RM (1990) Sequence logos: a new way to display consensus sequences. *Nucleic Acids Research* 18: 6097–6100.
  23. Mikelsons L, Carra C, Shaw M, Schweitzer C, Scaiano JC (2005) Experimental and theoretical study of the interaction of single-stranded DNA homopolymers and a monomethine cyanine dye: nature of specific binding. *Photochemical & Photobiological Sciences* 4: 798–802.
  24. Glen Research (2009) The Glen Report: NEW FLUORESCENT PHOSPHORAMIDITES - SIMA (HEX), DYLIGHT <http://www.glenresearch.com/GlenReports/GR21-110.html>. Accessed 1 July 2013.
  25. De Backer MD, Ilyina T, Ma X-J, Vandoninck S, Luyten WH, et al. (2001) Genomic profiling of the response of *Candida albicans* to itraconazole treatment using a DNA microarray. *Antimicrobial agents and chemotherapy* 45: 1660–1670.
  26. Jeon H, Choi S (2007) Fluorescence quenching causes systematic dye bias in microarray experiments using cyanine dye. *Genomics & Informatics* 5: 113–117.
  27. Fuller CW, Middendorf LR, Benner SA, Church GM, Harris T, et al. (2009) The challenges of sequencing by synthesis. *Nature Biotechnology* 27: 1013–1023.



## Nonivamide Enhances miRNA let-7d Expression and Decreases Adipogenesis PPAR $\gamma$ Expression in 3T3-L1 Cells

Barbara Rohm,<sup>1,2</sup> Ann-Katrin Holik,<sup>2</sup> Nicole Kretschy,<sup>3</sup> Mark M. Somoza,<sup>3</sup> Jakob P. Ley,<sup>4</sup> Sabine Widder,<sup>4</sup> Gerhard E. Krammer,<sup>4</sup> Doris Marko,<sup>5</sup> and Veronika Somoza<sup>1,2\*</sup>

<sup>1</sup>Christian Doppler Laboratory for Bioactive Aroma Compounds, Althanstraße 14, 1090 Vienna, Austria

<sup>2</sup>Department of Nutritional and Physiological Chemistry, Althanstraße 14, 1090 Vienna, Austria

<sup>3</sup>Department of Inorganic Chemistry, University of Vienna, Währinger Straße 42, Vienna, Austria

<sup>4</sup>Symrise AG, Mühlenfeldstraße, Holzminden, Germany

<sup>5</sup>Department of Food Chemistry and Toxicology, University of Vienna, Währinger Straße 38, Vienna, Austria

### ABSTRACT

Red pepper and its major pungent principle, capsaicin (CAP), have been shown to be effective anti-obesity agents by reducing energy intake, enhancing energy metabolism, decreasing serum triacylglycerol content, and inhibiting adipogenesis via activation of the transient receptor potential cation channel subfamily V member 1 (TRPV1). However, the binding of CAP to the TRPV1 receptor is also responsible for its pungent sensation, strongly limiting its dietary intake. Here, the effects of a less pungent structural CAP-analog, nonivamide, on adipogenesis and underlying mechanisms in 3T3-L1 cells were studied. Nonivamide was found to reduce mean lipid accumulation, a marker of adipogenesis, to a similar extent as CAP, up to 10.4% ( $P < 0.001$ ). Blockage of the TRPV1 receptor with the specific inhibitor *trans-tert*-butylcyclohexanol revealed that the anti-adipogenic activity of nonivamide depends, as with CAP, on TRPV1 receptor activation. In addition, in cells treated with nonivamide during adipogenesis, protein levels of the pro-adipogenic transcription factor peroxisome-proliferator activated receptor  $\gamma$  (PPAR $\gamma$ ) decreased. Results from miRNA microarrays and digital droplet PCR analysis demonstrated an increase in the expression of the miRNA mmu-let-7d-5p, which has been associated with decreased PPAR $\gamma$  levels. J. Cell. Biochem. 116: 1153–1163, 2015. © 2015 Wiley Periodicals, Inc.

**KEY WORDS:** *trans-tert*-BUTYLCYCLOHEXANOL; LIPID ACCUMULATION; 3T3-L1 ADIPOGENESIS; CELL DIFFERENTIATION; microRNA; PEROXISOME PROLIFERATOR-ACTIVATED RECEPTOR (PPAR); TRPV1

Adipose tissue plays a key role in metabolic homeostasis via secretion of adipokines, which interact with central and peripheral organs [Harwood, 2012]. Pathophysiological overgrowth of adipose tissue is associated with overweight, obesity, and subsequent diseases like diabetes type II, chronic inflammation, dementia, and macrovascular diseases [Kivipelto et al., 2005; Wahlqvist, 2005]. One possible mean to regulate total fat mass is

to reduce adipogenesis [Bray and Tartaglia, 2000], the differentiation of pre-adipocytes to mature adipocytes [Hausman et al., 2001], which determines the total number of adipocytes. This process starts during embryonic development, and white adipose tissue largely expands postnatal [Poissonnet et al., 1984]. However, adults are also capable of adipogenesis [Hausman et al., 2001]; about 10% of adipocytes are renewed per year, [Spalding et al., 2008] making the

Abbreviations: BCH, *trans-tert*-butylcyclohexanol; miRNA, microRNA; TRPV1, transient receptor potential cation channel subfamily V member 1.

Conflict of interest: The authors S. Widder, J.P. Ley, and G.E. Krammer are employees at Symrise AG, Holzminden, Germany.

Grant sponsor: The Austrian Federal Ministry of Economy, Family and Youth, the Austrian National Foundation for Research, Technology and Development, and the Austrian Science Fund; Grant number: FWF P23797; Grant sponsor: Christian Doppler Laboratory for Bioactive Aroma Compounds.

\*Correspondence to: Veronika Somoza, Department of Nutritional and Physiological Chemistry, Christian Doppler Laboratory for Bioactive Aroma Compounds, University of Vienna, Althanstraße 14, 1090 Vienna, Austria.

E-mail: Veronika.Somoza@univie.ac.at

Manuscript Received: 1 August 2014; Manuscript Accepted: 17 December 2014

Accepted manuscript online in Wiley Online Library (wileyonlinelibrary.com): 21 February 2015

DOI 10.1002/jcb.25052 • © 2015 Wiley Periodicals, Inc.



regulation of adipogenesis an interesting target in body weight maintenance.

Capsaicin (CAP), the most abundant capsaicinoid in red pepper, has been shown to be an effective anti-obesity agent. CAP reduces energy intake [Yoshioka et al., 1999], enhances energy metabolism, and decreases serum triacylglycerol content [Kawada et al., 1986]. In vitro, CAP has been demonstrated to inhibit adipogenesis in 3T3-L1 cells [Hsu and Yen, 2007], a widely studied in vitro model for the differentiation of pre-adipocytes to adipocytes. The anti-adipogenic activity in 3T3-L1 cells is accompanied by decreased peroxisome-proliferator activated receptor (PPAR $\gamma$ ), C/EBP $\alpha$ , and leptin expression [Hsu and Yen, 2007]. Using transient receptor potential cation channel subfamily V member 1 (TRPV1) deficient 3T3-L1 cells and knock-out mice, Zhang et al. [2007] demonstrated that prevention of adipogenesis depends on the activation of the TRPV1. However, binding of CAP to the TRPV1 receptor is also responsible for the pungency of CAP, limiting its dietary intake. This study focuses on the adipogenesis effects of the less pungent CAP-analog, nonivamide.

Nonivamide, which naturally occurs in *Capsicum oleoresin* as a minor component [Constant et al., 1996], is a direct structural analog of CAP (Fig. 1). It differs from CAP by one methyl group and one double bond on the carbon chain, and exhibits a markedly reduced TRPV1 binding affinity. An EC<sub>50</sub> value of 0.7  $\mu$ M for pure CAP has been calculated [Caterina et al., 1997], whereas twice as much of nonivamide is needed for the same effect (EC<sub>50</sub> = 1.4  $\mu$ M) [Thomas et al., 2011]. The decrease in TRPV1 binding affinity is accompanied by a major decrease in pungency; pure CAP is rated with 16,000,000 Scoville Heat Units (SHU), whereas nonivamide is rated at 9,200,000 SHUs [Haas et al., 1997]. To investigate the hypothesis, that the less pungent capsaicinoid nonivamide may produce anti-adipogenic activities similar to those of CAP, lipid accumulation after treatment with CAP and nonivamide was assessed in well-defined

pre-adipocytes, 3T3-L1 cells, as a model [Green and Kehinde, 1975]. The process of adipogenesis in 3T3-L1 cells is well investigated. After reaching confluence, contact inhibition leads to a growth arrest in 3T3-L1 pre-adipocytes. A standard hormone cocktail containing insulin, cAMP analogs, and glucocorticoids starts mitotic clonal expansion, involving replication of pre-adipocytes before terminal differentiation to adipocytes [Gregoire et al., 1998]. This process is regulated by a transcriptional cascade, which involves, but is not limited to peroxisome proliferator-activated receptor  $\gamma$  (PPAR $\gamma$ ), CCAAT-enhancer binding protein (C/EBP)  $\alpha$ ,  $\beta$ , and  $\delta$  and the transcription factors E2F1 and 4 [Rosen and Spiegelman, 2000; Farmer, 2006]. In this process, PPAR $\gamma$  and C/EBP $\alpha$  cross-activate each other through C/EBP regulatory elements, leading to the transcription of a large group of genes that finally produce the adipocyte phenotype [Clarke et al., 1997]. However, the involvement of several microRNAs (miRNAs) in the regulation of adipogenesis has also been demonstrated [McGregor and Choi, 2011]. miRNAs are small non-coding RNAs that repress translation and/or promote the decay of its target mRNA by binding to it, hence controlling physiological processes including metabolism, cell proliferation and differentiation [Eulalio et al., 2008]. For instance, the ectopic expression of pro-adipogenic miR-103 revealed an up-regulation of PPAR $\gamma$ <sub>2</sub>, which probably mediates the pro-adipogenic effects of miR-103 [Xie et al., 2009]. On the other hand, miR-27b was shown to directly target PPAR $\gamma$ , whose decreased expression led to an impaired adipogenesis [Karbiener et al., 2009]. However, also miR-143 and let-7a have been associated with an increased or decreased, respectively, of PPAR $\gamma$  expression [Esau et al., 2004; Sun et al., 2009].

In order to elucidate mechanisms by which the CAP analog nonivamide may regulate adipogenesis in 3T3-L1 cells, the dependency of the anti-adipogenic effects by CAP and nonivamide on TRPV1-receptor activation was examined using the specific TRPV1-inhibitor *trans-tert*-butylcyclohexanol (BCH) [Kueper et al., 2010]. In addition, PPAR $\gamma$  expression, which has previously been described as a target of CAP [Hsu and Yen, 2007], was determined at both the levels of gene expression regulation and protein abundance. To elucidate miRNA involvement in the effect of nonivamide, a genome-wide miRNA expression analysis was performed by means of a custom-made microarray. Effects for selected members of the *mmu-let-7* group were validated using digital droplet PCR.

## MATERIALS AND METHODS

### MATERIALS

Nonivamide and BCH were kindly provided by Symrise AG. Unless stated otherwise, all other chemicals were obtained from Sigma-Aldrich (Austria). Mouse fibroblasts (3T3-L1) were purchased at ATCC.

### CELL CULTURE

3T3-L1 pre-adipocytes cells were maintained in DMEM supplemented with 10% fetal bovine serum, 4% (v/v) L-glutamine and 1% (v/v) penicillin/streptomycin at 37°C and 5% CO<sub>2</sub> in a humidified atmosphere. Cells were passaged at ~75% to 80% confluence and used between passage 6 and 20.

Differentiation into adipocytes was carried out as described before [Riedel et al., 2012]. Briefly, differentiation was initiated 2 days

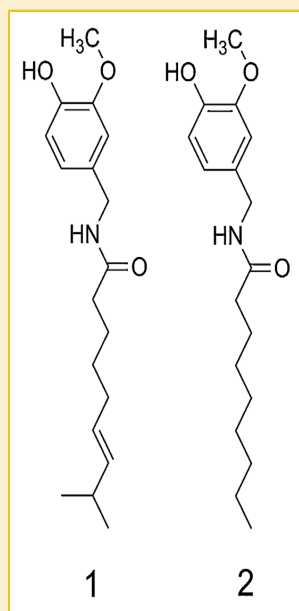


Fig. 1. Chemical structures of capsaicin (1) and its analog nonivamide (2).

post-confluence (Day 0) via the addition of differentiation media, consisting of growth medium supplemented with 0.5 mM 3-isobutyl-1-methylxanthine, 1  $\mu$ M dexamethasone, and 10  $\mu$ g/ml insulin. After 48 h, differentiation media was replaced by maturation media (DMEM supplemented with 10  $\mu$ g/ml insulin) on which cells were maintained for a further 48 h. Cells were kept in normal growth media for an additional 5 days. Mature adipocytes were used for experiments on Day 9 after initiation of differentiation. Only monolayers with a differentiation grade of  $\sim$ 90% or higher were used for the experiments.

The test compounds CAP, nonivamide, and BCH were dissolved in ethanol to 1,000 $\times$  stock solutions freshly each time and final ethanol concentration during the assays never exceeded 0.2% (v/v).

#### MTT ASSAY

Negative effects of a treatment with the test compounds on the number of metabolically active cells were excluded using the MTT assay in 96-well format. In the MTT assay, the reduction of yellow tetrazolium salt MTT (3-(4,5-dimethylthiazol-2-yl)-2,5-diphenyltetrazolium bromide) to a purple formazan by mitochondrial and ER enzymes is used as a measure for cell viability [Berridge et al., 2005].

Cells were seeded in 96-well plates and treated with 1 nM–10  $\mu$ M CAP or nonivamide with or without addition of 25–100  $\mu$ M BCH or the corresponding ethanol concentration (0.1–0.2% (v/v), solvent control) for 12 days after initiation of differentiation. Cell culture media was exchanged every second day. On Day 12, 100  $\mu$ l of the MTT working reagent (0.83 mg/ml MTT diluted in PBS/serum-free media (1:5)), was added to each well, and cells were incubated at 37°C for approximately 15 min. The MTT working solution was removed and the purple formazan formed during incubation was dissolved in 150  $\mu$ l DMSO per well. Absorbance was measured at 550 nm with 690 nm as reference wavelength using multiwell plate reader (Tecan infinite M200; Tecan Austria). The number of metabolically active cells was calculated relative to untreated control cells or the corresponding solvent control (100%).

#### OIL RED O STAINING

Accumulation of lipids was assessed by oil red O staining as described previously [Riedel et al., 2012]. Briefly, 3T3-L1 pre-adipocytes were seeded in 24-well plates at a density of  $2 \times 10^4$  cells/ml. Cells underwent differentiation as described above, but were maintained in maturation media for 10 days. Substance addition (1 nM–10  $\mu$ M CAP or nonivamide with or without the addition of 25, 50, or 100  $\mu$ M BCH, or the corresponding ethanol concentration solely) was started at Day 0 of the induction of differentiation. On Day 12, cells were fixated in 10% (v/v) formalin in PBS for 1 h. Cells were subsequently stained for 10 min with 200  $\mu$ l oil red O working solution, which contained 21 mg/ml oil red O dye in 60% (v/v) isopropanol. Residual oil red O

dye was removed by washing four times with double distilled water. Quantification of the staining was carried out by reading the 520 nm absorbance of the oil red dye from the lipid droplets of the cell monolayer, dissolved in 750  $\mu$ l isopropanol, on a Tecan infinite M200 multiwell plate reader. Lipid accumulation was calculated as percent of untreated control cells.

#### qRT-PCR

Quantitative Real-Time PCR was carried out for determination of gene expression levels of PPAR $\gamma$ , C/EBP $\alpha$ , FABP4, and CPT1 $\alpha$ . The RNA of 3T3-L1 cells was extracted on Day 0 (undifferentiated control) and Day 9 after initiation of differentiation with or without compound treatment using the RNeasy Lipid Tissue Mini Kit (Qiagen) according to manufacturer's protocol. Quality and concentration of the RNA was analyzed using the NanoQuant Plate on an infinite M200 Tecan reader. Reverse transcription was carried out using the high capacity cDNA Kit (Life Technologies, Austria). Increasing fluorescence signals during qRT-PCR reaction were measured in triplicate on a Step-One Plus device using the Fast SYBR green master mix (Life Technologies). Specific primers for each target gene were designed using NCBI Primer-BLAST and synthesized by Sigma-Aldrich (Austria) (Table I). Gene expression is given as fold change compared to undifferentiated control cells (=1), calculated from the respective starting mRNA levels, which were determined using LinRegPCR v.12.8 and normalized to hypoxanthine guanine phosphoribosyl transferase (*HPRT1*) as an endogenous control. *HPRT1* is a frequently used reference gene for white adipose tissue and 3T3-L1 cells [Han et al., 2002; Diaz-Villasenor et al., 2013].

#### PPAR $\gamma$ ELISA

Quantification of PPAR $\gamma$  was carried out using a specific ELISA Kit (mouse PPAR $\gamma$ ; Cloud-Clone Corp., USA) with a sensitivity of 0.66 ng/ml. 3T3-L1 cells were washed twice with ice-cold PBS and harvested in lysis buffer (50 mM Tris, 25 mM NaCl, 1 mM EDTA, 1 mM NaF, 1% (v/v) of the non-denaturing detergent Igepal, pH 7.4) supplemented with 1 mM PMSF, 1 mM sodium *ortho*-vanadate and protease inhibitor cocktail. Samples were homogenized by passing the lysate several times through a 20-gauge needle (Sterican, B.Braun Melsungen AG, Germany) and subsequent agitation for 30–45 min at 4°C. The lysate was centrifuged at 16,900g for 15 min at 4°C and the PPAR $\gamma$  content in the supernatant quantified by means of the ELISA as recommended by manufacturer's protocol.

#### CUSTOMIZED miRNA ARRAY

miRNA extraction and labeling. miRNA was extracted using the RNeasy Lipid Tissue Mini Kit (Qiagen) according to the manufacturer's protocol, but exchanging wash buffer RW1 with wash buffer RWT (Qiagen) to preserve RNA pieces <200 bp during

TABLE I. Oligonucleotides Used During PCR Reaction

Target	Forward primer	Reverse primer	Product length (bp)
HPRT	GAGAGCGTTGGCTTACCTC	ATCGCTAATCAGCAGCTGG	136
PPAR $\gamma$	GTGCCAGTTTCGATCCGTAGA	GGCCAGCATCGTGTAGATGA	142
C/EBP $\alpha$	GCCCCGTGAGAAAATGAAGG	ATCCCCAACCTAAGTCCC	129
FABP4	TTTGTCACCATCCGGTCAG	TGATGCTCTCACCTTCTGTGTC	110

washing. RNA quality and concentration was determined with a NanoQuant Plate on an infinite M200 Tecan reader. miRNA was labeled with synthetic 5'-phosphate-cytidyl-uridyl-DY547-3' RNA dinucleotides (Thermo Fisher Scientific) using T4 ligase (New England Biolabs). 300 ng of total RNA (plus synthetic spike-in controls) were added to the reaction mix containing 1 mM ATP, 50 mM Tris-HCl (pH 7.8), 10 mM MgCl<sub>2</sub>, 1 mM DTT, 10 µg/ml BSA, 25% (v/v) DMSO, 50 µM labeled dinucleotide, and 20 U T4 ligase. The reaction was allowed to take place for 2 h at 4°C and the labeled RNA was purified using a MicroBioSpin 6 column (Bio-Rad) [Wang et al., 2007].

**miRNA microarray design and synthesis.** Four identical customized microarrays were synthesized in situ on a glass substrate using a light-directed maskless array synthesizer as described before [Agbavwe et al., 2011]. The usage of a novel photochemical reaction cell allowed the simultaneous synthesis on two glass substrates, creating eight independently hybridizable microarrays at once [Sack et al., 2013].

Probes were designed for all mature mouse miRNA sequences in the Sanger miRNA database (MiRBase release 19). To equalize melting temperatures of the miRNA probes, microarray probes with very high melting temperatures were shortened at the 3' side. Since sequence homology among miRNA tends to be near the 5' end, this shortening has only little effect on sequence specificity; second, microarray probes corresponding to miRNA with very low melting temperatures were extended at the 5' end by the addition of G or 5'-AG-3' to allow pairing with one or two bases of the ligated dinucleotide [Wang et al., 2007].

**Hybridization and data analysis.** Each microarray was hybridized using a custom design adhesive hybridization chamber (SecureSeal, Grace Biolabs) with a separate compartment for each of the microarrays. The purified, labeled miRNA was applied to the microarray chamber in a hybridization solution containing 100 mM MES, 1 M Na<sup>+</sup>, 20 mM EDTA, 0.01% (v/v) Tween20, and 0.06% (w/v) BSA. Hybridization was carried out at 42°C with constant rotation. Microarrays were scanned with a GenePix 4400 microarray scanner (Molecular Devices, USA) and intensity data for each feature were extracted using NimbleScan software. Each hybridization was performed in duplicates and miRNA levels are presented as mean fold change of the two technical replicates compared to those of undifferentiated control cells.

#### DIGITAL DROPLET PCR

Absolute concentrations (copies/µl) of mmu-let-7a-5p, mmu-let-7b-3p, mmu-let-7d-5p, mmu-miR-143-3p, and mmu-miR-103-1-5p were determined using the Bio-Rad QX200 Droplet Digital PCR System. For this purpose, miRNA was extracted as described under the microarray section. Extracted miRNA from undifferentiated control cells or mature adipocytes treated with the compounds of interest for 9 days, was subsequently reversely transcribed using the TaqMan MicroRNA Reverse Transcription Kit with specific primers for the target miRNA (Life Technologies). PCR reaction was carried out on a C1000 thermocycler (Bio-Rad) out using droplet PCR supermix (Bio-Rad) and TaqMan miRNA Assays (Life Technologies) for each target miRNA after partition of the sample into 20,000 single droplets by means of the droplet generator. Per assay and treatment, between 11,300 and 17,800 droplets were analyzed and the absolute concentrations computed with the QuantaSoft software.

#### STATISTICAL ANALYSIS

Data are presented as means ± SEM or fold change compared to control cells (±SEM). Except for the microarray experiments, data are calculated from multiple experiments with at least two technical replicates as indicated in the figure or table legends, at which n refers to the number of biological replicates. Outliers were excluded from calculations after performing Nalimov outlier test. Significant differences between multiple treatments (compound and/or concentration) were determined using One- or Two-Way ANOVA with Holm-Sidak post hoc test. Significant differences between two groups were analyzed with Student's *t*-test and considered to be different at *P* < 0.05. Differences between groups are marked in figures and tables with \**P* < 0.05, \*\**P* < 0.01, and \*\*\**P* < 0.001.

## RESULTS

#### MTT ASSAY

Negative effects of long-term treatment with any of the test substances (CAP, nonivamide, and BCH) or a combination thereof, on the number of metabolically active cells were excluded using the MTT assay. There was no reduction in the number of metabolically active cells after a treatment with 0.01–10 µM CAP or nonivamide with or without the addition of 25–100 µM BCH for 12 days compared to control cells (One-Way ANOVA vs. control, *P* > 0.05, data not shown).

#### TREATMENT WITH CAPSAICIN AND NONIVAMIDE REDUCES LIPID ACCUMULATION IN 3T3-L1 ADIPOCYTES

Accumulation of lipids during the differentiation process, assessed via oil red O staining, is a frequently used functional marker for the degree of adipogenesis in 3T3-L1 cells [Hwang et al., 2005; Hsu and Yen, 2007; Zhang et al., 2007; Arumugam et al., 2008]. In the present study, the effect of the addition of 0.01–10 µM CAP or nonivamide during differentiation and maturation (12 days) of 3T3-L1 cells on lipid accumulation was assessed (Fig. 2). First, an effect of addition of 0.1% ethanol as a solvent control to the media was excluded (*P* > 0.05, data not shown). The effects of nonivamide and CAP are, thus, presented compared to cells treated with the solvent control. CAP reduced lipid accumulation by 5.76 ± 1.03% (*P* < 0.05) at 0.01 µM up to 10.1 ± 1.50% (*P* < 0.001) at 0.1 µM in comparison to control cells. Treatment with nonivamide reduced lipid accumulation to a similar extent as CAP; the effects were not different from the effects after CAP treatment at any of the tested concentrations. Compared to untreated control cells, treatment with nonivamide decreased lipid accumulation by 5.34 ± 1.03% (*P* < 0.05) at 0.01 µM up to 10.4 ± 2.47% (*P* < 0.001) at 1 µM.

#### REDUCTION IN LIPID ACCUMULATION BY CAPSAICIN AND NONIVAMIDE CAN BE BLOCKED BY THE ADDITION OF A TRPV1 INHIBITOR

Activation of the TRPV1 receptor has been shown to be responsible for the anti-adipogenic effects of CAP in vitro and in vivo [Zhang et al., 2007]. In order to examine whether the effects of nonivamide on lipid accumulation also depend on TRPV1 activation, 3T3-L1 cells were co-incubated with 1 µM nonivamide and 25–100 µM of the

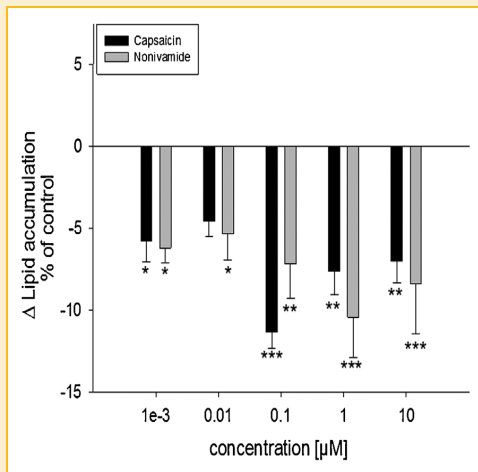


Fig. 2. Difference in lipid accumulation in % of control (0.1% EtOH)  $\pm$  SEM after addition of 0.01–10  $\mu$ M capsaicin or nonivamide during differentiation and maturation of 3T3-L1 cells. Lipids in fully mature adipocytes were stained 12 days after initiation of differentiation with oil red O and data are shown as means of control treated cells from three to four independent experiments with at least three technical replicates each. \* $P < 0.05$ , \*\* $P < 0.01$ , \*\*\* $P < 0.001$  versus control treated cells.

specific TRPV1-inhibitor BCH during differentiation and maturation for a total of 12 days (Fig. 3). A concentration of 1  $\mu$ M nonivamide was chosen for co-incubation studies, since this concentration demonstrated the greatest effect. As a positive control for TRPV1

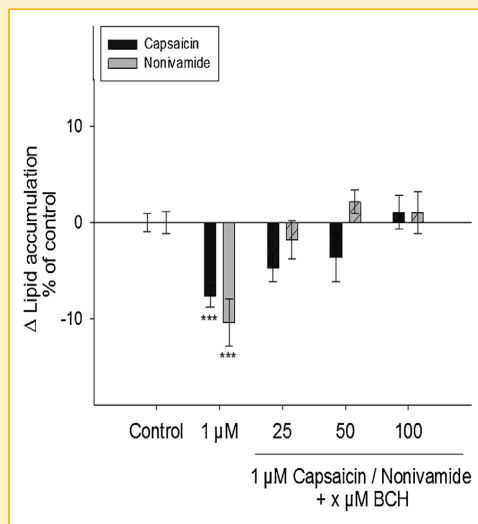


Fig. 3. Difference in lipid accumulation in % of control (0.1% EtOH)  $\pm$  SEM after treatment with 1  $\mu$ M capsaicin or nonivamide with or without the addition of 25–100  $\mu$ M of the selective TRPV1 inhibitor *trans*-*tert*-butylcyclohexanol (BCH) during differentiation and maturation (12 days) of 3T3-L1 cells. Lipids in fully mature adipocytes were stained 12 days after initiation of differentiation with oil red O and data are shown as means compared to control treated cells from three to four independent experiments with at least three technical replicates each. \*\*\* $P < 0.001$  versus control.

inhibition by BCH, the effect of concomitant incubation of the TRPV1 inhibitor BCH and CAP was determined. Addition of BCH to CAP-containing media prevented reduction in lipid accumulation by CAP, leading to no difference between control treatment and a treatment with 1  $\mu$ M CAP plus 25  $\mu$ M ( $-4.71 \pm 1.45\%$ ), 50  $\mu$ M ( $-3.62 \pm 2.49\%$ ) and 100  $\mu$ M BCH ( $+1.06 \pm 1.73\%$ ,  $P < 0.05$  vs. control), whereas treatment with 1  $\mu$ M CAP alone reduced lipid accumulation by  $7.63 \pm 1.41\%$  ( $P < 0.001$ , Fig. 3). Likewise, addition of 25, 50, and 100  $\mu$ M BCH to media containing 1  $\mu$ M nonivamide prevented reduction in lipid accumulation caused by 1  $\mu$ M nonivamide ( $-10.4 \pm 2.47\%$ ,  $P < 0.001$  vs. control, Fig. 3) as well. There was, similarly to the results obtained for CAP, no difference between control-treated cells and cells treated with 25  $\mu$ M ( $-1.83 \pm 2.00\%$ ), 50 ( $+2.15 \pm 1.25\%$ ), and 100  $\mu$ M BCH ( $+1.0 \pm 2.18\%$ ) in combination with nonivamide ( $P > 0.05$  for each treatment vs. control, Fig. 3). Incubation of 3T3-L1 cells for 12 days during differentiation and maturation with 25–100  $\mu$ M BCH did not affect lipid accumulation compared to control cells ( $P > 0.05$ ) and was between  $2.07 \pm 1.35\%$  and  $-0.96 \pm 1.93\%$  (data not shown in figure).

#### TREATMENT WITH NONIVAMIDE DECREASES EXPRESSION OF PPAR $\gamma$

PPAR $\gamma$  and C/EBP $\alpha$  are major factors regulating adipogenesis and have been demonstrated as a target of CAP [Hsu and Yen, 2007]. Thus, gene expression levels of PPAR $\gamma$ , C/EBP $\alpha$ , and FABP4 after treatment with 10  $\mu$ M nonivamide or CAP for 9 days or of control treated cells were determined using qPCR. Compared to undifferentiated control cells, gene expression of PPAR $\gamma$ , C/EBP $\alpha$ , and FABP4 increased to  $4.26 \pm 0.25$ ,  $7.51 \pm 0.43$ , and  $153 \pm 10.2$  in control treated cells (Fig. 4, Table II). However, there was no significant impact of CAP or nonivamide treatment on gene expression of C/EBP $\alpha$  and FABP4 and PPAR $\gamma$ , although there was a trend ( $P = 0.056$ ) toward a down-regulation of PPAR $\gamma$  mRNA levels after treatment with nonivamide ( $3.55 \pm 0.06$ , Fig. 4, left side).

In order to investigate whether PPAR $\gamma$  levels are down-regulated at the protein level, the PPAR $\gamma$  content per mg protein of 3T3-L1 cell lysates 9 days after initiation of differentiation with or without treatment with CAP or nonivamide was determined. Undifferentiated control cells had an average PPAR $\gamma$  content of  $59 \pm 16.7$  ng/mg protein. Upon differentiation, PPAR $\gamma$  levels increased by a factor of 132, to  $5894 \pm 416.6$  ng/mg protein ( $P < 0.001$ ) in control treated cells. Treatment with CAP did not change PPAR $\gamma$  levels ( $7882 \pm 3654$  ng/mg protein) compared to those of control treated cells, whereas treatment with nonivamide led to a decrease of PPAR $\gamma$  to  $4016 \pm 116$  ng/mg protein compared to control treated cells ( $P < 0.05$ , Fig. 4, right side).

#### TREATMENT WITH NONIVAMIDE REGULATES EXPRESSION OF mmu-let-7d-5p

Since several miRNAs have been associated with the regulation of adipogenesis and obesity (see review: [McGregor and Choi, 2011]), a genome-wide miRNA array was performed. By means of this customized array, miRNA levels of undifferentiated 3T3-L1 cells, control treated cells (0.1% EtOH) and cells treated with 10  $\mu$ M nonivamide during adipogenesis for 9 days were compared. Fold changes of control and nonivamide-treated cells compared to

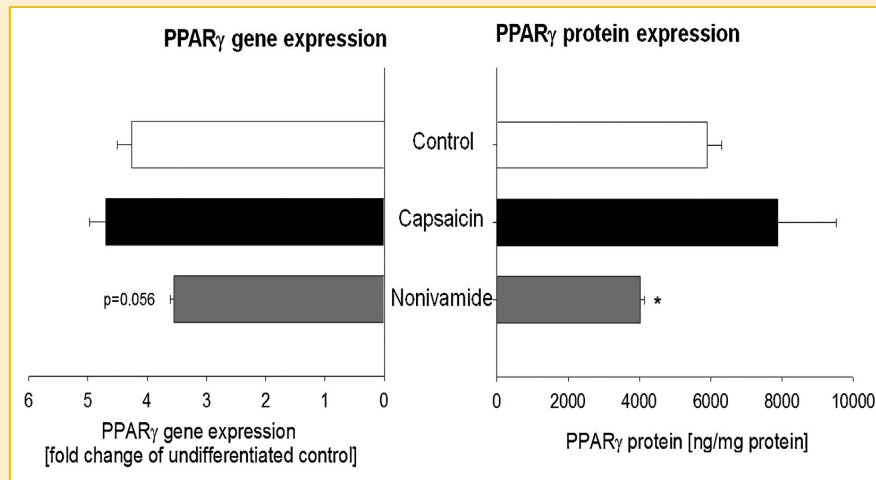


Fig. 4. PPAR $\gamma$  expression on genetic level (as mean fold change  $\pm$  SEM compared to undifferentiated control cells, left side) and protein (in ng/mg protein  $\pm$  SEM, right side) level in 3T3-L1 adipocytes. mRNA or protein was extracted on Day 9 after initiation of differentiation. During differentiation and maturation, 3T3-L1 cells were treated with either 0.1% EtOH, 10  $\mu$ M capsaicin, or nonivamide. Data are shown as mean from three independent experiments. \* $P$  < 0.05 versus control.

undifferentiated cells of selected miRNAs, which have been associated with the regulation of adipogenesis before, are displayed in Table III. On Day 9 after initiation of adipogenesis, expression levels of mmu-miR-103-3p (4.35), mmu-miR-210-3p (1.73), as well as mmu-let-7a-5p (2.04), and mmu-let-7d-5p (1.82) were increased compared to undifferentiated control cells (=1), using an absolute fold change of 1.5 as cut-off criteria [Li et al., 2011]. In contrast, there was neither an effect on other isoforms of the upregulated miRNAs, nor on further adipogenesis-regulating miRNAs like mmu-miR-143, mmu-miR-193, mmu-miR-27, or mmu-miR-448. However, treatment with nonivamide for 9 days increased expression of mmu-let-7a-5p from 2.04 (control treatment/undifferentiated control) to 3.38 (nonivamide treatment/undifferentiated control), corresponding to an absolute fold change of 1.66. Also other members of the let-7 group were up-regulated after nonivamide treatment, leading to an increased expression of mmu-let-7b-3p from 1.10 to 3.77, corresponding to an absolute fold change of 1.66, and mmu-let-7d-5p from 1.82 to 2.73, corresponding to an absolute fold change of 1.5. In

TABLE II. Results of the Gene Expression Analysis of C/EBP $\alpha$  and FABP4

Target gene	Solvent control	Capsaicin	Nonivamide
C/EBP $\alpha$	7.51 $\pm$ 0.43	7.69 $\pm$ 0.59	6.28 $\pm$ 0.33
FABP4	153 $\pm$ 10.2	155 $\pm$ 21.3	144 $\pm$ 9.78

Data are shown as fold changes compared to undifferentiated control cells (=1) from three independent experiments with at least two technical replicates. mRNA for the experiments was extracted on Day 0 (undifferentiated control) and Day 9 after initiation of differentiation, during which cells were either treated with 0.1% EtOH or 10  $\mu$ M capsaicin or nonivamide.

Fold changes in gene expression after treatment with 0.1% EtOH (solvent control) or 10  $\mu$ M capsaicin or nonivamide compared to undifferentiated control cells (=1). n = 3 with three technical replicates.

contrast, mmu-miR-103-1-5p and mmu-miR-103-2-5p were down-regulated after nonivamide treatment to 0.06 and 0.25 compared to 1.16 and 0.93 after control treatment. Nonivamide-treatment also reduced expression of mmu-miR-143-3p (0.06), mmu-miR-210-3p (0.14), mmu-miR-27a-3p and -5p to 0.17 or 0.09, respectively, and mmu-miR-27b-5p to 0.19 (Table III).

TABLE III. Results of the Customized miRNA Microarray Using an Absolute Fold Change (Compared to Undifferentiated Control Cells) of 0.5 or 1.5, Respectively, as Cut-Off Criteria

Mature miRNA	Solvent control	Nonivamide
mmu-let-7a-5p	2.04	3.38
mmu-let-7b-3p	1.10	3.77
mmu-let-7d-5p	1.82	2.73
mmu-miR-103-3p	4.35	6.37
mmu-miR-103-1-5p	1.16	0.06
mmu-miR-103-2-5p	0.93	0.25
mmu-miR-143-3p	1.29	0.06
mmu-miR-193a-3p	1.00	0.09
mmu-miR-193a-5p	0.94	0.01
mmu-miR-193b-5p	0.88	0.26
mmu-miR-27a-3p	1.03	0.17
mmu-miR-27a-5p	1.04	0.09
mmu-miR-27b-5p	0.79	0.19
mmu-miR-210-3p	1.73	0.14
mmu-miR-448-3p	0.79	0.02
mmu-miR-448-5p	0.81	0.10

Data are shown as fold changes compared to undifferentiated control cells (=1) of selected miRNAs, that were shown to regulate adipogenesis in 3T3-L1 cells. miRNA for the experiments was extracted on Day 0 (undifferentiated control) and Day 9 after initiation of differentiation, during which cells were either treated with 0.1% EtOH or 10  $\mu$ M nonivamide.

Fold changes in miRNA expression after treatment with 0.1% EtOH (solvent control) or 10  $\mu$ M nonivamide compared to undifferentiated control cells (=1). n = 1 with two technical replicates.

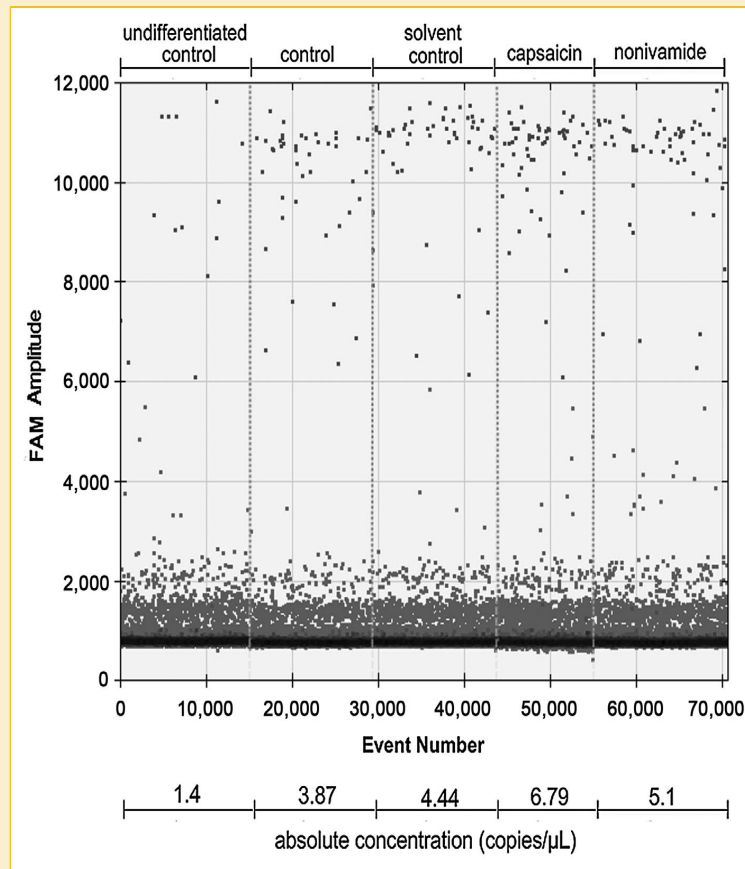


Fig. 5. Visual representation of one example measurement of the weakly expressed *mmu-let-7b-3p* using ddPCR. The x-axis shows the accumulating number of counted droplets. Per treatment, between 15,024 (capsaicin) and 16,357 (solvent control) droplets were accepted for analysis of a negative or positive FAM signal. FAM signal intensity is displayed on the y-axis. The lower cluster represents negative droplets, whereas the upper cluster represents droplets with a positive signal, allowing calculation of absolute copy numbers (copies/ $\mu$ L) using QuantaSoft software.

Since the present study detected a similar expression pattern after nonivamide treatment for several members of *mmu-let-7*, the expression of selected isoforms was validated using highly sensitive digital droplet PCR. This method allows an absolute quantification of the target gene copy number per  $\mu$ L by partition of the 20  $\mu$ L test sample into 20,000 single droplets that are separately analyzed for a positive or negative fluorescence signal (Fig. 5). Compared to undifferentiated control cells, expression of *mmu-let-7a-5p*, *mmu-let-7b-3p*, and *mmu-let-7d-5p* was increased to a fold change of  $1.44 \pm 0.07$ ,  $5.91 \pm 0.83$ , or  $2.22 \pm 0.19$ , respectively, within 9 days after initiation of differentiation in control cells. Treatment with the solvent control 0.1% EtOH during differentiation led to similar fold changes compared to undifferentiated cells with  $1.47 \pm 0.30$  for *mmu-let-7a-5p*,  $5.86 \pm 0.43$  for *mmu-let-7b-3p*, and  $2.47 \pm 0.28$  for *mmu-let-7d-5p* ( $P > 0.05$ ). In contrast to the miRNA array results, *mmu-let-7a-5p* expression was not affected by treatment with CAP or nonivamide with fold changes to the solvent control of  $1.11 \pm 0.26$  or  $1.18 \pm 0.08$ , respectively (Fig. 6). However, expression of *mmu-let-7b-3p* increased to  $8.05 \pm 0.64$  in CAP-treated cells compared to the solvent control ( $5.86 \pm 0.43$ ,  $P < 0.05$ ), corresponding to a fold change of  $1.38 \pm 0.11$  (Fig. 6). Treatment with

nonivamide increased *mmu-let-7b-3p* expression to a comparably mean fold change of  $8.32 \pm 2.46$  ( $1.42 \pm 0.42$  compared to the solvent control), without reaching the level of significance ( $P > 0.05$ ). Expression of *mmu-let-7d-5p* increased ( $2.95 \pm 0.13$ ) in nonivamide-treated cells compared to control cells ( $2.22 \pm 0.19$ ,  $P < 0.01$ ), but not compared to the solvent control (corresponding fold change  $1.20 \pm 0.05$ ,  $P > 0.05$ ). Treatment with CAP led to a similar fold change of undifferentiated control cells of  $3.25 \pm 0.17$ , corresponding to a fold change of  $1.32 \pm 0.28$  of the solvent control, without reaching the level of significance ( $P > 0.05$ ). No difference in *mmu-let-7* expression in response to CAP and nonivamide-treatment was found (Fig. 6).

## DISCUSSION

Red pepper and its major pungent principle, CAP are often discussed as anti-obesity agents. Beside reducing energy intake [Yoshioka et al., 1999], increasing energy metabolism and lowering serum triacylglycerol content [Kawada et al., 1986], administration of 0.01% (w/w) CAP has been shown to reduce visceral adipose tissue and subcutaneous fat in mice fed a high fat diet [Zhang et al., 2007]. In



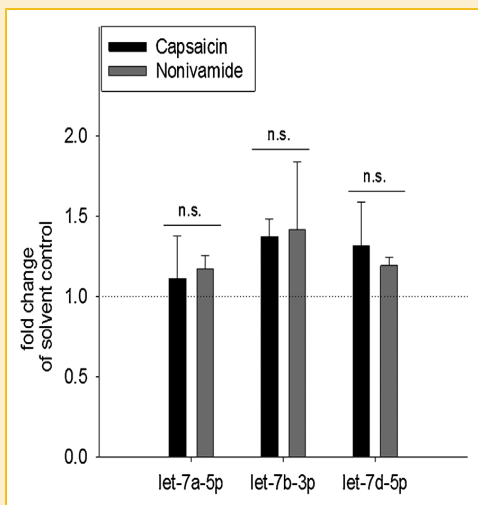


**Fig. 6.** Mean fold changes in *mmu-let-7a-5p*, *mmu-let-7b-3p*, and *mmu-let-7d-5p* expression were analyzed using digital droplet PCR. miRNA from 3T3-L1 cells was extracted on Day 9 after initiation of differentiation. During the process of differentiation and maturation, cells were treated with either 10  $\mu$ M capsaicin or nonivamide, or the corresponding ethanol concentration (0.1% ethanol; solvent control). An effect of the ethanol treatment was excluded. Data are displayed as mean fold changes  $\pm$  SEM compared to the solvent control ( $=1$ , dotted line) of three independent experiments.

addition, CAP has been shown to reduce adipogenesis in 3T3-L1 pre-adipocytes [Hsu and Yen, 2007; Zhang et al., 2007]. Knock out experiments in in vitro and in vivo model systems have shown that anti-adipogenic activity of CAP is mediated by activation of the TRPV1 cation channel [Zhang et al., 2007]. However, the downside of CAP, being a highly potential TRPV1 agonist, is that its contact with mucous membranes, for example, in the oral cavity, leads to a sharp burning pain in mammals. This pungency strongly limits dietary intake of CAP, especially in European countries. In the present study, we investigated whether the less pungent capsaicinoid, nonivamide, may exhibit similar effects on adipogenesis in 3T3-L1 cells as CAP. Nonivamide is a direct structural analog of CAP, although the slight structural difference reduces its TRPV1 binding affinity and hence, also its pungency by half. In the present study, we analyzed lipid accumulation by oil red O staining, as an indicator for adipogenesis. Oil red O staining is a frequently used marker for differentiation of pre-adipocytes to adipocytes in 3T3-L1 cells [Arumugam et al., 2008; Yoshitomia et al., 2012; Zhang et al., 2011]. Beside the visible accumulation of lipid droplets, the strong increase compared to undifferentiated control cells in PPAR $\gamma$  gene and protein expression as well as C/EBP $\alpha$  and FABP4 gene expression further confirmed the differentiation of 3T3-L1 pre-adipocytes to mature adipocytes upon addition of the hormone cocktail 2 days post-confluence.

The results demonstrate that addition of 0.01–10  $\mu$ M nonivamide reduces lipid accumulation in 3T3-L1 cells up to  $10.4 \pm 2.47\%$  when added at a final concentration of 1  $\mu$ M during differentiation and maturation for 12 days, which is comparable to the results obtained for CAP. Treatment with CAP reduced lipid accumulation up to

$10.1 \pm 1.50\%$  at 0.1  $\mu$ M, confirming the results of Zhang et al. [Hsu and Yen, 2007; Zhang et al., 2007], who showed reduced oil red O staining of 3T3-L1 cells after treatment with 1  $\mu$ M of CAP during adipogenesis. In order to investigate whether the nonivamide-induced reduction in lipid accumulation is mediated via TRPV1 activation, the effect of concomitant addition of the selective TRPV1 inhibitor BCH and nonivamide on lipid accumulation was analyzed. BCH has been successfully used as a TRPV1-inhibitor in previous studies [Rohm et al., 2013, 2015]. Since the anti-adipogenic effect of CAP depends on TRPV1 receptor activation [Hsu and Yen, 2007; Zhang et al., 2007], the effect of BCH on the reduction of lipid accumulation by CAP was used as a positive control for TRPV1 blockage by BCH. In the presence of 25–100  $\mu$ M BCH, addition of 1  $\mu$ M CAP did not reduce lipid accumulation, proving the effectiveness of BCH and confirming previous results [Hsu and Yen, 2007; Zhang et al., 2007]. However, addition of 25–100  $\mu$ M BCH to nonivamide-containing media prevented the anti-adipogenic activity of nonivamide, leading to no reduction in lipid accumulation compared to control treated cells. This result demonstrates that activation of the TRPV1 receptor by both CAP and nonivamide inhibits adipogenesis in 3T3-L1 cells. However, since ethanol has also been discussed to activate the TRPV1 receptor [Blednov and Harris, 2009; Trevisani et al., 2002], an effect of low doses of ethanol as solvent (0.1–0.2%) for the test substances on lipid accumulation was excluded in preliminary experiments.

As a signaling pathway for TRPV1-mediated inhibition of adipogenesis, increased calcium entry from the extracellular space via the TRPV1 channel with intracellular calcium accumulation targets adjacent calcineurin [Cioffi, 2007]. Activation of calcineurin is thought to inhibit the pro-adipogenic factors PPAR $\gamma$  and C/EBP $\alpha$ , thus repressing adipogenesis [Cioffi, 2007]. This suggested pathway is supported by a study from Hsu and Yen [2007], who demonstrated that treatment of mature 3T3-L1 adipocytes with high concentrations (25–100  $\mu$ M) CAP for 12–24 h down-regulated expression of PPAR $\gamma$  and C/EBP $\alpha$ . Thus, we investigated the effect of CAP and nonivamide treatment during adipogenesis on gene expression of C/EBP $\alpha$  and PPAR $\gamma$ , and, as a further marker for adipogenesis, FABP4. Gene expression of the three markers increased during adipogenesis, although there was no effect of CAP and nonivamide treatment compared to control treated cells. Since there was a trend ( $P = 0.056$ ) toward a PPAR $\gamma$  down-regulation after nonivamide treatment, PPAR $\gamma$  protein expression was analyzed as well. In contrast to CAP exposure, nonivamide-treatment reduced PPAR $\gamma$  expression compared to control-treated cells. This down-regulation of PPAR $\gamma$  could at least partly account for inhibition of adipogenesis by nonivamide. Although the comparable anti-adipogenic activities of CAP and nonivamide both depend on TRPV1 activation, treatment with CAP did not affect PPAR $\gamma$  treatment, contrary to the hypothesis and existing evidence from the literature. However, down-regulation of PPAR $\gamma$  after CAP treatment in the study by Hsu et al. was observed after treatment with far higher concentrations of CAP (25–100  $\mu$ M). In addition, in the study by Hsu and Yen [2007], mature 3T3-L1 adipocytes were treated, whereas in the present study, 3T3-L1 cells were treated during differentiation process. Also, a counter-regulation of other genes cannot be excluded. However, the differences in PPAR $\gamma$  expression between CAP and nonivamide

treatment are unexpected, and point to possible differences in signaling pathways. Differences in signaling after CAP and nonivamide treatment have been shown before in neural SH-SY5Y cells [Rohm et al., 2013], and can hence not be excluded for the present study as well. In addition, it remains to be clarified whether the differences in PPAR $\gamma$  expression after treatment with nonivamide or CAP originate at the pre- or at the post-transcriptional level.

The pro-adipogenic transcription factor PPAR $\gamma$  has been shown to be a target of some miRNAs, which have been recently identified as a novel group of adipogenic regulators. To investigate, whether the anti-adipogenic activity of nonivamide involves, beside TRPV1 activation and PPAR $\gamma$  down-regulation, also a regulation of miRNAs, a customized miRNA microarray was carried out for a first screening. During adipogenesis, miRNA-103-3p, miR-210-3p, and let-7a-5p, let-7b-3p, and let-7d-5p expression increased compared to undifferentiated control cells. This is in accordance with previous studies [Sun et al., 2009; Xie et al., 2009; Liang et al., 2013], although other isoforms of the presented miRNAs were not regulated.

Treatment with nonivamide led to a down-regulation of miR-27a-3p/-5p and miR-27b-5p compared to control treatment, which would rather argue for a PPAR $\gamma$  up-regulation than the analyzed PPAR $\gamma$  down-regulation after nonivamide treatment [Karbiener et al., 2009]. In contrast, the detected down-regulation of miR-143-3p after nonivamide treatment compared to control treatment could at least partly explain inhibition of PPAR $\gamma$  expression [Esau et al., 2004]. Also expression levels of the anti-adipogenic mmu-let-7a-5p, mmu-let-7b-3p, and mmu-let-7d-5p increased after nonivamide treatment compared to control treatment, which has been associated with an decreased PPAR $\gamma$  expression before [Sun et al., 2009]. Changes in expression of mmu-let-7a-5p, mmu-let-7b-3p, and mmu-let-7d-5p were validated using ddPCR, which allows a much more precise, absolute quantification of the target gene/miRNA than qPCR or microarray [Hindson et al., 2011, 2013]. Absolute quantification of these selected members of the let-7 group in undifferentiated control cells (Day 0) and 9 days after initiation of differentiation confirmed the results of the microarray by demonstrating an up-regulation of all three representatives of the let-7 group during adipogenesis. However, using ddPCR, there was no impact of CAP or nonivamide treatment on mmu-let-7a-5p expression. CAP-treated cells showed an increased let-7b-3p expression compared to solvent control-treated cells, whereas treatment with nonivamide led to an increased expression of mmu-let-7d-5p compared to the control. An increased expression of mmu-let-7d-5p after nonivamide-treatment compared to solvent control treated cells was also detected using the customized microarray, validating the stimulating impact of nonivamide treatment on mmu-let-7d-5p expression. Increased expression of let-7 has been shown to be accompanied by decreased PPAR $\gamma$  expression [Sun et al., 2009]. Thus, increased mmu-let-7d-5p may be responsible for the decreased PPAR $\gamma$  in nonivamide-treated cells and hence be involved in the anti-adipogenic activity of nonivamide in 3T3-L1 cells. Figure 7 provides an overview of the hypothesized signaling pathway for the anti-adipogenic activity of nonivamide. It is also remarkably that, although treatment with CAP did not reduce PPAR $\gamma$  expression, there was no difference in the expression of the investigated let-7 representatives between nonivamide and CAP treated cells.

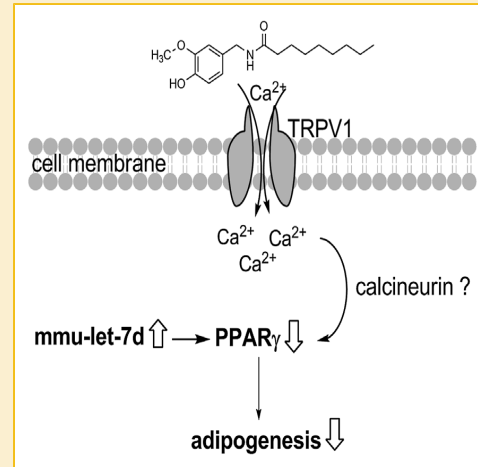


Fig. 7. Hypothesized pathway for the anti-adipogenic activity of nonivamide in 3T3-L1 cells. Binding of nonivamide to the TRPV1 cation channel increases intracellular Ca<sup>2+</sup>, which decreases expression of PPAR $\gamma$ , possibly via calcineurin. In addition, increased expression of the miRNA mmu-let-7d might decrease PPAR $\gamma$  expression as well, impairing differentiation of 3T3-L1 cells to an adipocyte phenotype.

In conclusion, the present study demonstrates for the first time that the less pungent CAP-analog nonivamide impairs adipogenesis to a similar extent as CAP. Using a specific inhibitor, it was demonstrated that the anti-adipogenic activity of nonivamide depends, like the anti-adipogenic activity of CAP, on the activation of the TRPV1 receptor. Nonivamide has a lower binding affinity than CAP to the TRPV1 receptor, however, in the tested range of concentrations, effects of nonivamide and CAP on adipogenesis were equal. The effects of lower test concentrations would be needed to clearly identify the activity threshold for both compounds, and to determine whether the threshold can be correlated with TRPV1 binding affinity, and thus, pungency. However, a different downstream-signaling pathway after TRPV1 activation is conceivable, since contrary to CAP, treatment with nonivamide decreased PPAR $\gamma$  levels. This could, at least partly, be explained by an increased expression of the miRNA mmu-let-7d. Since the capsaicinoid nonivamide is rated to almost half as pungent as CAP [Haas et al., 1997], an oral application of higher doses compared to CAP is possible and reveals nonivamide as a less pungent, but still potent novel anti-obesity compound from nature.

Although data from long-term human intervention studies with nonivamide are lacking, nonivamide seems to be a promising candidate to target different medicinal strategies in the treatment of obesity. Beside the inhibition of adipogenesis demonstrated here, nonivamide has also been shown to decrease fatty acid uptake in Caco-2 cells [Rohm et al., 2015], which may support the prevention of hyperlipidemia. In addition, administration of 0.15 mg nonivamide in an oral glucose tolerance test reduced total energy intake from a standardized breakfast in slightly overweight male subjects [Hochkogler et al., 2014], supporting the effectiveness of the less pungent CAP-analog.



## REFERENCES

- Agbavwe C, Kim C, Hong D, Heinrich K, Wang T, Somoza MM. 2011. Efficiency, error and yield in light-directed maskless synthesis of DNA microarrays. *J Nanobiotechnol* 9:1-17.
- Arumugam M, Vijayan P, Raghu C, Ashok G, Dhanaraj SA, Kumarappan CT. 2008. Anti-adipogenic activity of *Capsicum annuum* (Solanaceae) in 3T3 L1. *J Complement Integr Med* 5:1-9.
- Berridge MV, Herst PM, Tan AS. 2005. Tetrazolium dyes as tools in cell biology: New insights into their cellular reduction. *Biotechnol Annu Rev* 11:127-152.
- Blednov Y, Harris R. 2009. Deletion of vanilloid receptor (TRPV1) in mice alters behavioral effects of ethanol. *Neuropharmacology* 56:814-820.
- Bray GA, Tartaglia LA. 2000. Medicinal strategies in the treatment of obesity. *Nature* 404:672-677.
- Caterina MJ, Schumacher MA, Tominaga M, Rosen TA, Levine JD, Julius D. 1997. The capsaicin receptor: A heat-activated ion channel in the pain pathway. *Nature* 389:816-824.
- Cioffi DL. 2007. The skinny on TRPV1. *Circ Res* 100:934-936.
- Clarke SL, Robinson CE, Gimble JM. 1997. CAAT/enhancer binding proteins directly modulate transcription from the peroxisome proliferator-activated receptor gamma 2 promoter. *Biochem Biophys Res Commun* 240:99-103.
- Constant HL, Cordell GA, West DP. 1996. Nonivamide, a constituent of *Capsicum oleoresin*. *J Nat Prod* 59:425-426.
- Díaz-Villasenor A, Granados O, Gonzalez-Palacios B, Tovar-Palacio C, Torre-Villalvazo I, Olivares-García V, Torres N, Tovar AR. 2013. Differential modulation of the functionality of white adipose tissue of obese Zucker (fa/fa) rats by the type of protein and the amount and type of fat. *J Nutr Biochem* 24:1798-1809.
- Esau C, Kang X, Peralta E, Hanson E, Marcusson EG, Ravichandran LV, Sun Y, Koo S, Perera RJ, Jain R, Dean NM, Freier SM, Bennett CF, Lollo B, Griffey R. 2004. MicroRNA-143 regulates adipocyte differentiation. *J Biol Chem* 279:52361-52365.
- Eulalio A, Huntzinger E, Izaurralde E. 2008. Getting to the root of miRNA-mediated gene silencing. *Cell* 132:9-14.
- Farmer SR. 2006. Transcriptional control of adipocyte formation. *Cell Metab* 4:263-273.
- Green H, Kehinde O. 1975. An established preadipose cell line and its differentiation in culture. II. Factors affecting the adipose conversion. *Cell* 5:19-27.
- Gregoire FM, Smas CM, Sul HS. 1998. Understanding adipocyte differentiation. *Physiol Rev* 78:783-809.
- Haas JS, Whipple RE, Grant PM, Andresen BD, Volpe AM, Pelkey GE. 1997. Chemical and elemental comparison of two formulations of oleoresin capsicum. *Sci Justice* 37:15-24.
- Han J, Farmer SR, Kirkland JL, Corkey BE, Yoon R, Pirtskhalava T, Ido Y, Guo W. 2002. Octanoate attenuates adipogenesis in 3T3-L1 preadipocytes. *J Nutr* 132:904-910.
- Harwood HJ Jr. 2012. The adipocyte as an endocrine organ in the regulation of metabolic homeostasis. *Neuropharmacology* 63:57-75.
- Hausman DB, DiGirolamo M, Bartness TJ, Hausman GJ, Martin RJ. 2001. The biology of white adipocyte proliferation. *Obes Rev* 2:239-254.
- Hindson BJ, Ness KD, Masquelier DA, Belgrader P, Heredia NJ, Makarewicz AJ, Bright IJ, Lucero MY, Hiddessen AL, Legler TC. 2011. High-throughput droplet digital PCR system for absolute quantitation of DNA copy number. *Anal Chem* 83:8604-8610.
- Hindson CM, Chevillet JR, Briggs HA, Gallichotte EN, Ruf IK, Hindson BJ, Vessella RL, Tewari M. 2013. Absolute quantification by droplet digital PCR versus analog real-time PCR. *Nat Methods* 10:1003-1005.
- Hochkogler CM, Rohm B, Hojdar K, Widder S, Ley JP, Krammer GE, Somoza V. 2014. The pungent capsaicin analog nonivamide decreases total energy intake and enhances plasma serotonin levels in men when administered in an OGTT: A randomized, crossover intervention. *Mol Nutr Food Res* 58:1282-1290.
- Hsu CL, Yen GC. 2007. Effects of capsaicin on induction of apoptosis and inhibition of adipogenesis in 3T3-L1 cells. *J Agric Food Chem* 55:1730-1736.
- Hwang JT, Park IJ, Shin JI, Lee YK, Lee SK, Baik HW, Ha J, Park OJ. 2005. Genistein, EGCG, and capsaicin inhibit adipocyte differentiation process via activating AMP-activated protein kinase. *Biochem Biophys Res Commun* 338:694-699.
- Karbiener M, Fischer C, Nowitsch S, Opiessnig P, Papak C, Ailhaud G, Dani C, Amri EZ, Scheidele M. 2009. microRNA miR-27b impairs human adipocyte differentiation and targets PPARgamma. *Biochem Biophys Res Commun* 390:247-251.
- Kawada T, Hagihara K, Iwai K. 1986. Effects of capsaicin on lipid metabolism in rats fed a high fat diet. *J Nutr* 116:1272-1278.
- Kivipelto M, Ngandu T, Fratiglioni L, Viitanen M, Kåreholt I, Winblad B, Helkala E-L, Tuomilehto J, Soininen H, Nissinen A. 2005. Obesity and vascular risk factors at midlife and the risk of dementia and Alzheimer disease. *Arch Neurol* 62:1556-1560.
- Kueper T, Krohn M, Haustedt LO, Hatt H, Schmaus G, Vielhaber G. 2010. Inhibition of TRPV1 for the treatment of sensitive skin. *Exp Dermatol* 19:980-986.
- Li Y, Li J, Belisle S, Baskin CR, Tumpey TM, Katze MG. 2011. Differential microRNA expression and virulence of avian, 1918 reassortant, and reconstructed 1918 influenza A viruses. *Virology* 421:105-113.
- Liang WC, Wang Y, Wan DC, Yeung VS, Waye MM. 2013. Characterization of miR-210 in 3T3-L1 adipogenesis. *J Cell Biochem* 114:2699-2707.
- McGregor RA, Choi MS. 2011. microRNAs in the regulation of adipogenesis and obesity. *Curr Mol Med* 11:304-316.
- Poissonnet CM, Burdi AR, Garn SM. 1984. The chronology of adipose tissue appearance and distribution in the human fetus. *Early Hum Dev* 10:1-11.
- Riedel A, Pignitter M, Hochkogler CM, Rohm B, Walker J, Bytof G, Lantz I, Somoza V. 2012. Caffeine dose-dependently induces thermogenesis but restores ATP in HepG2 cells in culture. *Food Funct* 3:955-964.
- Rohm B, Holik AK, Somoza MM, Pignitter M, Zaunschirm M, Ley JP, Krammer GE, Somoza V. 2013. Nonivamide, a capsaicin analog, increases dopamine and serotonin release in SH-SY5Y cells via a TRPV1-independent pathway. *Mol Nutr Food Res* 57:2008-2018.
- Rohm B, Riedel A, Ley JP, Widder S, Krammer GE, Somoza V. 2015. Capsaicin, nonivamide and trans-pellitorine decrease free fatty acid uptake without TRPV1 activation and increase acetyl-coenzyme A synthetase activity in Caco-2 cells. *Food Funct* 6:172-184.
- Rosen ED, Spiegelman BM. 2000. Molecular regulation of adipogenesis. *Annu Rev Cell Dev Biol* 16:145-171.
- Sack M, Kretschy N, Rohm B, Somoza V, Somoza MM. 2013. Simultaneous light-directed synthesis of mirror-image microarrays in a photochemical reaction cell with flare suppression. *Anal Chem* 85:8513-8517.
- Spalding KL, Arner E, Westermark PO, Bernard S, Buchholz BA, Bergmann O, Blomqvist L, Hoffstedt J, Naslund E, Britton T, Concha H, Hassan M, Ryden M, Frisen J, Arner P. 2008. Dynamics of fat cell turnover in humans. *Nature* 453:783-787.
- Sun T, Fu M, Bookout AL, Kliewer SA, Mangelsdorf DJ. 2009. MicroRNA let-7 regulates 3T3-L1 adipogenesis. *Mol Endocrinol* 23:925-931.
- Thomas KC, Ethirajan M, Shahrokh K, Sun H, Lee J, Cheatham TE III, Yost GS, Reilly CA. 2011. Structure-activity relationship of capsaicin analogs and transient receptor potential vanilloid 1-mediated human lung epithelial cell toxicity. *J Pharmacol Exp Ther* 337:400-410.
- Trevisani M, Smart D, Gunthorpe MJ, Tognetto M, Barbieri M, Campi B, Amadesi S, Gray J, Jerman JC, Brough SJ, Owen D, Smith GD, Randall AD, Harrison S, Bianchi A, Davis JB, Geppetti P. 2002. Ethanol elicits and potentiates nociceptor responses via the vanilloid receptor-1. *Nat Neurosci* 5:546-551.

- Wahlqvist ML. 2005. Dietary fat and the prevention of chronic disease. *Asia Pac J Clin Nutr* 14:313-318.
- Wang H, Ach RA, Curry B. 2007. Direct and sensitive miRNA profiling from low-input total RNA. *RNA* 13:151-159.
- Xie H, Lim B, Lodish HF. 2009. MicroRNAs induced during adipogenesis that accelerate fat cell development are downregulated in obesity. *Diabetes* 58:1050-1057.
- Yoshioka M, St-Pierre S, Drapeau V, Dionne I, Doucet E, Suzuki M, Tremblay A. 1999. Effects of red pepper on appetite and energy intake. *Br J Nutr* 82: 115-123.
- Yoshitomia H, Qinb L, Liub T, Gaoa M. 2012. Guava leaf extracts inhibit 3T3-L1 adipocyte differentiation via activating AMPK. *J Nutr Ther* 1: 107-113.
- Zhang K, Guo W, Yang Y, Wu J. 2011. JAK2/STAT3 pathway is involved in the early stage of adipogenesis through regulating C/EBPbeta transcription. *J Cell Biochem* 112:488-497.
- Zhang LL, Yan Liu D, Ma LQ, Luo ZD, Cao TB, Zhong J, Yan ZC, Wang LJ, Zhao ZG, Zhu SJ, Schrader M, Thilo F, Zhu ZM, Tepel M. 2007. Activation of transient receptor potential vanilloid type-1 channel prevents adipogenesis and obesity. *Circ Res* 100:1063-1070.

# Simultaneous Light-Directed Synthesis of Mirror-Image Microarrays in a Photochemical Reaction Cell with Flare Suppression

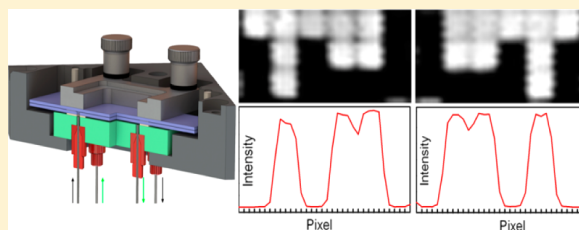
Matej Sack,<sup>†</sup> Nicole Kretschy,<sup>†</sup> Barbara Rohm,<sup>‡,§</sup> Veronika Somoza,<sup>‡,§</sup> and Mark M. Somoza<sup>\*,†</sup>

<sup>†</sup>Institute of Inorganic Chemistry, University of Vienna, Währinger Strasse 42, A-1090 Vienna, Austria

<sup>‡</sup>Department of Nutritional and Physiological Chemistry, University of Vienna, Althanstraße 14 (UZA II), A-1090 Vienna, Austria

<sup>§</sup>Christian Doppler Laboratory for Bioactive Aroma Compounds, University of Vienna, Althanstraße 14, A-1090 Vienna, Austria

**ABSTRACT:** The use of photolabile protecting groups is a versatile and well-established means of synthesizing high complexity microarrays of biopolymers, such as nucleic acids and peptides, for high-throughput analysis. The synthesis takes place in a photochemical reaction cell which positions the microarray substrate at the focus of the optical system delivering the light and which can be connected to a fluidics system which delivers appropriate reagents to the surface in synchrony with the light exposure. Here we describe a novel photochemical reaction cell which allows for the simultaneous synthesis of microarrays on two substrates. The reaction cell positions both substrates within the limited depth-of-focus of the optical system while maintaining the necessary reagent flow conditions. The resulting microarrays are mirror images of each other but otherwise essentially identical. The new reaction cell doubles the throughput of microarray synthesis without increasing the consumption of reagents. In addition, a secondary flow chamber behind the reaction cell can be filled with an absorbent and index-matching fluid to eliminate reflections from light exiting the reaction cell assembly, greatly reducing unintended light exposure that reduces the sequence fidelity of the microarray probes.



Microarrays are versatile and widely used analytical tools with the capacity to simultaneously detect several hundred thousand to millions of different biomolecules simultaneously. Microarrays can be made by presynthesizing the probe molecule and spotting it on a surface using appropriate tethering chemistry, but modern microarrays are made with *in situ* methods in which the biomolecules are synthesized directly on the substrate from their monomer components, which allows for high probe densities, high uniformity, and high reproducibility.

Light-directed *in situ* synthesis of microarrays derives from the photolithographic technology used in the semiconductor industry in combination with combinatorial chemistry based on the selective removal of photolabile protecting groups. The technology was first commercialized by Affymetrix, which used the photolabile MeNPOC group on the 5' end of DNA phosphoramidites to synthesize high-density DNA microarrays for genomics applications.<sup>1</sup> The synthesis technology was improved with the use of optical systems incorporating digital micromirror devices (DMD) to replace physical masks in the patterning of light on the microarray substrate, as well as by the use of the NPPOC photolabile group, which has significantly improved photodeprotection yield.<sup>2-7</sup> This maskless array synthesis (MAS) technology, originally used for DNA microarray synthesis has also been extended for the synthesis of RNA, aptamer,<sup>8</sup> and peptide microarrays.<sup>9-13</sup>

*In situ* microarray synthesis is robust and efficient in comparison with spotted synthesis; however, the total synthesis

time and the consumption of solvents and reagents are still a significant economic constraint. In addition, the light-directed chemistry is sensitive to stray light in the system, which leads to unintended photodeprotection which degrades the sequence fidelity of the microarray probes.<sup>7,14</sup> Here we present an improved microfluidic photochemical reaction cell for use in light-directed synthesis that addresses both of these concerns. This reaction cell places two microarray substrates within the depth-of-focus plane of the optical system, so that two microarrays are synthesized simultaneously using the same reagents. The microarrays thus synthesized are mirror images of each other but otherwise essentially identical. The microarrays can be used independently but may have additional utility as matched pairs for experiments that would benefit from very close data comparisons; the quality of *in situ* synthesized microarrays, however, is very high and in most common applications, variations in quality between microarrays synthesized at different times are not experimentally relevant. In addition, the reaction cell assembly has a secondary chamber that can be filled with a light-absorbing and index-matching fluid to eliminate reflections that are a primary source of sequence error in light-directed synthesis.

**Received:** August 2, 2013

**Accepted:** August 22, 2013

**Published:** August 22, 2013

## MATERIALS AND METHODS

### Photochemical Reaction Cell Concept and Assembly.

The reaction cell needs to position the two microarray substrates at the focal plane of the optical system. There is some tolerance to this positioning: the depth of focus of the imaging optics. The imaging optics are a 1:1 Offner relay system,<sup>15,16</sup> an off-axis conjugate system composed of two spherical concentric mirrors, primary and secondary. The system was designed with a numerical aperture (NA) of 0.08 to result in a resolving power of  $2.7 \mu\text{m}$ . This resolving power is sufficient since it is significantly smaller than the size of individual mirrors of the digital micromirror device (DMD),  $13 \mu\text{m} \times 13 \mu\text{m}$ , separated by a  $0.7 \mu\text{m}$  gap and is similar or better than those of most available microarray scanners. A low value of numerical aperture lowers the cost of the primary mirror but, more importantly, reduces the amount of scattered light originating from dust and imperfections in the optical system, which is proportional to  $\text{NA}^2$ . Unintended photodeprotection, from scattering, diffraction, and local flare, is the largest source of sequence error in light-directed microarray synthesis.<sup>7</sup> The depth of focus is intrinsically limited by diffraction to  $< \sim \lambda / \text{NA}^2$ ,  $\sim 60 \mu\text{m}$ , but in practice, the positioning of the microarray substrates in the focal plane is somewhat less restricted due to limited resolution of microarray scanners. Therefore, the primary optical constraint in the simultaneous light-directed synthesis of microarray pairs is that the two substrates must be within  $\sim 60$ – $100 \mu\text{m}$  of each other, depending on the scanner resolution.

A secondary constraint is imposed by reagent delivery. A larger reaction cell volume requires larger flow rates of solvents and reagents, the consumption of which scales with cell volume. Since our original reaction cell (for synthesizing microarrays on a single surface) had a depth of  $70 \mu\text{m}$  and worked well with a standard oligonucleotide synthesizer (Expedite 8909), we took this value as a starting point. Thus, the reaction cell should consist of two standard microarray substrates ( $75 \text{ mm} \times 25 \text{ mm} \times 1 \text{ mm}$ ) separated by a uniform gap of  $\sim 70 \mu\text{m}$ . The microarray substrates form the entrance and exit windows for the ultraviolet light used in the synthesis. Reagents need to be introduced into this gap and to uniformly flow across the surface before exiting. We used these criteria to design and built the reaction cell shown in Figure 1. The reaction cell assembly consists of a black anodized aluminum support block, a quartz block, the two microarray substrates, two gaskets, and a clamping frame and screws to hold the parts together. Reagent delivery tubes attach to the underside of the quartz block and connect to the oligonucleotide synthesizer.

The support block forms the rigid structure for the assembly of the reaction cell and allows for the reaction cell to be precisely positioned in the focal plane. Three alignment points make contact with ball-tipped, high-precision adjustment screws (Newport AJS127-0.5H) in the optical system. After initial adjustment of the screws, the reaction cell assembly can be quickly and reproducibly positioned. The support blocks hold a quartz block. The quartz block has four  $0.8 \text{ mm}$  through-holes (two inlets, two outlets) that are countersunk on the back side to accommodate microfluidics ports. The microfluidics ports (IDEX 6-32 Coned NanoPort Assemblies) were turned on a lathe to reduce their diameter to  $6.4 \text{ mm}$  and attached within each countersunk hole with common cyanoacrylate adhesive. The front and back surfaces of the quartz block were machined to a surface parallelism error of  $< 30$  arc sec and

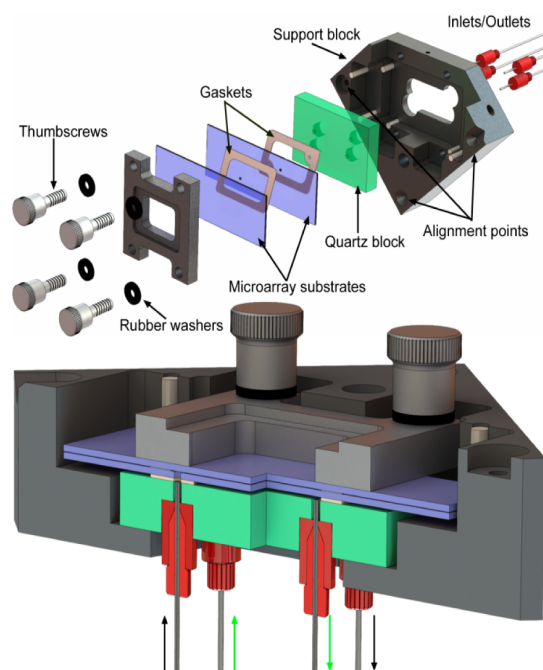


**Figure 1.** Exploded and section view of reaction cell assembly. The reaction cell is formed by two microarray substrates ( $75 \text{ mm} \times 25 \text{ mm} \times 1 \text{ mm}$ ) separated by a  $50 \mu\text{m}$  PTFE gasket. Reagents enter and exit the cell via two  $0.9 \text{ mm}$  holes through the lower substrate. These holes are coupled to the inlets/outlets via an additional  $250 \mu\text{m}$  thick FFKM gasket separating the lower substrate from the quartz block. The lower gasket forms a chamber that can be independently filled with a light-absorbing and index-matching fluid to reduce reflections from both quartz surfaces and from the back surface of the lower substrate. The thickness of the upper and lower gaskets in the section view have been exaggerated by a factor of 2 for visual clarity.

polished to an optical flatness of  $\lambda/4$  (Mindrum Precision). During reaction cell assembly, the lower gasket is placed on the quartz surface. This gasket forms the lower chamber, which can be filled via two of the fluidics ports. Prior to microarray synthesis, this chamber can be filled with an index-matching and light absorbing fluid to prevent light reflections from light exiting the reaction chamber. In the legacy reaction cell design, an antireflective coating on the back surface of the quartz block can reduce the back reflection to a minimum of about 0.25% when new, but this value is typically larger,  $\sim 1\%$ , due to the presence of dust, chemical films, and scratches. This 0.25–1% value is sufficient to make this unintended light exposure the largest source of error after diffraction, but unlike diffraction, the error is not confined primarily to the gaps between microarray features.<sup>7</sup> An alternative strategy to reduce back reflections is to fill the lower chamber with an index-matching fluid with dissolved chromophores which absorb the light exiting the reaction chamber and which either convert the light to heat or Stokes shift it beyond the absorption band of the light-labile group.

The lower gasket has two holes that align with two of holes in the quartz block. These holes couple the corresponding fluidics ports to the microarray synthesis cell. This gasket is made from  $250 \mu\text{m}$  thick Chemraz 584 perfluoroelastomer (FFKM), cut to shape with a laser cutter (Spirit GX). The microarray synthesis cell is a chamber consisting of two glass substrates separated by a very thin gasket. This chamber is

accessed via two 1 mm holes, in the lower substrates, which align with the holes in the lower gasket.

The thickness of the upper gasket determines the depth of the photochemical reaction cell and therefore needs to be  $\sim 70$   $\mu\text{m}$  thick, chemically resistant and sufficiently elastic to form a seal for the duration of the synthesis, up to  $\sim 12$  h for an array of 70mers. These requirements are quite exceptional and we were unable to find any references to such thin gaskets in the scientific or engineering literature. A perfluoroelastomer, such as Chemraz, would likely work, but the manufacturer is unable to make them thinner than 250  $\mu\text{m}$ . We tried expanded polytetrafluoroethylene (ePTFE), which is commonly used in gasket applications due to its chemical resistance and ability to compress to form a seal, but found seepage through the gasket, presumably due to its porous nature. In the end we found that the common PTFE tape used for plumbing applications works well. This tape is made from unsintered PTFE and is therefore sufficiently compressible to form a seal but not porous. PTFE tape is made in many thicknesses and densities, which allowed for some experimentation. We initially used  $\sim 100$   $\mu\text{m}$  (120  $\mu\text{m}$  uncompressed) PTFE with a density of  $\sim 1.4$   $\text{g}/\text{cm}^3$  (Gasoila yellow tape), sintered PTFE has a density of about 2  $\text{g}/\text{cm}^3$ , but found some loss of focus when microarrays were scanned at a resolution of 2.5  $\mu\text{m}$ . Another problem with the 100  $\mu\text{m}$  gap were indications that reagents were flowing in a channel through the center of the reaction cell rather than sweeping the whole surface. This was particularly apparent with the helium drying step, which was not capable of fully removing solvent from the corners of the reaction cell. Switching to thinner and lower density PTFE tape (Gasoila Industrial Strength SD,  $\sim 0.7$   $\text{g}/\text{cm}^3$ ) gave a thickness of  $\sim 50$   $\mu\text{m}$  under compression. With this thickness, both of the paired arrays produce sharp scans with resolution limited only by the 2.5  $\mu\text{m}$  pixel size of the scanner and both reagent and helium flow sweep uniformly across the entire surface of both substrates. The 50  $\mu\text{m}$  PTFE gaskets are also formed with a laser cutter. Because of their thinness, they are too delicate to be reusable but can be made quickly and inexpensively.

**Microarray Synthesis and Hybridization.** Schott Nexte-rion Glass D slides functionalized with *N*-(3-triethoxysilylpropyl)-4-hydroxybutyramide (Gelest SIT8189.5). The arrays with holes were drilled with a 0.9 mm diamond bit and washed and rinsed in an ultrasonic bath prior to functionalization. The slides were loaded in a metal staining rack and completely covered with a 500 mL of a solution of 10 g of the silane in 95:5 (v/v) ethanol–water and 1 mL of acetic acid. The slides were gently agitated for 4 h and then rinsed twice for 20 min with gentle agitation in the same solution but without the silane. The slides were then drained and cured overnight in a preheated vacuum oven (120 °C). After cooling to room temperature, the slides were stored in a desiccator cabinet until use. Microarrays were synthesized directly on the slides using a maskless array synthesizer, which consists of an optical imaging system that used a digital micromirror device to deliver patterned ultraviolet light near 365 nm to the synthesis surface. Microarray layout and oligonucleotide sequences are determined by selective removal of the NPPOC photocleavable 5'-OH protecting group. Reagent delivery and light exposures are synchronized and controlled by a computer. The chemistry is similar to that used in conventional solid-phase oligonucleotide synthesis. The primary modification is the use of NPPOC phosphoramidites. Upon absorption of a UV photon, and in the presence of a weak organic base, e.g., 1% (m/v) imidazole in DMSO, the

NPPOC group comes off, leaving a 5'-terminal hydroxyl which is able to react with an activated phosphoramidite in the next cycle. The DNA sequences on the microarrays in this project were synthesized with a light exposure dose of 4.5  $\text{J}/\text{cm}^2$ , with coupling time of 40 s at monomer concentrations of 30 mM. After synthesis, the microarrays were deprotected in 1:1 (v/v) ethylenediamine in ethanol for 2 h at room temperature, washed twice with distilled water, dried with argon, and stored in a desiccator until hybridization.

Microarrays were hybridized in an adhesive chamber (SecureSeal SA200, Grace Biolabs) with a solution consisting of 0.3 pmol of 5'-Cy5-labeled probe and 200  $\mu\text{g}$  of acetylated BSA in 400  $\mu\text{L}$  of MES buffer (100 mM MES, 1 M NaCl, 20 mM EDTA, 0.01% Tween-20). After 2 h of rotation at 42 °C, the chamber was removed and the microarrays were vigorously washed in a 50 mL centrifuge tube with 30 mL of nonstringent wash buffer (SSPE; 0.9 M NaCl, 0.06 M phosphate, 6 mM EDTA, 0.01% Tween-20) for 2 min and then with stringent wash buffer (100 mM MES, 0.1 M NaCl, 0.01% Tween-20) for 1 min. The microarrays were then dipped for a few seconds in a final wash buffer (0.1 $\times$  SSC) and then dried with a microarray centrifuge. Arrays were scanned with a Molecular Devices GenePix 4400A at a resolution of 2.5  $\mu\text{m}$ .

**Detection and Suppression of Reflected Light.** To test the possibility of eliminating reflected light reaching the synthesis area, a small piece of radiochromic film (Far West Technology, FWT-60-20f), with a 2 mm punched hole, was placed in the reaction cell. A 9.5 mm metal disk with a 1 mm pinhole (Edmund Optics, 39730) was aligned over the hole in the film to serve as a physical mask. The entire reaction cell assembly was tilted by  $\sim 7^\circ$  to move the reflection spot away from the mask hole. The lower chamber was filled with either DMSO (control) or UV absorbers dissolved in DMSO or dichloromethane. The UV absorbers (beta carotene, 9-methylanthracene, and riboflavin) were chosen for high extinction coefficients near 365 nm, high Stokes shift, low fluorescence quantum yield, and solubility in DMSO. The synthesis cell was exposed using all mirrors, with an exposure of 60  $\text{J}/\text{cm}^2$  (80  $\text{mW}/\text{cm}^2$  for 750 s).

## RESULTS AND DISCUSSION

**Synthesis of Mirror-Image Microarrays.** Simultaneous synthesis of mirror-image microarrays in this microfluidic photochemical reaction chamber produces high-quality microarrays with little additional cost or effort beyond those of the single microarray synthesis of the legacy method. The primary concern with this method is that both arrays are in focus. To test the image quality of paired microarrays, we initially synthesized simple microarrays of 30mers (GTC ATC ATC ATG AAC CAC CCT GGT CTT TTT), hybridized them with labeled complementary oligonucleotides and scanned them at high resolution. The results of one such experiment is shown in Figure 2. The top row shows pixel-level close-ups from both of the arrays. Each white square corresponds to a microarray feature synthesized with a single DMD mirror. In both close-ups, the features are individually resolved, and the 0.7  $\mu\text{m}$  gap between features are also clearly visible. The middle row shows plots of the scan image intensity along a horizontal line through the center of each of the pixel-level close-ups. The intensity drops by  $\sim 1000$ -fold between the center of hybridized pixels and unhybridized pixels, which is a typical signal/background for this type of microarray. The gap between immediately adjacent hybridized pixels is visible as a drop in intensity of



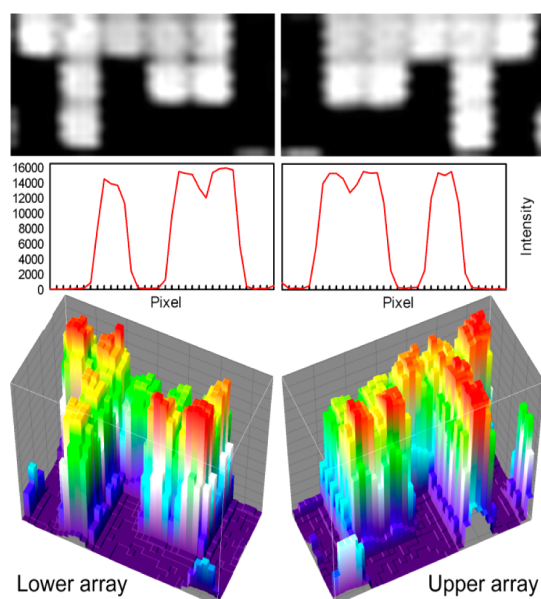


**Figure 2.** Scanned images and pixel intensities from two mirror-image microarrays synthesized simultaneously. Figures on the left are from the lower substrate (closest to quartz block in Figure 1), and those on the right are from the upper substrate. Top row:  $3 \times 6$  array of features from the center of a  $1024 \times 768$  array, scanned at  $2.5 \mu\text{m}$ . Each feature measures  $13 \mu\text{m} \times 13 \mu\text{m}$  and are separated by a  $0.7 \mu\text{m}$  gap. Middle row: Intensity profiles of lines drawn horizontally through the close-ups above. Lower row: 3D surface intensity plots of the same close-ups.

about 20%. This interstitial intensity is due to the limited resolution of the scanner ( $2.5 \mu\text{m}$ ), which leads to image pixels that derive most of their intensity from the adjacent bright microarray features. Diffraction also contributes significantly to intensity in gaps between microarray features, about 40% of the intensity of adjacent features when both features are exposed, and about 20% of the intensity of an adjacent feature when only one of the features is exposed.<sup>7</sup> The vertical sawtooth pattern probably originates from signal latency during rastering by the scanner. The microarrays are fully resolved within the constraints of scanner resolution and diffraction. The bottom row of Figure 2 shows 3-D surface intensity plots of the same close-ups. From the perspective of common microarray use, each of the mirror image microarrays from the pair can be used as an individual microarray, but in some experimental contexts requiring close comparisons, matched pairs might be used to increase confidence in the comparison.

**Blocking Reflections.** The use of a light-absorbing fluid in the lower chamber resulted in the complete blockage of reflected light. Initial trials with 9-methylanthracene and riboflavin in DMSO were only partially successful due to incomplete absorption of violet light from the mercury lamp. Most of the photodeprotection of NPPOC results from the 365 nm line, but the mercury lines at 405 and 436 nm are also transmitted through the optical system and result in measurable deprotection. Beta carotene was able to completely absorb the incident light and prevent any reflection. Beta carotene is insufficiently soluble in DMSO but is highly soluble in dichloromethane,<sup>17</sup> which also has an index of refraction similar to that of glass. Figure 3 shows the effect of 5.5 mM beta carotene in dichloromethane. The control experiment (left film) has DMSO in the lower chamber and clearly shows the

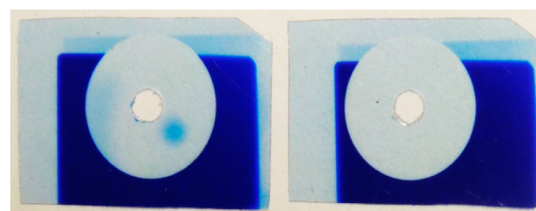


**Figure 3.** Visualization of light reflected into the synthesis chamber from the back surface of the quartz block and the complete suppression thereof using a light-absorbing fluid in the lower chamber. A 9.5 mm metal disk with a 1 mm diameter pinhole was used to mask radiochromic film in the synthesis chamber. The pinhole was aligned with a 2 mm hole in the film to allow the passage of light ( $60 \text{ J}/\text{cm}^2$ ), and the reaction cell assembly was tilted  $7^\circ$  to direct the reflection away from the hole. With the secondary chamber filled with a nonabsorbing fluid (left), there is a clear reflection to the lower right of the hole. When the secondary chamber is filled with a light-absorbing fluid, the reflection is completely suppressed (right).

reflection from the light transmitted through the 1 mm pinhole as a round exposed spot on the lower right-hand side. Another reflection is also apparent on the left side of the circle; this originates from transmission outside the pinhole disk that is not entirely absorbed by the radiochromic film. The film on the right shows that the beta carotene solution completely suppresses the reflections.

There are four principle sources of unintended photodeprotection: (1) global scattering, (2) edge scattering, (3) local flare (which includes reflections), and (4) diffraction.<sup>7</sup> Global scattering from imperfections and dust in the optical system is relatively small and results in a contrast ratio of better than  $1/2500$ . Edge scattering originates primarily from the edges of the micromirrors and has a similar magnitude as global scattering. Diffraction is an intrinsic limitation of all imaging systems and results in partial exposure ( $\sim 20\%$ ) of the area of the synthesis surface corresponding to the gaps between mirrors. Local scattering is primarily due to reflections of light exiting the reaction block but also includes scattering from bubbles in the exposure solvent. Bubbles can be eliminated by using appropriate fluidics protocols, primarily the use of helium as the blanket gas and adequate flushing of the reaction cell with exposure solvent before exposure. Reflection and diffraction remain alone as the largest sources of unintended exposure, each contributing approximately 1–2% of incident light. The use of an effective light absorber in the lower chamber, as demonstrated here, therefore reduces unintended exposure by approximately 50%. Diffraction remains as a large source of unintended exposure, but because the intensity is mostly confined to the gaps between microarray features (“spots”), it does not strongly affect the sequence fidelity within the features.

## CONCLUSIONS

We have presented a method for doubling the efficiency of *in situ*, light directed microarray synthesis by assembling a reaction cell from two very closely spaced substrates. The method is straightforward, and we have adopted the method for routine synthesis of both DNA and RNA microarrays and for applications including gene expression and miRNA expression studies.<sup>18,19</sup> For microarray applications requiring high sequence fidelity, the reaction cell assembly provides a chamber that can be used to completely suppress reflections.

## AUTHOR INFORMATION

### Corresponding Author

\*E-mail: mark.somoza@univie.ac.at.

### Notes

The authors declare no competing financial interest.

## ACKNOWLEDGMENTS

Funding by the University of Vienna, the Faculty of Chemistry of the University of Vienna, the Austrian Science Fund (Grant FWF P23797), the Austrian Federal Ministry of Economy, Family and Youth, and the Austrian National Foundation for Research, Technology and Development is gratefully acknowledged. We thank John Wallace and Kurt Heinrich for providing assistance with material sourcing, specifications, and mechanical drawings from the original reaction cell and Walter Leuthner for machining the support block and prototypes of various components.

## REFERENCES

- (1) Fodor, S. P.; Read, J. L.; Pirrung, M. C.; Stryer, L.; Lu, A. T.; Solas, D. *Science* **1991**, *251*, 767–773.
- (2) Singh-Gasson, S.; Green, R.; Yue, Y.; Nelson, C.; Blattner, F.; Sussman, M.; Cerrina, F. *Nat. Biotechnol.* **1999**, *17*, 974–978.
- (3) Beier, M.; Hoheisel, J. D. *Nucleic Acids Res.* **2000**, *28*, e11.
- (4) Hasan, A.; Stengele, K.; Giegrich, H.; Cornwell, P.; Isham, K.; Sachleben, R.; Pfeleiderer, W.; Foote, R. *Tetrahedron* **1997**, *53*, 4247–4264.
- (5) Pirrung, M. C.; Wang, L.; Montague-Smith, M. P. *Org. Lett.* **2001**, *3*, 1105–1108.
- (6) Agbavwe, C.; Somoza, M. M. *PLoS ONE* **2011**, *6*, e22177.
- (7) Agbavwe, C.; Kim, C.; Hong, D. G.; Heinrich, K.; Wang, T.; Somoza, M. M. *J. Nanobiotechnol.* **2011**, *9*, 57.
- (8) Franssen-van Hal, N. L. W.; van der Putte, P.; Hellmuth, K.; Matysiak, S.; Kretschy, N.; Somoza, M. M. *Anal. Chem.* **2013**, *85*, 5950–5957.
- (9) Bhushan, K. R. *Org. Biomol. Chem.* **2006**, *4*, 1857–1859.
- (10) Shin, D.-S.; Lee, K.-N.; Yoo, B.-W.; Kim, J.; Kim, M.; Kim, Y.-K.; Lee, Y.-S. *J. Comb. Chem.* **2010**, *12*, 463–471.
- (11) Lackey, J. G.; Mitra, D.; Somoza, M. M.; Cerrina, F.; Damha, M. *J. Am. Chem. Soc.* **2009**, *131*, 8496–8502.
- (12) Wang, T.; Oehrlin, S.; Somoza, M. M.; Perez, J. R. S.; Kershner, R.; Cerrina, F. *Lab Chip* **2011**, *11*, 1629–1637.
- (13) Lackey, J. G.; Somoza, M. M.; Mitra, D.; Cerrina, F.; Damha, M. *J. Chim. Oggi* **2009**, *27*, 30–33.
- (14) Garland, P. B.; Serafinowski, P. *J. Nucleic Acids Res.* **2002**, *30*, e99.
- (15) Offner, A. *Opt. Eng.* **1975**, *14*, 130–132.
- (16) Offner, A. *Photogr. Sci. Eng.* **1979**, *23*, 374.
- (17) Craft, N. E.; Soares, J. H. *J. Agric. Food Chem.* **1992**, *40*, 431–434.
- (18) Holik, A.-K.; Rohm, B.; Somoza, M. M.; Somoza, V. *Food Funct.* **2013**, *4*, 1111–1120.
- (19) Rohm, B.; Holik, A.-K.; Somoza, M. M.; Pignitter, M.; Zaunschirm, M.; Ley, J. P.; Krammer, G. E.; Somoza, V. *Mol. Nutr. Food Res.* **2013**, DOI: 10.1002/mnfr.201200846.

## 2.0. Conclusions

In these studies we have shown the potential of the light directed in situ synthesis of DNA microarrays and how it can be increased if the suitable conditions are present. By using BTA-NPPOC as the photolabile protecting group a two fold increase in photodeprotection efficiency in comparison with the commonly used NPPOC group could be achieved. By using SPh-NPPOC, which is based on intra- and intermolecular energy transfer from a triplet sensitizer the photodeprotection efficiency could be increased by twelve fold. This results in a significant decrease of expenditure of time to synthesize an array. Further these results offer a possibility to adapt the specific photolabile protecting group to the required conditions of the synthesis.

Intensive research was also focused on the development of high density RNA microarrays. First we tried to find the right synthesis conditions for DNA and RNA microarrays. These include coupling time, the activator type, capping and oxidation steps. Additionally a new cleavage method was developed to cleave the RNA from the surface without contamination and degradation and to analyze the pureness of the RNA after the deprotection process. To detect the sufficiency the RNA/DNA was analyzed by MS or HPLC. The analysis of the DNA and RNA arrays showed sufficient cleavage and deprotection and the confirmation of the chosen synthesis conditions of the DNA and RNA.

The modification of the photochemical cell allowed us to double the efficiency of the in situ light directed microarray synthesis. It was proven that the modification has no negative effect on the quality of the synthesis. The testing includes image quality, possible leaking due the synthesis and also the possibility that eliminating reflected light reaches the synthesis. The modification is important especially for high density microarrays, like gene expression and miRNA expression studies which have a long synthesis time.

The interaction between the dye and the nearby sequence plays a crucial role in



hybridization experiments which are commonly used in microarray technology. In our studies we tried to determine the sequence-dependent fluorescence for DY547 and DY647, which are becoming more and more important in labelling experiments, and to compare it with the common used dyes Cy3 and Cy5. To determine the sequence dependence pattern of Cy3, Cy5, DY547 and DY647 all four dyes were tested. The testing includes the usage of all four bases and the testing of all possible combination of bases in an in situ microarray experiment. The results indicate that DY547 and DY647 are less likely resulting to result in sequence-dependent labeling artifacts in comparison to Cy3 and Cy5 and it was found that the DY-dyes have a slightly higher quantum yield. This reveals the urgency to determine the sequence dependence pattern, to understand the full spectra of the influences which can affect the intensity of hybridization signals.

The application of microarrays includes a very wide area. The most recent technology to provide sensitive and accurate multiplexed protein measurements are aptamer microarrays. With this approach it is possible to test the binding of aptamer and protein by a high density microarray which can include about 750sevenfitfy thousand experimental sequences per array. Yet the right conditions of the synthesis of aptamer microarrays was not explored till now, so we detected the optimal conditions and have proven them in an on-array streptavidin binding assay in cooperation with Flexgen. Furthermore we have explored the impact of synthesis parameters on aptamer microarray performance and made direct comparisons with similar hybridization-based arrays. Also the higher complexity of aptamer microarray in comparison with hybridization experiments was noticed.

Another important application of microarrays are gene expression experiments. In cooperation with the Nutrition Department of the University of Vienna it was tested, if a less pungent structural analog of capsaicin, nonivamide (NV), has similar effects on lipid accumulation in 3T3-L1 cells and if TRPV1 receptor activation and miRNA regulation is involved in the underlying pathways. The involvement of the miRNA regulation was tested by a gene expression experiment. The testing proved that capsaicin and NV reduces lipid accumulation in 3T3-L1 cells and that the effectiveness of capsacin and nonivamide depends on

the activation of the TRPV1 receptor and on the miRNA regulation.

These studies had the main focus on optimization of the fabrication of a high density light directed microarray which includes synthesis, deprotection and hybridization in different fields of applications. All the areas which are necessary to create such microarrays are involved in these studies, the synthesis by using a modified photochemical cell and by using a photolabile group with higher photodeprotection efficiency. The deprotection was improved by and the development of a new cleavage method to analyze the pureness of the DNA/RNAs by MS and HPLC after the deprotection of the base protection groups and the ALE group. The results of analysis by MS and HPLC revealed that an optimization was achieved in every field. It creates an incentive to further develop inventions in this field such as the fabrication of high density RNA microarrays which detect regulatory protein binding patterns, with the goal to better understand the mechanisms of post-transcriptional gene regulation, as well as the binding of small molecules to RNA for potential therapeutic applications. Additional, the high complexity of aptamers could lead to further analysis with a variety of aptamers to understand the full extent of variability.

### 3.0. Abstract

Light-directed in situ microarray synthesis is a powerful tool to detect over a hundred thousand of sequences simultaneously. The microarrays are produced by using MAS (maskless array synthesizer). The MAS combines the optical and chemical synthesis. The optical synthesis provides a spatially addressable illumination of light performed by using a digital micromirror device, while the chemical system delivers solvents and reagents to the functionalized glass surface where the microarray synthesis takes place. The synthesis offers high spectra of designs and modifications to adapt to the requirements of the applications. Therefore there is a need to investigate the optimization of the synthesis and the ensuing processes which involves deprotection and hybridization to assure the consistent quality of the microarray.

In this thesis the main focus was to achieve optimization in every field which is needed to create a light directed in situ microarray. Due our research the efficiency of the synthesis was doubled by using a modified photochemical cell where the synthesis takes place. Additional the development of a new cleavage method which is also suitable for in situ microarrays enables analysis of the deprotection status by MS or HPLC. Through usage of different photolabile deprotection groups, the photodeprotection was increased by two to twelve folds. The determination of the sequence dependence pattern of DY547 and DY647 in comparison with the well-established cyanine dyes Cy3 and Cy5 extended the spectra of the possible influence which can affect the hybridization signal and helped to understand them better. Further the identification of the optimized conditions for the fabrication of an aptamer microarray and also the confirmation that miRNA regulation has an influence of on adipose was achieved.

The exploration of the optimization of the fabrication of DNA Microarrays creates also an incentive to further develop inventions towards this field. One of the possibly further inventions could be the fabrication of high density RNA microarrays. Additionally, the high complexity of aptamers could lead to further analysis with a variety of aptamers to understand the full extent of variability.

## 4.0. Zusammenfassung

Die lichtinduzierte in situ MAS (Maskless Array Synthesis) ist eine leistungsstarke Methode um Mikroarrays zu produzieren, mit deren Hilfe eine Analyse von hunderttausend Sequenzen simultan möglich ist. Chemische und optische Komponenten werden durch die MAS kombiniert. Die optischen Komponenten ermöglichen die räumliche zielgerichtete Illumination durch Licht welche durch einen Mikrospiegelaktor kontrolliert wird. Das chemische System hingegen liefert Reagenzien und Lösungsmittel an die funktionalisierte Glasoberfläche wo die Synthese des Mikroarrays stattfindet. Die Synthese von Microarrays erlaubt durch ein hoch flexibles aber auch komplexes Design eine Anpassung an die Anforderungen der verschiedensten Anwendungen. Ein Bedarf für die weitere Erforschung und Optimierung der Synthese und der darauffolgenden Prozesse wie die Entfernung der Schutzgruppen und die Hybridisierung ist aber dennoch gegeben.

In dieser Doktorarbeit ist der Hauptfokus auf die Optimierung der Herstellung und auf alle Prozesse die eine Herstellung eines hoch verdichteten „light directed“ Mikroarrays beinhalten gerichtet. Durch unsere Forschung konnte die Effizienz der Synthese mittels Benutzung einer modifizierten photochemischen Zelle verdoppelt werden. Zusätzlich wurde eine neue Methode entwickelt die die Spaltung und das Sammeln der produzierten Oligonukleotiden beinhaltet. Diese kann genutzt werden um die Effizienz der Entschützung und die Genauigkeit mit der die Oligonucleotide synthetisiert wurden zu bestimmen. Die Bestimmung gelingt durch HPLC und Massenspektrometrie. Durch Nutzung einer anderen photolabilen Entschützungsgruppe wurde die Effizienz der Photoentschützung um das Zwei- bis Zwölfwache erhöht. Die Ermittlung des sequenzabhängigen Musters von DY547 und DY647 das mit den etablierten Cyaninfarbstoffe Cy3 und Cy5 verglichen wurde, ermöglicht es zu bestimmen wie die Interaktion des Farbstoffes das Fluoreszenzsignal in Mikorarray-, PCR-, FRET- und Sequenzierungs-experimenten beeinflusst. Weiteres wurde die Identifizierung der optimalen Bedingungen für die Herstellung eines Aptamer Mikroarrays erreicht und eine

Bestätigung, dass miRNA Regulation Einfluss auf Fettgewebe hat erzielt.

Die Erforschung der Optimierung der Produktion von DNA-Mikroarrays kreiert einen Ansporn für neue Erfindungen auf diesem Gebiet. Eine der möglichen weiteren Erfindungen könnte die Produktion von hochverdichteten RNA Microarrays beinhalten. Die hohe Komplexität der Aptamere könnte zu weiteren Analysen mit einer Vielzahl

## 5.0. References

1. Kilian Dill, Robin Liu, Piotr Grodzinsky, Microarrays, Preparation, Microfluidics, Detection Methods, and Biological Application, 2009, pp 139-167,
2. Xiaolian Gao, Xiaochuan Zhou, Erdogan Gulari Light directed massively parallel on-chip synthesis of peptide arrays with t-Boc chemistry, Proteomics, 2003
3. Sun H, Lu CH, Uttamchandani M, Xia Y, Liou YC, Yao SQ., Peptide microarray for high-throughput determination of phosphatase specificity and biology, Angew Chem Int Ed Engl. 2008;47(9):1698-702. doi: 10.1002/anie.200703473.
4. Leszek Rychlewski, Maik Kschischo, Liying Dong, Mike Schutkowski Ulf Reimer, Target Specificity Analysis of the Abl Kinase using Peptide Microarray Data, Journal of Molecular Biology 2004
5. Burton E. Tropp, Molecular Biology: Genes to Proteins, 2012, p S129
6. Jane B. Reece, Lisa A. Urry, Michael L., Cain Campbell Biology 10th Edition, 2013, p 78
7. Bruce Alberts, Dennis Bray, Karen Hopkin, Alexander Johnson, Julian Lewis, Martin Raff, Keith Roberts, Peter Walter, Essential Cell Biology, Fourth Edition, 2013, pp139-140
8. Shaohui Hu, Zhi Xie, Jiang Qian, Seth Blackshaw, and Heng Zhu, Functional Protein Microarray Technology, Wiley Interdiscip Rev Syst Biol Med. May 2011; 3(3): 255–268.
9. David A. Hall, Jason Ptacek, and Michael Snyder, Protein Microarray Technology” Mech Ageing Dev. Jan 2007; 128(1): 161–167.
10. [www.elmat.lth.se/forskning/nanobiotechnology\\_and\\_lab\\_on\\_a\\_chip/research/nanoporous\\_silicon\\_based\\_protein\\_arrays/](http://www.elmat.lth.se/forskning/nanobiotechnology_and_lab_on_a_chip/research/nanoporous_silicon_based_protein_arrays/)
11. Cloud P Paweletz, Lu Charboneau, Verena E Bichsel, Nicole L Simone, Tina Chen, John W Gillespie, Michael R Emmert-Buck, Mark J Roth, Emanuel F Petricoin and Lance A Liotta, Reverse phase protein microarrays which capture disease progression show activation of pro-survival pathways at the cancer invasion front, Oncogene, 2001
12. Bruce Alberts, Essential Cell Biology, 1998, p168
13. Bruce Alberts, Alexander Johnson, Julian Lewis, Martin Raff, Keith Roberts, and Peter Walter, Molecular Biology of the Cell. 4th edition, Chapter 4,

## The Structure and Function of DNA

14. T. Strachan, Andrew P. Read, *Human Molecular Genetics* 3, 2004, pp16-19,22-24
15. Wilfried Janning, Elisabeth Knust, *Genetik: Allgemeine Genetik - Molekulare Genetik – Entwicklungsgenetik*, 2008, p163
16. Leonard H. Augenlicht and Diane Kobrin, *Cloning and Screening of Sequences Expressed in a Mouse Colon*, 1982 *Cancer Research*
17. Leonard H. Augenlicht, Miryam Z. Wahrman, Heidi Halsey, Leigh Anderson, John Taylor, and Martin Lipkin, *Expression of Cloned Sequences in Biopsies of Human Colon Tissue and in Colon Carcinoma Cells Induced to Differentiate in Vitro*, 1987 *Cancer Research*
18. Mark Schena, Dari Shalon, Ronald W. Davis, Patrick O. Brown, *Quantitative Monitoring of Gene Expression Patterns with a Complementary DNA Microarray*; *Science, New Series*, Vol. 270, No. 5235 (Oct. 20, 1995), pp. 467-470
19. Deval A. Lashkari, Joseph L. DeRisi, John H. McCusker, Allen F. Namath, Christl Gentile, Seung Y. Hwang, Patrick O. Brown and Ronald W. Davis, *Yeast microarrays for genome wide parallel genetic and gene expression analysis*, 1997 *Nov 25;94(24):13057-62*.
20. <http://www.atdbio.com/content/17/Solid-phase-oligonucleotide-synthesis>
21. Masad J. Damha, Paul A. Giannaris and Steven V. Zabalylo, *An improved procedure for derivatization of controlled-pore glass beads for solid-phase oligonucleotide synthesis*, 1990, *Nucleic Acids Research*
22. Fernando Albericio, *Solid-Phase Synthesis: A Practical Guide*, 2000
23. Cheng-Chung Lee, Thomas M. Snyder, and Stephen R. Quake, *A microfluidic oligonucleotide synthesizer*, 2010, *Nucleic Acids Research*
24. Agnieszka B. Sierzchala, Douglas J. Dellinger, Jason R. Betley, Tadeusz K. Wyrzykiewicz, Christina M. Yamada, and Marvin H. Caruthers, *Solid-Phase Oligodeoxynucleotide Synthesis: A Two-Step Cycle Using Peroxy Anion Deprotection*, 2003, *Journal of the American Chemical Society*
25. Ann Caviani Pease, Dennis Solas, Edward J. Sullivan, Maureen T. Cronin, Christopher P. Holmes, Stephen P.A. Fodor, *Light-generated oligonucleotide arrays for rapid DNA sequence analysis*, 1994. Vol. 91, pp. 5022-5026.
26. Fodor SP, Read JL, Pirrung MC, Stryer L, Lu AT, Solas D. *Science*. 1991 Feb 15;251(4995):767-73.



27. Hasan, A., K.-P. Stengele, H. Giegrich, P. Cornwell, K.R. Isham, R.A. Sachleben, W. Pfeleiderer, and R.S. Foote, Photolabile protecting groups for nucleosides: Synthesis and photodeprotection rates. *Tetrahedron*, 1997. 53(12): p. 4247-4264.
28. Christy Agbavwe, Changan Kim, DongGee Hong, Kurt Heinrich, Tao Wang, and Mark M Somoza, Efficiency, error and yield in light-directed maskless synthesis of DNA microarray, *J Nanobiotechnology*. 2011; 9: 57
29. Nicole Kretschy, Mark M. Somoza, Comparison of the Sequence-Dependent Fluorescence of the Cyanine Dyes Cy3, Cy5, DyLight DY547 and DyLight DY647 on Single-Stranded DNA, January 15, 2014DOI: 10.1371/journal.pone.0085605
30. <http://www.genelink.com/newsite/products/>
31. Jennifer Villaseñor-Park and Alex G Ortega-Loayza, Microarray Technique, Analysis, and Applications in Dermatology, *Journal of Investigative Dermatology*, 2013
32. Kilian Dill, Robin Liu, Piotr Grodzinsky, *Microarray Technology in Practice*; Steven Russel, 2008 p4
33. Hughes, TR Roberts, CJ Dai, HY , Jones AR; Meyer MR; Slade, Burchard, J. Dow, Ward, TR ,Kidd, MJ, Friend SH, Marton MJ, Widespread aneuploidy revealed by DNA microarray expression profiling, 2000, *Nat. Genet* 25:333-37
34. Phillips JL, Hayward SW, Wang Y, Vasselli J, Pavlovich C, et al, 2001, The consequences of chromosomal aneuploidy on gene expression profiles in a cell line model for prostate carcinogenesis. *Cancer Res.* 61:8143–49
35. Hye Jin Lee , Alastair W. Wark , Yuan Li , and Robert M. Corn, Fabricating RNA Microarrays with RNA–DNA Surface Ligation Chemistry, *Anal. Chem.*, 2005, 77 (23), pp 7832–7837
36. Sukeerthi Seetharaman, Maris Zivarts, Narasimhan Sudarsan, Ronald R. Breaker, Immobilized RNA switches for the analysis of complex chemical and biological mixtures, *Nature Biotechnology* 19, 336 - 341 (2001)
37. Hye Jin Lee , Alastair W. Wark , Yuan Li , and Robert M. Corn, Fabricating RNA Microarrays with RNA–DNA Surface Ligation Chemistry, *Anal. Chem.* 2005, 77, 7832-7837
38. Lackey, J.G., D. Mitra, M.M. Somoza, F. Cerrina, and M.J. Damha, Acetal Levulinyl Ester (ALE) Groups for 2'-Hydroxyl Protection of Ribonucleosides in the Synthesis of Oligoribonucleotides on Glass and Microarrays, *J. Am. Chem. Soc.*, 2009. 131(24): p. 8496-8502.

## Curriculum Vitae



### Personal

Name: Kretschy  
First name: Nicole  
Nationality: Austria

### Experience

- 2012 January - present      **Ph.D. project at the University of Vienna**,  
Department of Inorganic Chemistry  
Dr. Mark Manuel Somoza  
PhD thesis: Photolithographic Synthesis of Microarrays
- 2010 February – 2011 May      Diploma project at the Medical University of Vienna,  
Diploma thesis: The suppression of in vitro breast cancer  
metastasis by approved pharmaceutical drugs (Grade: 1)  
First Examiner: Univ. Prof. Dr. Georg Krupitza,  
Clinical Institute for Pathology  
Examination subject: Tumor Biology
- Second Examiner: Univ. Prof. Dr. Sylvia Kirchengast Institute of  
Anthropology  
Examination subject: Sexual Biology
- 2009      **Student apprentice at the Medical University of Vienna**,  
Department of Medicine I,  
Division of Haematology/Haemostaseology  
Head of Laboratory: Priv. Doz. Dr. Medhat Shehata

### Education

- 2011      Master degree in Biology, branch of study Anthropology with  
specialisation in human genetics
- 2003      High School Diploma – Vienna

### Professional qualification

- Analytical methods: In situ microarray synthesis, PCR, western blot, FACS-analysis,  
apoptose assay, RNA isolation, microarray analysis
- Languages: English, French (school knowledge)